Simulation of externally fired gas turbine configurations for micro-scale biomass applications

G Bernard

orcid.org/0000-0003-4810-9614

Dissertation submitted in partial fulfilment of the requirements for the degree *Master of Engineering in Mechanical Engineering* at the North-West University

Supervisor: Prof. M van Eldik

Co-supervisor: Dr. P.V.Z. Venter

Graduation: November 2019

Student number: 22178457

PREFACE

First and foremost, I would like to thank the Lord for my health, talent, and ability to have come this far. Blessed is His name!!

A big thank you to my study leaders, Prof. Martin van Eldik and Dr Phillip Venter, for the opportunity and their guidance and input during the study, I appreciate it so much.

I would also like to thank my friends and family for their continuous support and encouragement.

And lastly, thank you might not be enough, but I would like to thank my parents for their love and support, especially my mom who is my best friend and biggest cheerleader. Thank you for believing in me and for giving me more than any child could hope for. You're the best.

ABSTRACT

Title:	Simulation of externally fired gas turbine configurations for micro-scale biomass applications.
Author:	Gezelle Bernard
Supervisor:	Prof. M. van Eldik
Co-supervisor:	Dr. P.V.Z. Venter
School:	Mechanical and Nuclear Engineering
Degree:	Master of Engineering

Most rural communities in South Africa are forced to rely on alternative energy resources such as biomass, gas, liquid fuels and waste materials for the provision of energy to fulfil their lighting and cooking needs since electrification in rural areas is problematically low. Biomass as a source of renewable energy is a promising, ecological and sustainable solution for electricity generation. A micro-scale externally fired gas turbine (EFGT) fuelled by biomass provides a suitable solution for electricity generation in rural areas. The EFGT holds the advantage of being able to operate with poor quality and a variety of biomass fuels since the combustion gasses is not in direct contact with the working fluid of the cycle. The purpose of this study is to evaluate different EFGT configurations using thermal-fluid simulation models developed for micro-scale EFGT biomass applications, typically with an electricity generation capacity in the region of 5 kW that will be suitable for a small rural community. The conceptual simulation models can be used to assist farming and rural communities, who are interested and capable of implementing micro-scale generation to fulfil their basic electricity needs, to gain practical insight into different cycle configurations and its operating conditions.

Verification was done by comparing the results of the simple EFGT cycle configuration against that found in the literature of a similar biomass cycle. The comparative results were within 5% correlation. Within this study, four different system configurations of a micro-scaled EFGT cycle were modelled with different levels of complexity, but with rural applications in mind. The different cycle configurations were evaluated for different operating conditions and component efficiencies. The performance of the EFGT cycles was investigated to evaluate the effect of varying parameters such as turbine inlet temperature, mass flow of air, combustion heat and COP of the pre-cooling unit respectively. The individual models showed promising results, such as cycle efficiencies ranging from 12.58% for the simple cycle 30.07% for the heat recovery cycle with pre-cooled air.

Key Words: Open Brayton cycle, EFGT cycle, Thermal fluid simulation, Power generation.

OPSOMMING

Titel:	Simulasie van ekstern-aangedrewe gasturbine konfigurasies vir mikroskaal biomassa toepassings.
Outeur:	Gezelle Bernard
Studieleier:	Prof. M. van Eldik
Medestudieleier:	Mnr. P.v.Z. Venter
Skool:	Skool vir Meganiese - en Kerningenieurswese
Graad:	Meestersgraad in Ingenieurswese

Die meeste landelike gemeenskappe in Suid-Afrika word gedwing om staat te maak op alternatiewe energiebronne soos biomassa, gas, vloeibare brandstof en afvalstowwe vir die verskaffing van energie om hul beligtings en kookbehoeftes te vervul, weens ‘n gebrek aan elektrisiteit. Biomassa as bron van hernubare energie is 'n belowende, ekologiese en volhoubare oplossing vir die opwekking van elektrisiteit. ‘n Eskterne verbranding gasturbine (EVGT), met biomassa as brandstof, bied 'n geskikte oplossing vir die opwekking van elektrisiteit in landelike gebiede. Die EVGT het die voordeel dat dit met swak gehalte en 'n verskeidenheid van biomassa brandstof kan funksioneer, aangesien die verbrandingsgasse nie direk in kontak met die werkvloeistof van die siklus is nie.

Die doel van hierdie studie is om verskillende EVGT-konfigurasies te evalueer deur gebruik te maak van termo-vloei simulasiemodelle wat ontwikkel is vir mikroskaal-EVGT-biomassa-toepassings, tipies met 'n kragopwekkingskapasiteit van 5 kW wat geskik sal wees vir 'n klein landelike gemeenskap. Die konseptuele simulasiemodelle kan gebruik word om boere en landelike gemeenskappe wat belangstel en in staat is om mikroskaalopwekking te implementeer om hul basiese elektrisiteitsbehoeftes te vervul, te help om praktiese insig te verkry in verskillende sikluskonfigurasies en die bedryfstoestande van so toepassing.

Modelverifikasie was gedoen deur die resultate van die eenvoudige EVGT-sikluskonfigurasie te vergelyk met dié van 'n soortgelyke biomassa-siklus wat in die literatuur gepubliseer is. Die vergelykende resultate was binne 5% korrelasie.

In hierdie studie word vier verskillende stelselkonfigurasies van 'n mikroskaal EVGT-siklus gemodelleer met verskillende vlakke van kompleksiteit, maar met landelike toepassings in gedagte. Die verskillende sikluskonfigurasies is geëvalueer vir verskillende operasionele toestande en komponent rendemente. Die prestasie van die EVGT-siklusse is ondersoek om die effek van varierende parameters soos die turbineinlaat temperatuur, massa vloei van lug,

verbrandingshitte en prestasie koëffisiënt van die voorafverkoelde eenheid te evalueer. Die individuele modelle het belowende resultate getoon, soos sikluseffektiewiteite wat wissel van 12.58% vir die eenvoudigde siklus tot 30.07% vir die hitteherwinningsiklus met voorverkoelde lug.

Sleutelwoorde: Oop Brayton siklus, EVGT- siklus, Termo-vloei simulasie, Kragopwekking.

DECLARATION

I, **Gezelle Bernard (ID: 910506 0195 086)**, declare that this report is a presentation of my own original work. Whenever contributions of others are involved, every effort was made to indicate this clearly, with due reference to the literature. No part of this work has been submitted in the past, or is being submitted, for a degree or examination at any other university or course.

Gezelle Bernard

TABLE OF CONTENTS

LIST OF TABLES

LIST OF FIGURES

NOMENCLATURE

Symbol	Description	Unit
Δ	Variation of a variable	Variable based
C_P	Specific Heat Coefficient at Constant Pressure	J/kg-K
E	Energy	J
h	Enthalpy	kJ/kg
P	Pressure	Pa or Bar
$\dot{m}$	Mass flow	kg/s
Q	Heat transferred	kW
T	Temperature	℃
W	Work Done	kW
ρ	Density	kg/m^3
Δp_{0L}	Pressure drop	Pa or Bar
α	Fraction value	-
p_{0i}	Inlet pressure	Pa or Bar
p_{0e}	Outlet pressure	Pa or Bar
PR	Pressure ratio	-
η	Efficiency	-
$\dot{Q}$	Heat transfer rate	kJ/kg
$\dot{Q}_{max}$	Maximum heat transfer rate	kJ/kg
ε	Heat Exchanger Effectiveness	-
C_{min}	Minimum heat capacity	J/kg-K
K	Temperature (Kelvin)	K

ABBREVIATIONS & ACRONYMS

Abbreviation / Acronym	Definition
AFR	Air to Fuel Ratio
APU	Auxiliary Power Unit
CHP	Combined Heat and Power
COP	Coefficient of performance
DFGT	Directly fired gas turbine
EES	Engineering Equation Solver
EFGT	Externally fired gas turbine
EFGMT	Externally fired gas microturbine
Eskom	Refers to the South African electrical supply utility
HE	Heat Exchanger
HTHE	High Temperature Heat Exchanger
PR	Pressure Ratio
RPM	Revolutions Per Minute
TIT	Turbine Inlet Temperature
ORC	Organic Rankine Cycle
HED	Temperature difference of heat exchanger terminals

CHAPTER 1

INTRODUCTION

CHAPTER 1:

INTRODUCTION

"Why not take something ordinary, and turn it into something extraordinary?"

1.1 Background

South African electricity users place a large demand on the national supplier, Eskom, especially during morning and early evening peak periods. Eskom generates approximately 95% of the country's electricity and considering load shedding implemented a few years ago, it is safe to say that this demand is at times higher than what can be generated (Eskom, 2016a).

The country has experienced a large increase in the percentage of households requiring access to electricity. Between 2002 and 2013, the percentage of households having access to electricity increased from 77,1% to 85,4% (Stats SA, 2016). Despite these improvements, electrification of households in rural areas is hampered by concerns of practicality and cost-effectiveness. For instance, where informal areas have not been proclaimed, electricity cannot be installed due to the threat of relocation. Similarly, the electrification programme in rural areas is troubled by the topography, a lack of infrastructure, and low population/household density (Stats SA, 2016). This has resulted in rural communities needing to rely on alternative energy resources such as biomass, gas, liquid fuels and waste materials for the provision of energy to fulfil their lighting and cooking needs.

There has been a rapid increase in the generation of green power globally. Green power refers to power generation where different kinds of natural resources and waste materials are being utilized in a variety of applications to positively contribute to society and the environment (EPA, 2018). The motivation behind this movement is not just to reduce health and environmental hazards, but to rather focus on establishing a prosperous economic future in alternative energy (Habboush, 2016). A progression in innovation transforms this movement into a rapidly growing competitive industry and creates a platform for creative solutions for common real-life problems and obstacles.

The advantages of renewable energy are that it is sustainable (non-depletable), abundant (found everywhere across the world, in contrast to fossil fuels and minerals), and essentially non-

polluting (Nelson, 2011). Biomass is without a doubt a very attractive resource of renewable energy that can be utilized in innovative solutions.

Biomass refers to any plant mass harvestable for conversion, as well as animal and human wastes convertible to solid gaseous fuels (Smil, 1983). Biomass as a fuel holds many advantages over other energy sources. Biomass fuel is a renewable source of energy, unlike fossil fuels. A variety of biomass fuel sources are available in abundance in the form of agriculture, forestry, animal and biodegradable urban wastes. CO_2 gas emissions from biomass combustion do not have an adverse effect on the environment, as it is consumed by the growing plants.

According to McKendry (2002), biomass can be converted into three main products of which two are related to energy in the form of power/heat generation and transportation fuels and the third product is used as a chemical feedstock. The first two products rely on thermo-chemical conversion and the third on bio-chemical conversion. In terms of power generation, the focus is on thermo-chemical conversion from biomass, where four process options are available namely combustion, pyrolysis, gasification and liquefaction (McKendry, 2002). A number of different thermodynamic cycles are used for power generation as well as combined heat and power (CHP) generation. Among these cycles is the Brayton cycle, which refers to externally or directly fired gas turbines (Pilavachi, 2000). Schematic drawings of the externally and directly fired gas turbines are shown in Figure 1-1.

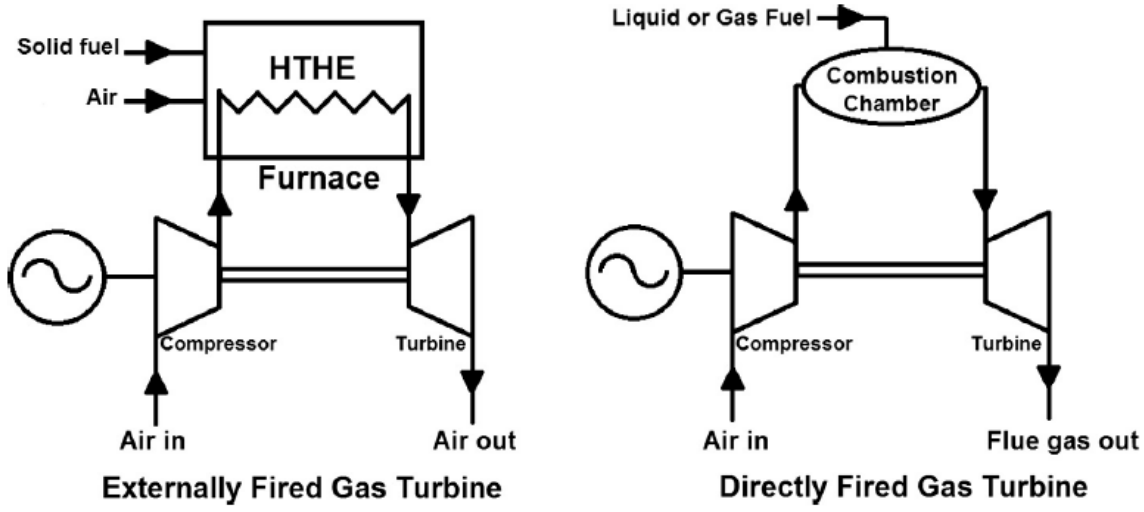

Figure 1-1: Simple externally and directly fired gas turbine cycles (Al-attab & Zainal, 2015).

The directly fired gas turbines (DFGT) can achieve higher specific output power mainly due to its higher turbine inlet temperature (TIT), but it can deal only with clean fuels. Although the DFGT

can provide higher thermal efficiency, the externally fired gas turbine (EFGT) can deal with a wide range of fuels even solid fuels without cleaning systems, fuel compression and injection equipment (Al-attab & Zainal, 2015).

An externally or indirectly fired gas turbine configuration means that the hot combustion gases are not in direct contact with the turbine blades. The thermal power of the combustion gases is transferred to the working fluid via a high-temperature heat exchanger (HTHE) and unlike directly fired gas turbines, EFGT's can be an open cycle with air as the working fluid.

The use of biomass in small scale power or CHP-EFGT standalone systems in the off-grid sites presents a very attractive option since biomass is usually available in sufficient quantities and does not require costly fuel transportation (Al-attab & Zainal, 2015). Since a variety of biomass fuels are usually available to rural communities and based on the simplicity, flexibility and the ability to operate with varying quality biomass fuels and using air as a working fluid, the EFGT thermodynamic cycle will be the focus of this study.

1.2 Problem Statement

Electrification in most rural areas is problematically low, therefore only a few are fortunate to have the minimum electricity for lighting and cooking. The use of micro-scale biomass EFGTs needs to be investigated as a possible solution.

1.3 Purpose of this Study

The purpose of this study is to evaluate different micro-scale externally fired cycle configurations in terms of simplicity, efficiency and TIT for a biomass application with an electricity generation capacity in the region of 5 kW that will be suitable for a small rural community.

1.4 Method of Investigation

- A literature survey will be conducted on biomass-fueled micro-scale EFGTs and its system components to obtain insight into what has been done by researchers to date, and to gain knowledge into the working principals and operating conditions of these different cycles.
- Simulation models will be developed in Engineering Equation Solver (EES) to simulate various cycle configurations and operating conditions.
- This is a conceptual study and will not focus on the detail design of the individual components nor the system itself.

- An analysis of the different configurations will determine practical and viable configurations for a micro-scale biomass application.
- Verification will be done using information from a published study into the use of a simple EFGT cycle fueled by olive residues with a power output in the region of 1.5 to 3 kW.

1.5 Impact of the Study

On completion of this study verified thermodynamic simulation models of a micro-scale biomass EFGT-cycle in the order of 5 kW will be available. The evaluation of different cycle configurations will be of great assistance to understand and develop or expand local expertise on the operating conditions and thermodynamic performance of different simple micro-scale biomass EFGT-cycle configurations. These simulations and the evaluation thereof can especially be useful should such an application be implemented in small rural communities with biomass abundantly available to provide the minimum electricity needed to informal dwellings.

CHAPTER 2

LITERATURE SURVEY

CHAPTER 2:

LITERATURE SURVEY

2.1 Introduction

The focus of this chapter is to gain knowledge into developments of micro-scaled power as well as combined heat and power generating technologies based on EFGTs. Gas turbines i.e. externally fired gas turbines have the same basic operation principle as the open Brayton cycle (Nascimento *et al*., 2014). An overview of the history and application of gas turbines, micro-turbines, auxiliary power units and EFGTs is covered in this chapter. The externally fired gas microturbines (EFGMT) are researched in terms of different sizes, output performance, system components and layout configurations, which will also be investigated in this chapter. Furthermore, the thermodynamic simulation approaches followed in literature will also be outlined for these type of cycles.

2.2 The History and background on Gas Turbines

Saravanamuttoo *et al*. (2009) affirm that the gas turbine is unquestionably one of the most important inventions of the 20th century, which impacted human life in many ways. The first important application of the gas turbine was the development of the military jet engine towards the end of the Second World War. These early engines were fuel inefficient, unreliable and noisy, but in less than 20 years they had matured to become the standard form of propulsion for civil aircraft (Saravanamuttoo *et al*., 2009).

Microturbine technology is based on historical research and development, as it came into the automotive market between 1950 and 1970, when the automotive industry viewed the possibility of using microturbines to replace traditional reciprocating piston engines (Nascimento *et al*., 2014). The first microturbines were based on a gas turbine designed to be used in generators of missile launching stations, as well as aircraft and bus engines, among other commercial means of transport. The use thereof in the energy market increased between 1980 and 1990 when the demand for distributed generating technologies increased (Liss, 1999).

Another well-known application of microturbines is the auxiliary power unit (APU) which originated from aircraft, such units are based on relatively small gas turbines to deliver electrical power and heat independent of the main engines and specifically designed to meet the onboard demands of

the aircraft. They operate preferably on the ground (Henne & Friedrich, 2009). In the earliest form, the APU was a single-shaft unit in which the compressor was oversized relative to the turbine, allowing up to 30% of the inlet flow to be bled off at compressor delivery for aircraft services. With the simple arrangement, the pressure ratio of the APU is limited to 4 and results in a very inefficient cycle. The standard approach used in modern APUs is to use a separate load compressor driven by the gas turbine using a common air intake for both compressors. This allowed the load compressor to be designed for a pressure ratio of about 4, while the gas turbine pressure ratio can be significantly higher (8-12). Companies well-known for the early development of APUs are Honeywell and Pratt & Whitney.

Although early gas turbines for power generation applications had a low power output and their thermal efficiency was too low to be competitive (Saravanamuttoo *et al*., 2009), gas turbines became widely used in power generation by the end of the 20th century due to remarkable development enabling outputs of up to 300 MW with thermal efficiencies of 40 percent.

Saravanamuttoo *et al*. (2009) explain that it is important to realize that in the gas turbine, the processes of compression, combustion and expansion do not occur in a single component as they do in a reciprocating engine. They occur in components which are separate in the sense that they can be designed, tested and developed individually, and these components can be linked together to form a gas turbine unit in a variety of ways. Other compressors and turbines can be added, with intercoolers between the compressors and reheat combustion chambers between the turbines. However, these refinements may increase the power output and efficiency of the system at the expense of complexity, weight and cost (Saravanamuttoo *et al*., 2009).

The basic principle of operation of microturbines is based on open cycle gas turbines, which could present several typical features, such as variable speed, high speed operation, compact size, simple operability, easy installation, low maintenance, air bearings, low nitrogen oxide emissions as well as heat recovering systems (Hamilton, 2001).

According to Nascimento *et al*. (2014), power generating turbines are classified as microturbines for capacity ranges up to 300 kW. Microturbines have similar setups to those of small, medium and large size gas turbines, as explained by Nascimento and Santos (2011).

2.3 Externally Fired Gas Turbines

The EFGT is not a new concept, as several EFGT plants were built between the years 1930-1960. At that stage in time, it was used to fire fuels like coal, mine gas and blast furnace gas.

Nevertheless, accessibility and reduction in the cost of “clean” fossil fuels like natural gas and oil, which could be burnt in internally fired gas turbines lead to a diminishing of interest in EFGT technology. (Anheden, 2000)

As mentioned in chapter 1, the greatest distinction between an internal and an externally fired gas turbine is that an EFGT has an atmospheric pressure combustor and a high-temperature heat exchanger in place of the combustion chamber. Therefore, with the EFGT, the combustion occurs outside the circuit of the working fluid. Most of the system components and operating rational of an internal gas turbine is also applicable and can be incorporated for the EFGT, i.e. adding compressors, turbines and other refinements to the system.

2.3.1 The Externally Fired Gas Microturbine Cycle Configurations

This section will focus on the system components and layout configuration of an EFGMT well as operating conditions, examples and previous studies conducted on EFGT's found in literature.

Externally fired gas microturbines in its simplest form are formed by an assembly of a compressor, an atmospheric combustion chamber with a high-temperature heat exchanger and a turbine, as shown in the simplified schematic in Figure 2-1.

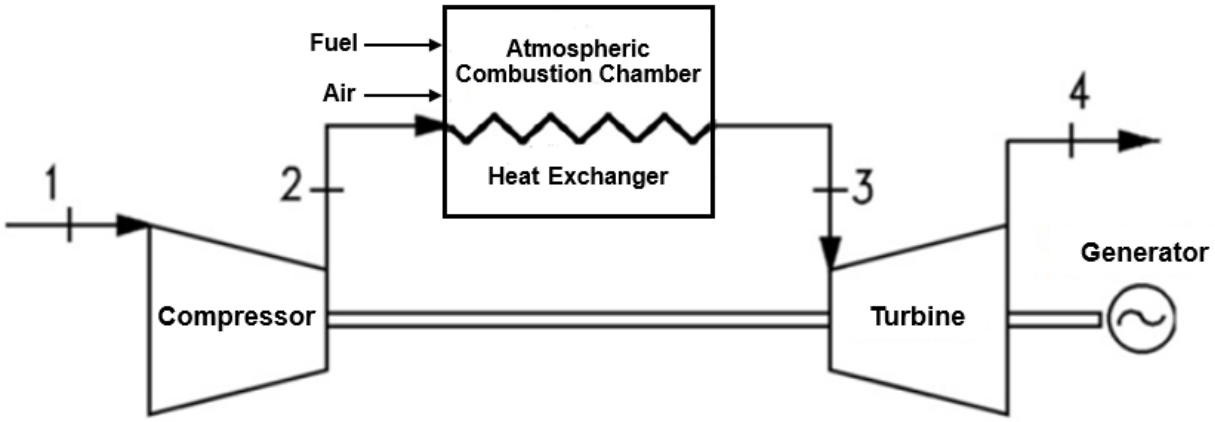

Figure 2-1: Schematic of a simple externally fired gas turbine system (Adapted from Nascimento *et al.*, 2014).

In this simple EFGT, the ambient air is first compressed by the compressor, then flows through the heat exchanger where it receives energy (heat) from the fuel source burnt in the atmospheric combustion chamber, thereby further raising its temperature of the compressed air. Leaving the heat exchanger, the high temperature working fluid is directed to the turbine, where it is expanded

before being discharged back into the open air, while the turbine supplies work to the compressor and drive the electric generator (Nascimento *et al*., 2014).

State-of-the-art microturbines have markedly improved in the last years in terms of components and cycle configuration. The microturbine's optimum rotational speeds are between 60,000 to 90,000 rpm and have a pressure ratio of 3:1 or 4:1, in a single stage configuration (Nascimento *et al*., 2014).

Bdour *et al.* (2016) claim that typical electrical efficiencies for systems like ORC and EFGT are in the range of 10%–20%, although higher efficiencies of 25% for EFGT have been reported by Schmid (2007).

To produce an acceptable efficiency, the heat in the turbine exhaust system can be partially recovered and used to preheat the turbine air supply before it enters the combustor, using an air-to-air heat exchanger called a recuperative process. This allows the net cycle efficiency to be increased to as much as 30% while the average net efficiency of a cycle without recuperation is in the region of 17% (Rodgers *et al*., 2001). A precondition for recuperative heat transfer is that the exhaust gas is at a higher temperature than the compressed air (Kautz & Hansen, 2007).

As with gas turbines, the maximum net power provided by a microturbine is limited by the temperature threshold of the materials used in manufacturing the turbine. Nascimento *et al*. (2014) cite the two main factors affecting the performance of microturbines to be the component efficiencies and the gas temperature at the turbine inlet, whereas Saravanamuttoo *et al*. (2009) add a third factor, namely the compressor pressure ratio, while also claiming that the overall efficiency of the gas turbine is primarily dependent on this third factor. The higher the values of all three these factors, the better the performance of the overall system will be.

2.3.2 Previous studies on biomass-fuelled Externally Fired Gas Turbines

Being able to process a wide variety of fuels, including those with suboptimal combustion properties, EFGT is considered to be a promising option for small- to medium-scale plant sizes. This section will summarise some of the studies conducted on EFGT cycles in the micro range and also look at some cases in detail.

Literature on EFGT cycles in the range of this study is extremely scarce, whereas it is abundantly available in the range of 50kW and upward.

2.3.2.1 Thermodynamic simulation of a multi-step externally fired gas turbine powered by biomass (Durante *et al.*, 2017)

Durante *et al.* (2017) developed a thermodynamic model for a realistic Brayton cycle, working as an EFGT fuelled with biomass. The model incorporates a high-temperature heat exchanger and an arbitrary number of turbines and compressors, with the corresponding number of intercoolers and reheaters. It considers irreversibilities such as non-isentropic compressions and expansions, and pressure losses in heat input and release. Their study presents a valuable overview of the different cycle configurations and its performance with regard to certain parameters since it incorporates the simple configuration as well as more complex models.

Durante *et al.* (2017) investigated the influence of two parameters, the pressure ratio as well as the influence of the fuel moisture, on different cycle configurations. The input parameters of their model were based on the parameters obtained from the data sheet of the Turbec T100 turbine.

Durante *et al.* (2017) show curves on the dependence of thermal efficiency and power output with the overall pressure ratio for several plant configurations with a variable number of compression/expansion stages.

The pressure ratio is one of the basic design parameters influencing the Brayton cycle performance. The EFGT plant performance was computed as a function of pressure ratio for different configurations. The different configurations are defined as follows, according to Horlock's notation (Horlock, 2003):

- CT - Single-step plant with one compressor and one turbine.
- CICT - Two compressors, one intercooler, and one turbine.
- CTBT - One compressor and two turbines with an intermediate burner.
- CICTBT - Two compressors with intercooling, and two turbines with reheating.

Pressure ratio was varied from 2 to 16 and eucalyptus wood was taken as fuel with 25% moisture on dry basis. The air mass flow was set to 1.0 kg/s, the ambient temperature to 300 K and the turbine inlet temperature to 1273 K. All other parameters, such as compressors and turbine isentropic efficiencies are the same as that for the Turbec T100 turbine.

Figure 2-2 and Figure 2-3 respectively show the power output and cycle efficiency for each of the four different plant layouts.

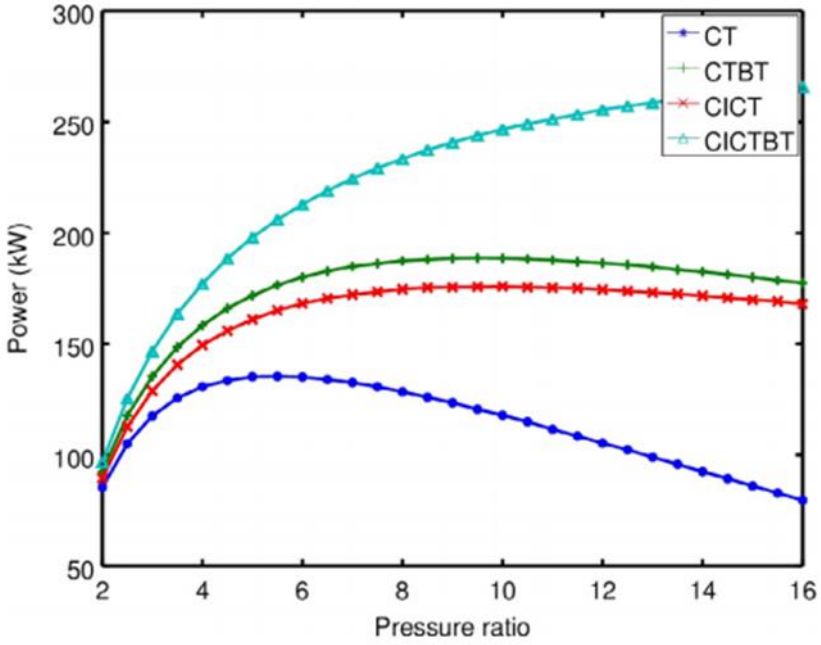

Figure 2-2: Evolution of power output with increasing pressure ratio (Durante *et al.*, 2017).

In Table 2-1 the maximum power output at corresponding pressure ratios for all four configurations are listed alongside its corresponding pressure ratio, $r_{c,max\,P}$, at which the maximum power is achieved.

Table 2-1: Maximum power output at corresponding pressure ratios (Durante *et al.*, 2017).

Configuration	$r_{c,max\,P}$	P_{max} (kW)
CT	5.5	136
CTBT	9.5	189
CICT	10.0	176
CICTBT	>16	>266

From the table above it is evident that the compressor pressure ratio for the simple configuration is relatively lower than that of the more complex models at which point it reaches P_{max}.

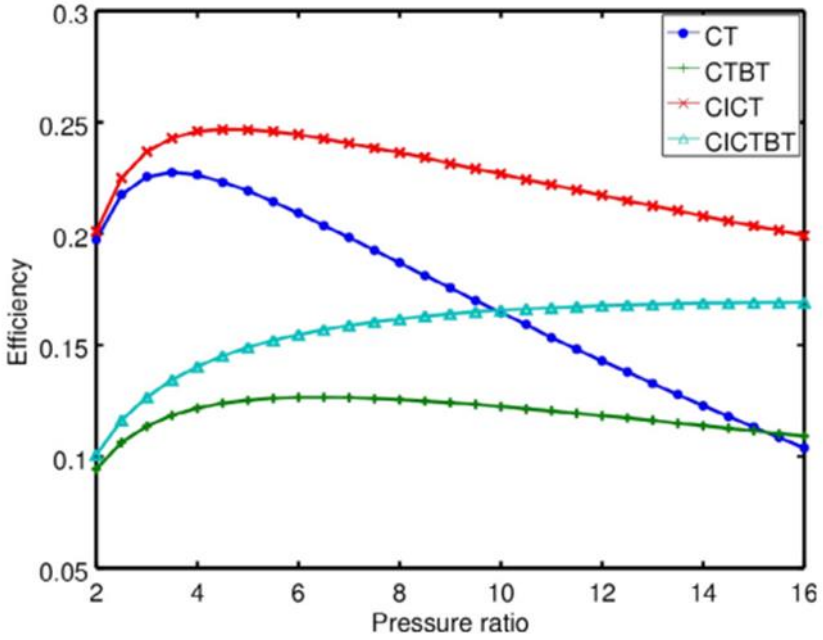

Figure 2-3: Evolution of cycle efficiency with increasing pressure ratio (Durante *et al*., 2017).

In Table 2-2 the maximum efficiency, η_{max}, for all four configurations are listed alongside its corresponding pressure ratio, $r_{c,max\,\eta}$, at which the maximum efficiency is achieved.

Table 2-2: Maximum power output at corresponding pressure ratios (Durante *et al*., 2017).

Configuration	$r_{c,max\,\eta}$	η_{max}
CT	3.5	0.23
CTBT	6.0	0.13
CICT	4.5	0.25
CICTBT	16.0	0.17

For a single step plant layout fuelled with eucalyptus wood an efficiency of 23% is predicted, whereas, for a configuration with two compressors and one turbine, efficiency increases to 25%. It is remarkable that the latter also leads to a 29% increase in power output.

Furthermore, Durante *et al.* (2017) also analysed the influence of fuel moisture in the case of eucalyptus wood biomass and claims that the cycle net power output is independent of fuel moisture if ambient and turbine inlet temperatures, as well as the air mass flow rates, are fixed. On the contrary, fuel consumption and efficiency are sensitive to moisture. With increasing moisture, a larger fuel mass rate is required to keep the turbine inlet temperature at the desired value, because less useful energy is contained in the fuel per unit mass.

The influence of fuel moisture on fuel consumption, efficiency, exhaust gas temperature and the adiabatic flame temperature was investigated. They found that fuel consumption and exhaust gas temperature increase linearly as the fuel moisture content increases. The opposite linear effect on cycle efficiency and adiabatic flame temperature resulted in fuels containing higher moisture content.

The moisture of biomass has a clear influence on fuel consumption, efficiency, and exhaust gas temperature. For instance, a decrease of moisture from 50% d.b. to 0% can lead to an increase in efficiency of between 8% and 14%, depending on the particular plant layout.

2.3.2.2 Determination of Optimized Parameters for the Flexible Operation of a Biomass-Fueled, Micro-scale Externally Fired Gas Turbine (EFGT) (Bdour *et al*., 2016)

The study of Bdour *et al*. (2016) will be discussed extensively and in great detail, since this was the smallest EFGT system found in literature that revealed detailed results and relates to the purpose of this study. Bdour *et al*. (2016) modelled a micro-scale EFGT as a decentralized power plant, within the range of 15 kW_{th}, using olive residues as a fuel source. It was modelled using Aspen Plus 8.6 software with the aim of providing a technical analysis for such a plant. Optimized parameters for pressure ratio and turbine air-mass flow have been mapped for several loads to provide information for process control. For all cases, the mechanical output, efficiency curves, and the compressor work (back-work) ratio have been calculated.

Methodology followed by Bdour et al. (2016)

For the model, a 15 kW_{th} with an electrical output of between 1.5 and 3 kW_{el} EFGT cycle was suggested in order to illustrate the idea of decentralized power generation from olive waste. As mentioned above, Aspen Plus 8.6 was used to not only simulate the complete EFTG cycle as shown in Figure 2-4, but also calculate the stoichiometric combustion equation for a complete combustion analysis of the system.

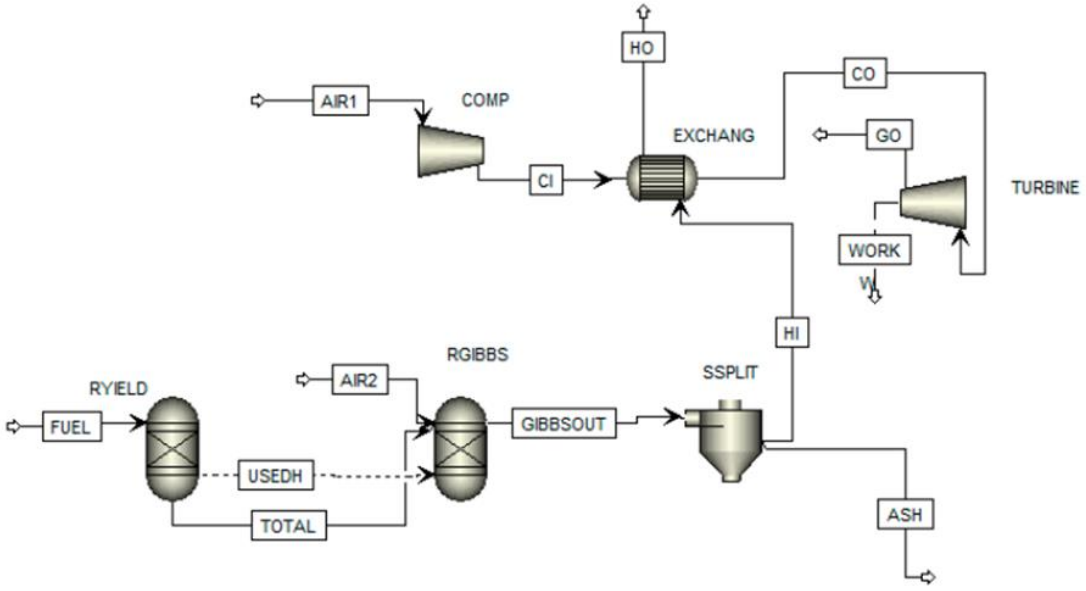

Figure 2-4: Combustion model in Aspen Plus (Bdour *et al.*, 2016).

To study the cycle's behaviour for different operational cases, it was necessary to first develop a reference base case. Table 2-3: Reference base case simulation parameters (Bdour *et al.*, 2016) displays the parameters for the base case.

Table 2-3: Reference base case simulation parameters (Bdour *et al.*, 2016).

General Parameters	
Ambient temperature	300 K
Operating pressure	4 bar
Air-mass flow rate	0.017 kg/s
Thermal power input	15 kW
Compressor isentropic efficiency	0.78
Turbine isentropic efficiency	0.82
Electrical generator efficiency	0.90
Temperature difference of heat exchanger terminals (HED)	20 K

Results and discussion by Bdour et al. (2016)

The results obtained from their study showed that for the base case scenario of Table 2-3, the compressor consumes 3.2 kW_m (mechanical power) while the gas turbine delivers 4.9 kW_m, resulting in 1.7 kW_m generated from the cycle configuration. The generated power is a direct function of the pressure variation and the combustion temperature.

After depicting the power output against an increasing pressure ratio, the researchers did the same for a variating air mass flow through the turbine, keeping the operating pressure constant at 4 bar.

Figure 2-5 shows that the maximum power net output is found for a 0.017 kg/s air-mass flow rate through the turbine.

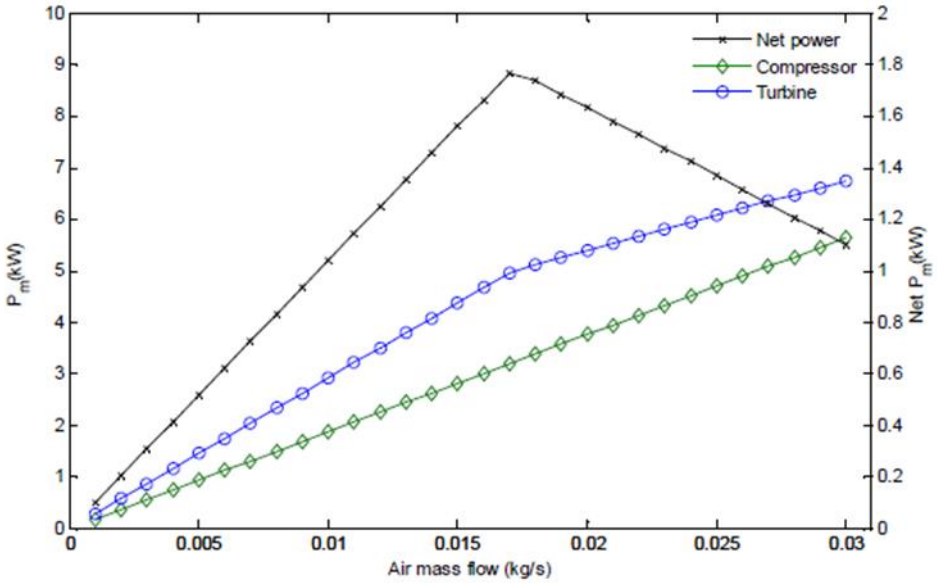

Figure 2-5: Compressor, turbine and net output power as a function of turbine air-mass flow rate (Bdour *et al*., 2016).

Bdour *et al*. (2016) analysed this further and showed that the electrical efficiency is highly affected by the turbine inlet temperatures as shown in Figure 2-6. While for 1060 K it reaches 10% at 4 bar, it is significantly lower at turbine inlet temperatures of 938 K and 988 K.

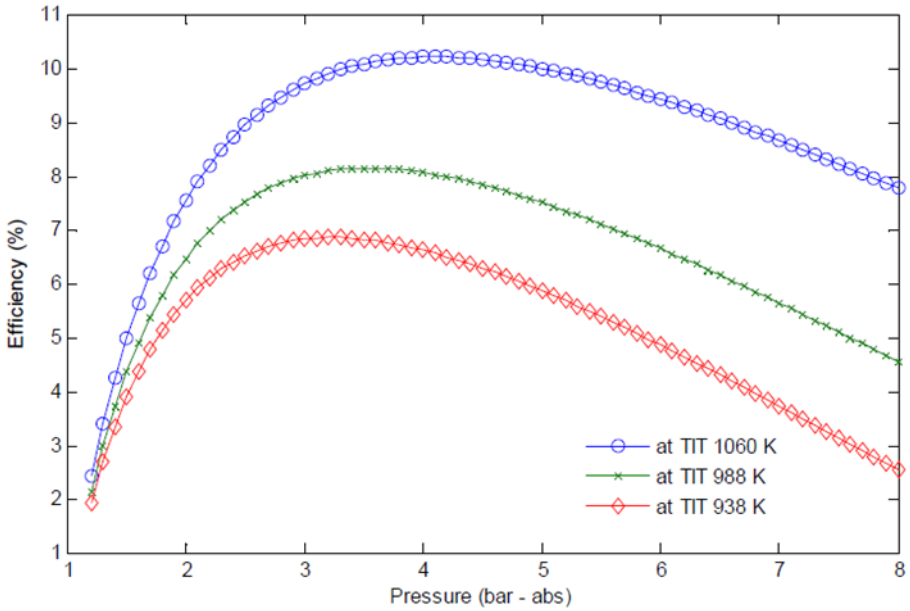

Figure 2-6: Electrical efficiency as a function of pressure at selected turbine inlet temperature (TIT) at 20 K HED (Bdour et al., 2016).

Furthermore, Bdour *et al*. (2016) performed an analysis by using the built-in sensitivity tool of Aspen to do an optimization of the process. At each flue gas temperature, the air mass flow rate was varied within a range from 0.001 to 0.03 kg/s in steps of 0.001 kg/s and the pressure was simultaneously varied within the range of 1.4 to 8 bar (abs.) in steps of 0.3 bar**.** At the same time, the analysis considered the maximum net output power from the cycle and then registered both the pressure and mass flow rate, and so on, until about 1850 K flue gas temperature.

For the analysis outlined above it was concluded that at low turbine inlet temperature values, it is necessary to keep a low pressure and a high mass flow rate. This is explained by the compressor power consumption, which depends on the operating pressure of the cycle.

The results of the study conducted by Bdour *et al.* (2016) show that a plant has an electrical efficiency of between 5% and 17% is realizable. This variation in efficiency is due to the investigation being performed for several combustion temperatures, power output and varying heat exchanger temperatures and heat transfer efficiencies. The efficiency can be improved when using a more efficient compressor and gas turbine set, in addition to the potential implementation of waste heat recovery. The turbine inlet temperature is a dominant factor in terms of the electrical efficiency, so higher temperature values in combustion flue gas could provide a more efficient operation.

The study by Bdour et al. (2016) was chosen for the comparison against the EES model to be developed for the current study (verification of the model is discussed in Chapter 4) based on its size, simplicity and availability of operating conditions.

2.3.2.3 Other studies on micro-scaled biomass-fuelled EFGT cycles

Most of the biomass-fuelled EFGT cycles found in literature classified as micro-scaled is still quite large in comparison to the model being introduced in this study, with the study presented by Bdour *et al.* (2016) being an exception.

Kautz & Hansen (2007) investigated the advantage of utilizing waste heat from the turbine in a recuperative process to increase the efficiency of the cycle and reduce fuel consumption. In the recuperative gas turbine heat from the hot turbine exhaust gas is transferred to the colder compressed air in a heat exchanger between compressor and combustor. The EFGT has the thermodynamic advantage of the preheated air and that the combustion gases do not pass through the turbine. However, the heat can also be provided by placing the combustor in the hot exhaust-air stream from the turbine, as shown in Figure 2-7.

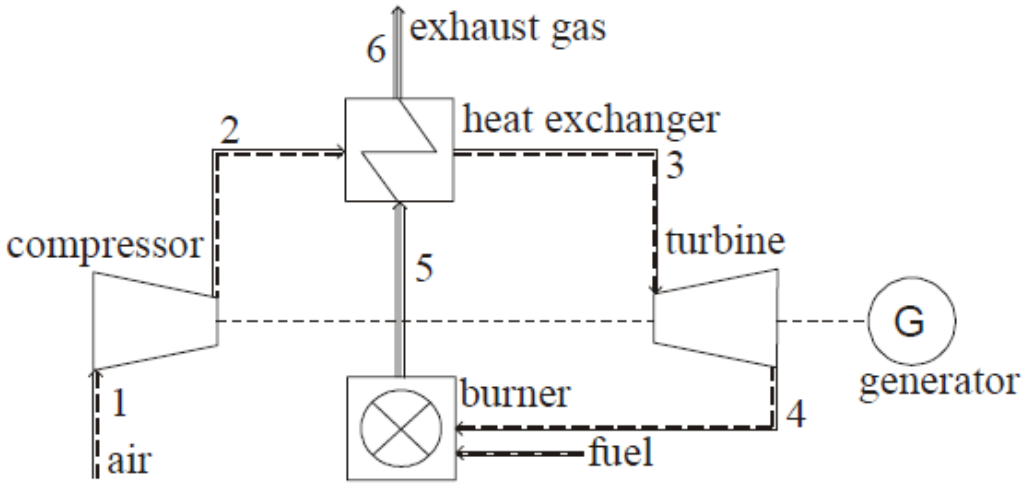

Figure 2-7: EFGT with combustor in the exhaust-air stream of the turbine (Kautz & Hansen, 2007).

Kautz & Hansen (2007) went one step further by stating that in an indirectly heated gas turbine any heat at a sufficiently high temperature can be used and they found solar energy to be a possible heat source. In a solar thermal-electric system the EFGT has the same role as the Stirling engine. The solar heat from the collector is focussed on a hot air heat exchanger and either alone or together with a backup fuel, serves as the energy input to the gas turbine process. This innovative system is shown in Figure 2-8. For smaller power units parabolic or dish collectors

would be suitable whereas for larger units solar towers are more appropriate. With biofuels to make-up for solar deficiencies and the diurnal variation, the system would rely fully on renewable energy resources.

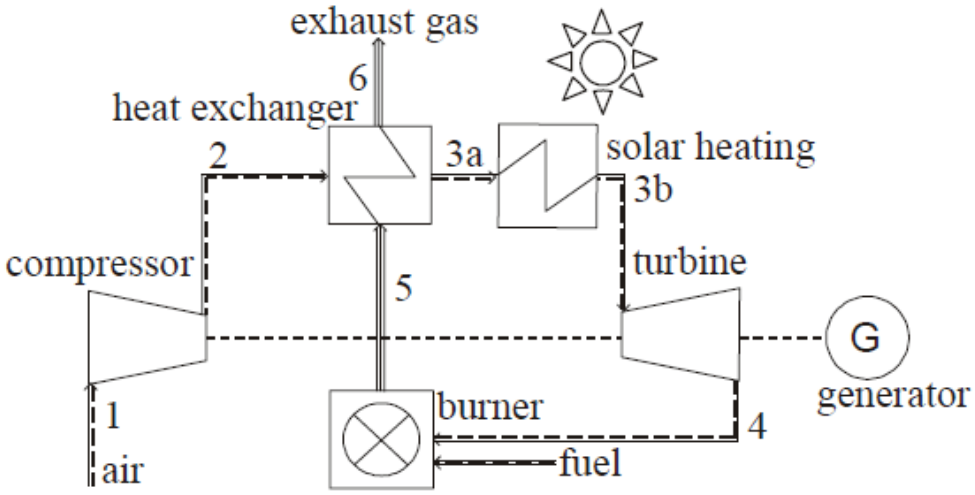

Figure 2-8: Simplified diagram of an EFGT with solar-energy input (Kautz & Hansen, 2007).

Cocco *et al.* (2006) evaluated the performance of a small scale (about 100 kW_e), externally fired gas turbine fuelled by residual biomass and integrated with a biomass dryer. The hot air expands in the turbine and then feeds the biomass furnace. The exhaust waste heat is recovered by drying the raw biomass in a rotary dryer and, in case, in a low temperature heat exchanger for hot water production. The system is shown in

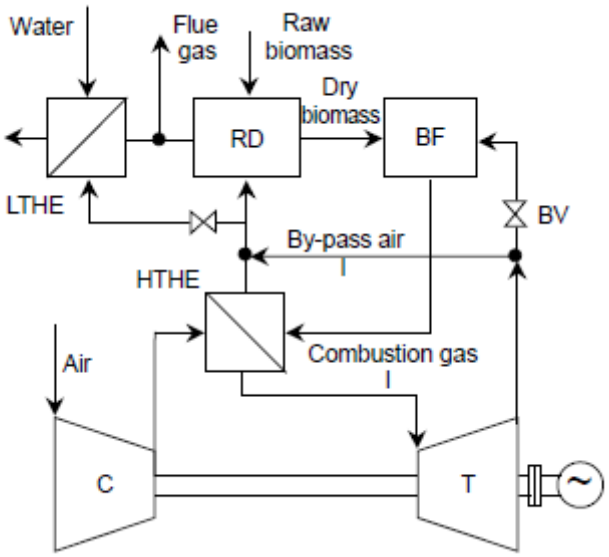

Figure 2-9: Simplified scheme of the EFGT power plant integrated with a biomass rotary dryer (Cocco *et al.* 2006).

A parametric analysis was conducted in order to evaluate the influence of the most important operating parameters, such as the pressure ratio, the turbine inlet temperature, the temperature difference in the heat exchanger and the biomass moisture content. They claim that the use of dry biomass and recovered heat allows efficiency values of about 22–33% to be obtained, depending on the turbine inlet temperature assumed for the different EFGT configurations. Moreover, since the rotary dryer is able to dry more biomass (about 3.5–4.0 times) than they need, the integration of the EFGT power plant with the biomass dryer allows a very flexible operation to be achieved, particularly in the presence of a seasonal heat power demand and/or other external biomass uses.

Brayton Energy (2019) designed and built an intercooled recuperated gas turbine with two operating points. Brayton's design entails a two-stage centrifugal compressor with a 1.2 MW two stage axial turbine combined with an intercooled externally fired recuperated system. To effectively achieve direct biomass combustion in a gas turbine, Brayton's approach burns the solid fuel at atmospheric pressure in the turbine exhaust, thereby preventing erosion in the turbine section, and simplifying the fuel delivery system. The high-temperature reaction zone provides complete combustion and low emission levels. The layout of their design is shown in Figure 2-10.

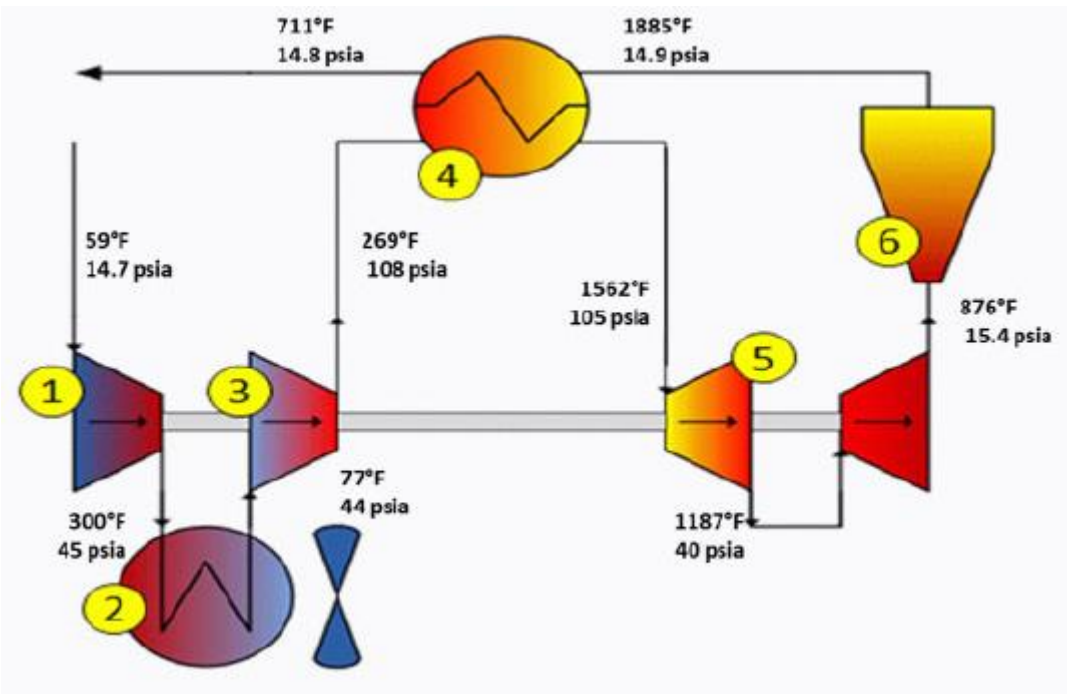

Figure 2-10: An intercooled recuperated gas turbine (Brayton Energy, 2019).

The intercooled recuperated gas turbine by Brayton Energy is much larger than the unit under consideration for this study, but its cycle configuration and operation approach is worth noting. The gas turbine delivers 1.2 MW_e fuelled by natural gas or liquid fuel with an efficiency of 40%, while delivering 900 kW_e when fuelled by back-heated solid biomass with an efficiency of 24% (Brayton Energy, 2019).

A summarised overview of some other existing research on EFGT is given in Table 2-4. The table presents some of the key input parameters used in each study (turbine inlet temperature, pressure ratio and type of fuel) as well as the power output and efficiency achieved by the cycle.

Table 2-4: Overview of previous studies on biomass-fuelled EFGT.

Study conducted by:	Turbine Inlet Temp.	Pressure Ratio	Fuel	Power	Efficiency
	[K]	[-]	[-]	[kW] (Electric)	[%]
Al-Attab and Zainal, 2015	1073	4.5	Biomass	50	15%
Pantaleo *et al*., 2013	1173	n/a	Biomass	66	19%
Kautz and Hansen, 2007	1173	2-8	Biomass (gasification)	100	16% and 30% with recuperator
Al-Attab and Zainal , 2010	967	n/a	Biomass (gasifier)	57 (Thermal)	n/a
Cocco *et al., 2006*	1223	3.5	Residual biomass	100	22%–33% using drier
Vera *et al*., 2011		2–6	Olive tree prunings and leaves	30	19.1%
Datta *et al*., 2010	1050–1350	2–8	Biomass (gasifier)	100	16%–34% (Thermal)
De Mello and Monterio, 2012	1223	4.5	Biomass	100	20%–30%

2.3.3 Commercially available micro-turbine power units

Commercially a variety of micro biogas turbine generators are available in terms of scale and configuration. Most of these available units rely on direct/internal combustion of fuels such as biogas, natural gas or liquid fuels. Capstone and MTT are companies which specialise in these type of units.

MTT (2018) have commercialised recuperated micro gas turbines for micro CHP systems. The MTT recuperated gas turbine design is based on low-cost high-performance micro turbomachinery technology suitable for efficient gas turbine cycles in the 4 kW electrical power output range. With a recuperator, a large portion of the exhaust gas heat is recovered and electrical efficiency levels beyond 20% can be realized.

One of these developments by MTT is the EnerTwin. The EnerTwin is a micro-CHP system (Combined Heat and Power) where a boiler and a small power plant are combined in a single robust and sustainable device. The core of the EnerTwin is a recuperated micro gas turbine, fuelled by natural gas, that drives a generator. The microturbine, based on existing turbocharger components from the automotive industry, delivers 3.2 kW electrical power and 15.6 kW thermal power for heating and the production of hot water (MTT, 2018). The component configuration of the EnerTwin is shown in Figure 2-11.

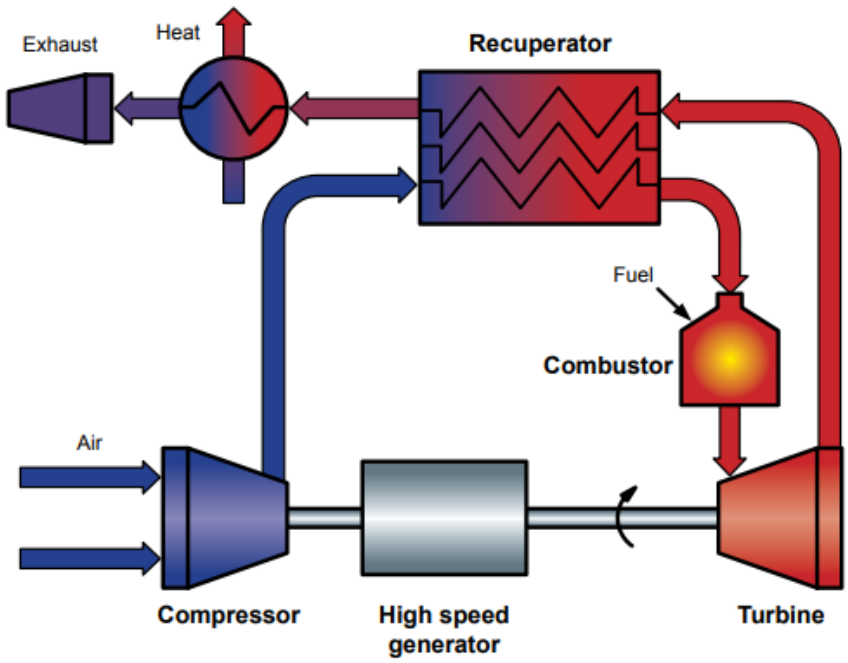

Figure 2-11: MTT EnerTwin recuperated microturbine in a CHP configuration (MTT, 2018).

Capstone (2019) has a 30 kW_e microturbine generating reliable electricity from high-pressure natural gas, liquid fuels or biogas. The system has an efficiency of 26% (LHV). The Capstone C30 has the same cycle configuration and basic operation as the MTT EnerTwin. Figure 2-12 shows the engine components of the Capstone C30 Microturbine.

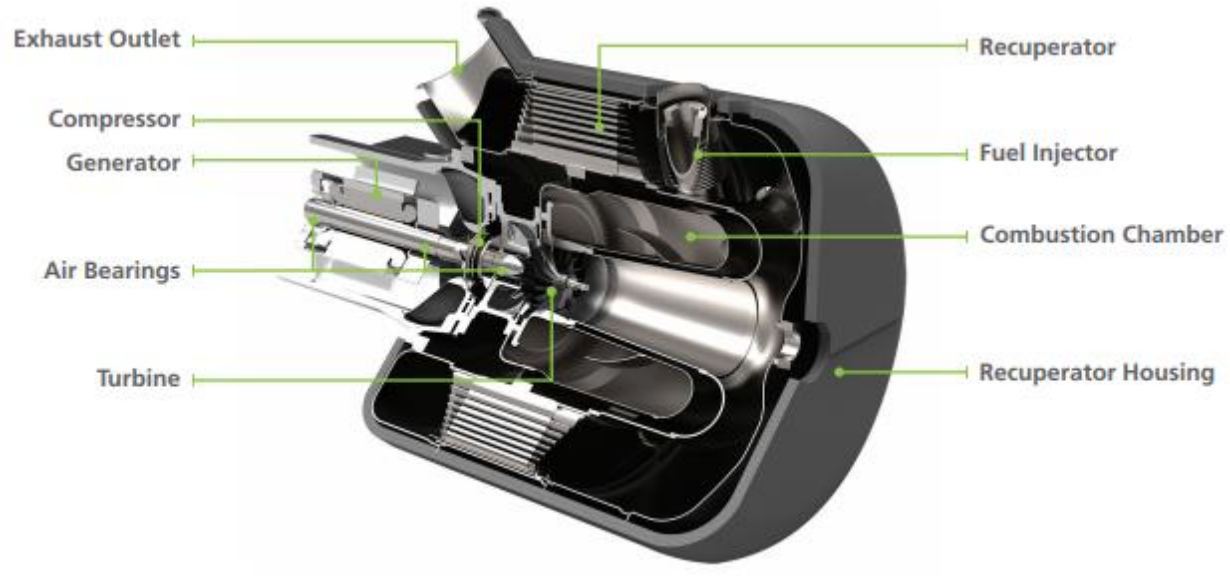

Figure 2-12: Capstone C30 Microturbine (Capstone, 2019)

Since both the above-mentioned microturbines by Capstone and MTT are directly fired and fuelled by “clean” fuels, it falls outside the scope of the current study. But this shows that microturbine units are commercially available and used on a residential and industrial level.

Micro EFGTs are not as commonly commercially available such as the micro DFGTs, although off-the-shelf EFGT units are available. Ansaldo Energia (2019) has an EFGT unit available known as the AE-T100E, which much larger than the unit under consideration. The system has been designed to combine all the advantages of a micro gas turbine with the opportunity to exploit different energy sources as, for instance, biomass burner or solar concentrator. The system is composed by an external boiler that uses a high-temperature heat exchanger to transfer the thermal energy to a micro gas turbine, that operates in an open Brayton cycle, incorporating a single stage centrifugal compressor and a single stage radial turbine, placed on a single shaft. The use of an external boiler allows obtaining the thermal energy required to operate the gas turbine from the combustion of different sources of biomass. Due to the split-up between combustion and evolving fluid (air), this system allows the use of solid fuels/waste fuels otherwise not usable in small size plants based on gas turbines (Ansaldo Energia, 2019).

The AE-T100E has a maximum rated electrical output of 75 kW_e, a maximum TIT of 830˚C and an electrical efficiency determined by the external heat source. Low maintenance requirements, with service intervals of 6,000 operating hours, makes this power generation system extremely attractive and competitive when compared to more conventional solutions (Ansaldo Energia, 2019).

2.3.4 Conclusion

It can be concluded that turbine inlet temperatures for EFTGs can be as high as 1350 K and pressure ratio ranges between 2 and 8 in a single stage. The maximum net power provided by a microturbine is limited by the temperature that the turbine materials can support. Consequently, the three main factors affecting the performance of microturbines are component efficiency, the gas temperature at the turbine inlet and the pressure ratio of the system. Heat recovery allows the net cycle efficiency to be increased to as much as 30% while the average net efficiency of microturbines with no heat recovery is in the region of 17%.

The literature shows that multiple configurations, very simple to very complex, have been researched and investigated in terms of performance, components and operating conditions. Heat recovery can be incorporated for different applications depending on the need. Applications such as drying fuel, pre-heating fuel, pre-heating compressed air or even water or space heating.

In Chapter 3 the cycle development and evaluation methodology of the simulation models will be discussed. Furthermore, the fundamental thermodynamic equations used in the simulations are explained for each of the components and the practicality and choice of components are discussed.

CHAPTER 3

CYCLE DEVELOPMENT AND THEORETICAL BACKGROUND

CHAPTER 3:

CYCLE DEVELOPMENT AND THEORETICAL BACKGROUND

3.1 Introduction

In order to develop EFGT simulation models, it is important to fully understand the theory and fundamental principles governing such a cycle. Firstly, the cycle development and simulation process will be discussed per configuration in terms of analysis, methodology and component layouts. Secondly, each component will be described in terms of the function it fulfils within the cycle as well as its governing equations and calculations leading up to the overall cycle efficiency. Within each component section, a practical discussion will follow regarding the component choice, size, operating properties and availability of components suitable for the micro-scale EFGTs evaluated in this study.

3.2 Cycle Development

Since the focus of the study is based on the evaluation of micro-scale EFGTs for rural applications, the configuration should be kept simple and the number of components should be limited to avoid practical and maintenance issues. Therefore, for the purpose of this dissertation only the following cycles will be considered:

- A simple EFGT cycle.
- An EFGT cycle incorporating heat recovery.
- A simple EFGT cycle with pre-cooled air.
- An EFGT cycle with pre-cooled air incorporating heat recovery.

The simple cycle and the heat recovery cycle are common configurations for micro-scaled EFGTs found in literature. The pre-cooled cycles, however, serve as a unique contribution to evaluate the potential improvement of the simple EFGT and the EFGT with heat recovery especially for applications situated in region known for higher ambient temperatures. The aim of the pre-cooled cycle will be to decrease the temperature of the inlet air to the compressor and therefore decreasing the work needed by the compressor.

3.2.1 The simple EFGT cycle

The simple EFGT cycle shown in Figure 3-1 consists of an air filter, a compressor, an atmospheric combustion chamber (open to the atmosphere) with an integrated high-temperature heat exchanger and a turbine. The numbers (1-9) defines the different working points within the cycle. Each point represents thermodynamic properties of the working fluid (air) at a critical point (component inlet or outlet) within the cycle. These points will be used to set up the simulation model and evaluate certain parameters in the cycle.

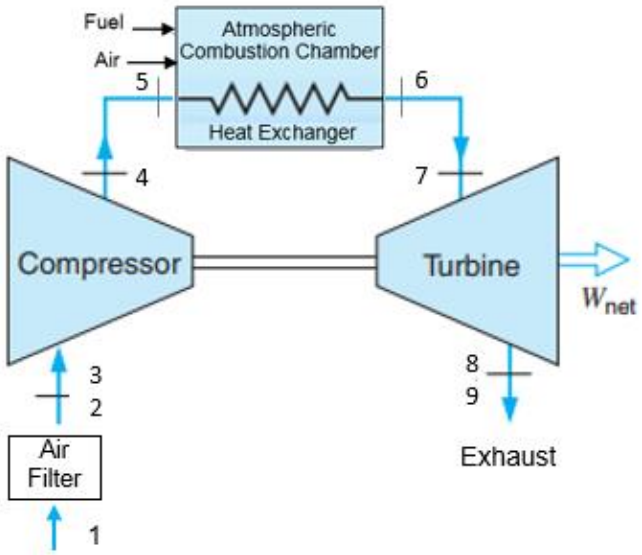

Figure 3-1: Schematic of the simple EFGT cycle (Adapted from Borgnakke & Sonntag, 2009).

The working points for the simple EFGT cycle are defined as follows:

- Working point 1 ~ Inlet air at ambient conditions.
- Working point 2 ~ Air filter Outlet.
- Working point 3 ~ Compressor Inlet.
- Working point 4 ~ Compressor Outlet.
- Working point 5 ~ Heat Exchanger Inlet.
- Working point 6 ~ Heat Exchanger Outlet.
- Working point 7 ~ Turbine Inlet.
- Working point 8 ~ Turbine Outlet.
- Working point 9 ~ Exhaust air.

For the simple cycle, a reference case will be set up with specific input parameters to establish basic results that can be used comparatively to gain insight on the effect of various parameters.

The following will be simulated to investigate the effect of the respective turbine inlet temperature (TIT):

- The effect of adjusting the turbine inlet temperature based on the reference case input parameters.
- The effect of turbine inlet temperature at a fixed net power output is used to evaluate other cycle parameters such as different heat input values and mass flow of the air.

3.2.2 The EFGT cycle incorporating heat recovery

By adding an additional heat exchanger between the compressor and combustion chamber within the simple EFGT cycle, the heat recovery cycle is formed and configured as shown in Figure 3-2. Waste heat from the turbine outlet is used to preheat the compressed air passing through the heat exchanger within the atmospheric combustion chamber.

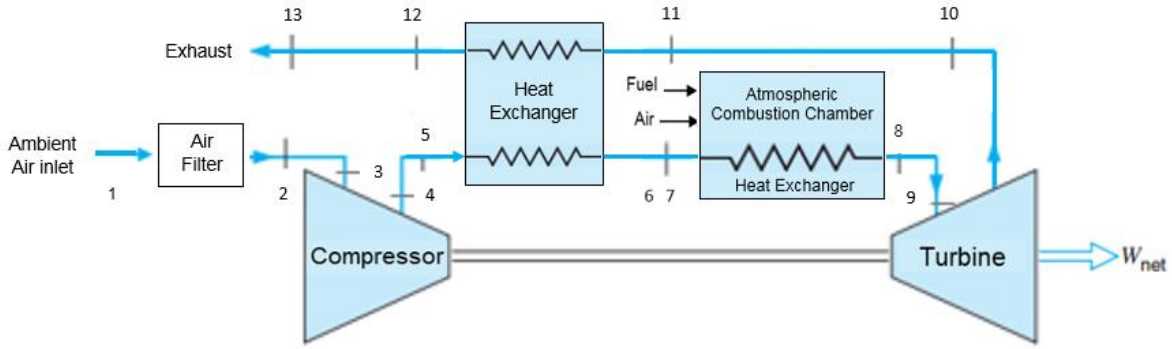

Figure 3-2: Schematic of the EFGT cycle configuration with waste heat recovery (Adapted from Borgnakke & Sonntag, 2009).

The working points for the heat recovery EFGT cycle are defined as follows:

- Working point 1 ~ Inlet air at ambient conditions/Air filter inlet.
- Working point 2 ~ Air filter outlet.
- Working point 3 ~ Compressor inlet.
- Working point 4 ~ Compressor outlet.
- Working point 5 ~ Heat exchanger primary side inlet (Heat Recovery).
- Working point 6 ~ Heat exchanger primary side outlet (Heat Recovery).
- Working point 7 ~ Heat Exchanger inlet (Combustion chamber).

- Working point 8 ~ Heat Exchanger outlet (Combustion chamber).
- Working point 9 ~ Turbine inlet.
- Working point 10 ~ Turbine outlet.
- Working point 11 ~ Heat exchanger secondary side inlet (Heat Recovery).
- Working point 12 ~ Heat exchanger secondary side outlet (Heat Recovery).
- Working point 13 ~ Exhaust air.

The results generated by the heat recovery cycle will be compared with that of the simple cycle to investigate the improvement. Furthermore, the heat recovery cycle will be analysed in terms of operating conditions by adjusting the mass flow and combustion heat to further improve the cycle.

3.2.3 The pre-cooled air EFGT cycles

The working points for both the simple pre-cooled and the pre-cooled heat recovery cycles will remain the same except for the addition of working point 01 which refers to air at ambient conditions at the inlet of the pre-cooling unit and working point 1 will now represent the air properties at the outlet of the pre-cooler, which is also the air filter inlet. The configurations for the simple pre-cooled EFGT cycle and pre-cooled heat recovery EFGT cycle are shown in Figure 3-3 and Figure 3-4 respectively.

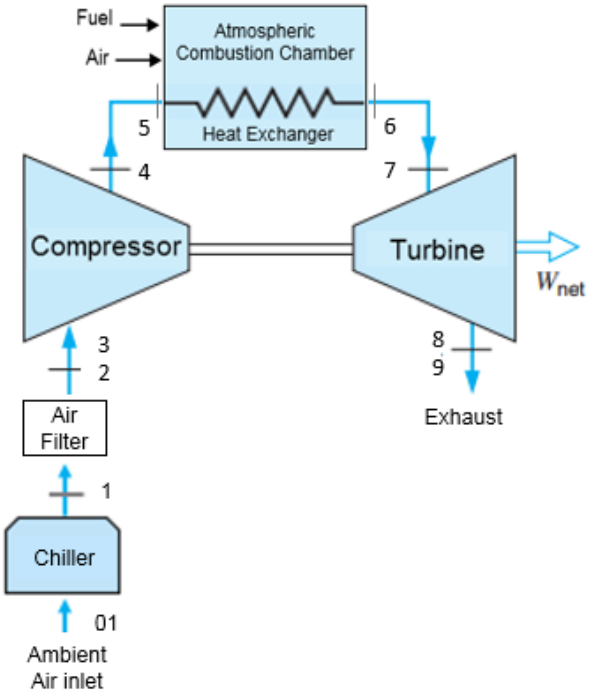

Figure 3-3: Schematic of the pre-cooled air simple EFGT cycle configuration (Adapted from Borgnakke & Sonntag, 2009).

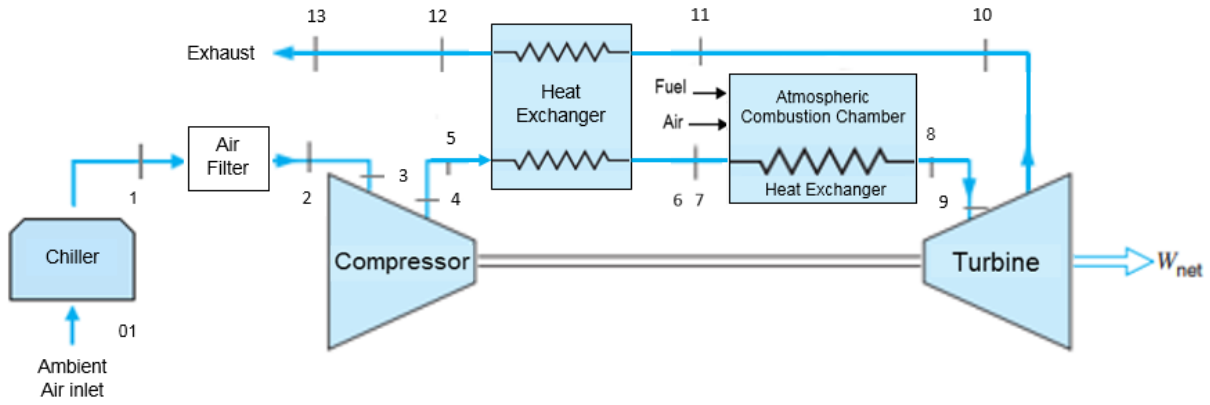

Figure 3-4: Schematic of the pre-cooled air heat recovery EFGT cycle configuration (Adapted from Borgnakke & Sonntag, 2009).

The performance of the pre-cooled cycle simulations will be investigated based on the prescribed parameters for the simple and heat recovery cycles respectively. Furthermore, the simulations will be set up to investigate the following:

- The effect of the temperature difference initiated by the pre-cooling unit.
- The effect of the COP of the chilling unit.

The four cycles will be compared to one another in terms of performance although the heat recovery and pre-cooled cycles are based on the simple cycle with additional components to improve the performance of the simple cycle. Each cycle will also be investigated individually to establish the effect of different operating conditions.

3.3 Cycle Components

In this section, the cycle components are discussed in terms of practical implementation, function, component characteristic and availability as well as governing equations used to simulate each of the components incorporated within the different simulation models.

The following components will be discussed:

- Air filter and ducting.
- Compressor.
- Combustion chamber.
- Turbine.
- Heat exchanger.

- Chilling unit.
- The externally fired gas turbine cycle.

3.3.1 Air inlet filter and ducting

The purpose of the inlet duct is to provide clean and unrestricted air flow to the system. Clean and undisturbed inlet air flow extends the life of the compressor and all other components in the system by preventing erosion, corrosion, etc.

The selection and operation of an inlet filtration system are highly dependent on the environment where the gas turbine is operating. The contaminant present in the ambient air will dictate the type filters that are used. It is important to quantify what type and size of contaminants are present in order to correctly select the filters to be used. Temporary and seasonal variations must also be considered for the inlet filtration system.

Usually, the inlet duct assembly is designed and produced as a separate system rather than as part of the design and production of the gas turbine engine.

Filtration systems are distinctively classified as high, medium, or low-velocity systems. The velocity of the filtration system is defined as the actual volumetric air flow divided by the total filter face area. Low-velocity systems are the standard on land-based applications and have airflow at less than 2.54 m/s at the filter face. (Wilcox *et al*., 2012)

Wilcox *et al*. (2012) further claim that typical pressure losses in gas turbine inlet filtration systems can range from 500 to 1500 Pa. However, a higher pressure loss occurs with a more efficient filter due to airflow restrictions. Pressure loss has a direct impact on the gas turbine performance, as it causes a reduction in compressor inlet pressure. For the compressor to overcome the inlet system losses, the gas turbine will consume more fuel, and it also has a reduced power output.

Based on the fact that this is only a conceptual design, the calculations for this section will be done according to Rousseau's (2013) method discussed below. Therefore specific air filter and duct sizes will not be calculated, but it will rely on applicable empirical values used in previous studies.

A simplified schematic for a pipe (liquid flow) or duct (gas flow) is shown in Figure 3-5.

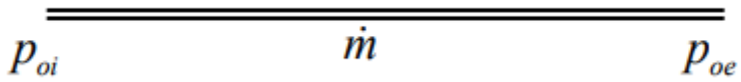

Figure 3-5: Simple duct schematic (Rousseau, 2013).

Rousseau (2013) explains that the simplest way to estimate the pressure drop in a duct is to write it as a fraction (*α*) of the average pressure level namely

$$\Delta p_{0L} = \alpha \left(\frac{p_{0i}+p_{0e}}{2}\right) \quad \text{(E.3.1)}$$

Where:

Δp_{0L} = Pressure drop

α = Fraction

p_{0i} = Initial pressure

p_{0e} = End pressure

With the typical pressure losses mentioned by Wilcox *et al*. (2012) being only 0.5% to 1.5% of the ambient pressure used in the study (1 bar), the fraction value (*α*) of 0.01 is used for the calculation of the pressure drop through the air filter.

Within this simulation model, it will be assumed that all ducting is properly insulated and the pressure loss through the ducting will be considerably less than that through the air filter, therefore the fraction value (α) of 0.00005 is used for the calculation based on the pressure drop in the heat exchanger. Further explanation follows in the heat exchanger section.

3.3.2 Compressor

There are two main types of compressors: axial and centrifugal. Each compressor is assumed to contain a certain number of stages of rotor blades and stator vanes. In an axial flow compressor, each stage incrementally boosts the pressure from the previous stage. A single stage of compression consists of a set of rotor blades attached to a rotating disk, followed by stator vanes attached to a stationary ring.

Due to the divergent duct shape, the stator vanes slow the air, converting the accelerated velocity to a higher static pressure. The vanes ought to be positioned at an angle such that the exiting air is directed into the rotor blades of the next stage at the most efficient angle. This process ought to be repeated for each stage of the compressor. In addition to the number of stages of blades and vanes, the compressor also incorporates the inlet guide vanes and the outlet guide vanes. These vanes, located at the inlet and outlet of the compressor, direct air to the first stage compressor blades at the "best" angle. The outlet guide vanes "straighten" the air to provide the combustor with the proper airflow direction. Axial flow compressor is more popular due to high delivery capacity, high compression ratio due to many stages, high efficiencies of 85% to 90%, and low cross-sectional area. Its drawback is its sophisticated design and appreciable length due to a large number of stages, the narrow operating range for good efficiency, higher weight and cost.

For an application such as this micro-scale EFGT, a centrifugal compressor is a more practical choice since centrifugal compressors are known for being used in gas turbines such as turboshaft, turboprop, microturbines and auxiliary power units. A centrifugal/radial-flow type compressor mainly consists of stationary inlet casing, rotating impeller and the stationary diffuser. Pressure ratios of 4:1 are typical in a single stage, and ratios of 7:1 are possible if exotic material is used for impeller manufacture. The best efficiencies are 3% to 4% below those obtainable from an axial flow compressor designed for the same duty (Sayers, 1990). Figure 3-6 shows a centrifugal compressor with its stationary inlet casing, rotating impeller and the stationary diffuser.

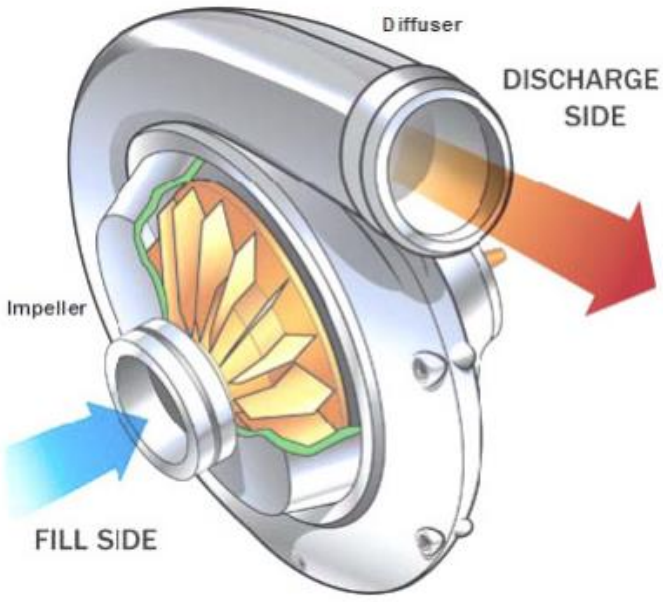

Figure 3-6: Centrifugal compressor (Howstuffworks, 2006).

Advantages of centrifugal compressors are that it is simple in design, easy to manufacture, rugged in construction and less costly. Due to its short length higher pressure ratios are attained in a single stage. They are more reliable in operation under all operating conditions and less susceptible to the effects of deposits left on and fouling of the flow path.

Al-attab & Zainal (2006) did a study into a simple EFGT cycle, incorporating a turbocharger for a truck, in the same power output range as this study presents. The turbo compressor had a pressure ratio of 3 and the air flow rate was low, between 0.09 to 0.12 kg/s, because the turbocharger is not expected to run in full speed because of the low turbine inlet temperatures. They found that the compressor power to be around 18 kW.

Automotive turbochargers by Garrett (2018) are available in applicable sizes ranging from 25 kW to 100 kW, with rotational speeds ranging from 2000 rpm to 6000 rpm. These turbochargers are typically used for vehicles like the TATA Ace, Chevrolet Aveo, Cruze and Captiva. These turbochargers are commercially available and will be suitable to use within an EFGT cycle such as this study presents (Data sheets available in Appendix B).

A schematic of a compressor is presented in Figure 3-7.

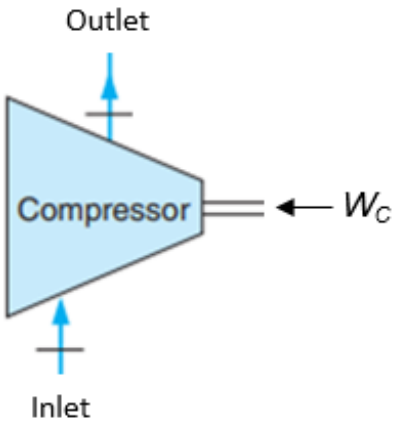

Figure 3-7: Simple schematic of a compressor (Adapted from Borgnakke & Sonntag, 2009).

The pressure ratio for a compressor is defined as:

$$PR = \frac{Outlet\ Pressure}{Inlet\ Pressure} \qquad \text{(E.3.2)}$$

For the compressor simulation the mass flow rate can be determined, but also the work on the working fluid by using the following equation:

$$W_C = \dot{m}\,(h_{out} - h_{in}) = \dot{m}\,Cp(T_{out} - T_{in}) \quad \text{(E.3.3)}$$

Where:

W_C = Work done on compressor per unit mass

$\dot{m}$ = Mass flow rate of air

h_{in} = Specific enthalpy of inlet fluid

h_{out} = Specific enthalpy of outlet fluid

And,

C_P = Heat constant at constant pressure

T_{in} = Temperature of inlet fluid

T_{out} = Temperature of outlet fluid

The outlet enthalpy can be calculated by using the equation for isentropic efficiency, defined as:

$$\eta_C = \frac{(h_{out,is} - h_{in})}{(h_{out} - h_{in})} \quad \text{(E.3.4)}$$

Where:

η_C = Compressor isentropic efficiency

$h_{out,is}$ = Isentropic enthalpy of outlet fluid

h_{in} = Specific enthalpy of inlet fluid

h_{out} = Specific enthalpy of outlet fluid

(Borgnakke & Sonntag, 2009).

3.3.3 Combustion Chamber

The combustion section has the function of controlling the burning of large amounts of fuel and to release the heat in a manner that the air is expanded and accelerated to provide a smooth and stable stream of uniformly-heated gas at all starting and operating conditions

Once the air flows through the compressor, the compressed air passes through a high-temperature heat exchanger where the compressed air is heated by solid fuel burnt in the atmospheric combustor. A schematic of the process is shown in Figure 3-8.

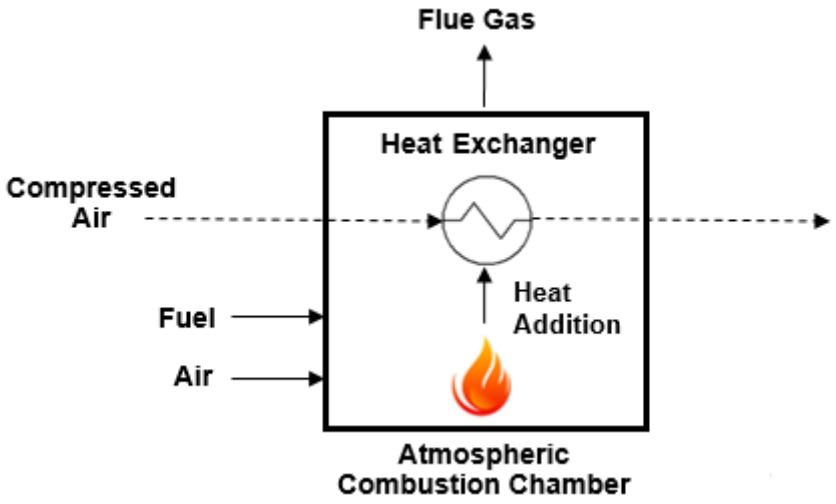

Figure 3-8: Schematic of an atmospheric combustion chamber and heat exchanger.

The heat added to the system can be calculated as follows:

$$Q_{CC} = \dot{m}\,(h_{out} - h_{in}) = \dot{m}\,Cp(T_{out} - T_{in}) \qquad \text{(E.3.5)}$$

Where,

Q_{CC}	=	Heat added by the combustion chamber
$\dot{m}$	=	Mass flow rate of air
h_{in}	=	Specific enthalpy of inlet fluid
h_{out}	=	Specific enthalpy of outlet fluid

And,

C_P	=	Heat constant at constant pressure
T_{in}	=	Temperature of inlet fluid
h_{out}	=	Temperature of outlet fluid

(Borgnakke & Sonntag, 2009)

The fuel, air and flue gas will not form part of the simulation since the flue gas will not be used for heat recovery whatsoever. The simulations will focus only on the air stream and the heat added to it. Therefore the equation above (E.3.5) will be used to calculate the heat added to the air stream in the heat exchanger. A temperature difference will be used to accommodate the heat

loss between the combustion chamber and the heat exchanger. This will be discussed in the heat exchanger section.

In order to calculate the combustion heat available it is important to know the chemical composition of the fuel being burnt and to calculate the adiabatic flame temperature for the specific fuel.

According to Chen (2014), cell walls of plants consist mainly of three organic compounds: cellulose, hemicellulose and lignin. Besides these three components, natural lignocellulosic materials contain a small amount of pectin, nitrogenous compounds, and the secret ash. For instance, the element content of wood is about 50 % carbon, 6 % hydrogen, 44 % oxygen, and 0.05–0.4 % nitrogen.

Cellulose is the main component of the plant cell. It is a natural high molecular polymer composed of glucose residues. It is the most abundant renewable organic resource on earth and is widespread in higher plants, bacteria, marine algae, and other biomass. Although the structure and composition of the cell walls of plants vary widely, the cellulose content usually accounts for 35–50 % of dry weight and, peculiarly, almost 100 % for cotton.

Based on this, cellulose will be used to represent the chemical composition of the solid fuel used in the study. It mainly contains carbon (44.44 %), hydrogen (6.17 %), and oxygen (49.39 %). The chemical formula of cellulose is ($C_6H_{10}O_5$) (Chen, 2014).

The combustion equation and adiabatic flame temperature will be calculated based on the chemical composition of cellulose as a fuel source. Borgnakke & Sonntag (2009) states that for a given fuel and given pressure and temperature of the reactants, in this case, 25℃ and 1 bar, the maximum adiabatic flame temperature that can be achieved is with a stoichiometric mixture. The adiabatic flame temperature can be controlled by the amount of excess air that is used. This is especially important for gas turbines, where the maximum permissible temperature is determined by metallurgical considerations in the turbine and close control of the temperature of the products is essential.

The adiabatic combustion process for cellulose at 25℃ is shown in Figure 3-9.

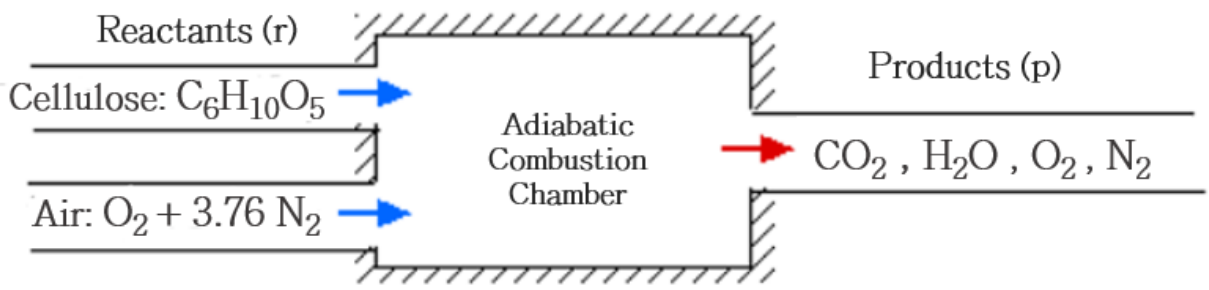

Figure 3-9: Adiabatic combustion process of cellulose.

The chemical reaction for the combustion of cellulose is given below.

$$C_6H_{10}O_5 + (6)(3)(O_2 + 3.76\ N_2) \longrightarrow 6\ CO_2 + 5\ H_2O + 12\ O_2 + 67.68\ N_2$$

Bdour *et al.* (2016) used an air-to-fuel ratio (AFR) of 20 for their base case and McAllister *et al. (*2011) claims that for most hydrocarbon fuels, 14 to 20 kg of air is needed for complete combustion of 1 kg of fuel.

Therefore, the air-to-fuel ratio for the complete combustion of cellulose is calculated with 200% excess air. This resulted in an AFR value of 15.3 kg of air per 1 kg fuel, which falls within the relevant AFR range provided by McAllister *et al. (*2011).

The calculation is done as follows:

$$AFR = \frac{m_{air}}{m_{fuel}} = \frac{18(4.76)(29)}{1(162)} = 15.3\left[\frac{kg_{air}}{kg_{fuel}}\right]$$

Where, m_{air} and m_{fuel} respectively represents the mass of the air and fuel present in the chemical reaction.

The molecular mass and enthalpy of formation (h^0_f) of the elements taking part in the chemical reaction above are listed in Table 3-1.

Table 3-1: Enthalpy of formation and molecular mass of different chemical elements (Borgnakke & Sonntag, 2009).

Element	Formula	Molecular Mass	h^o_f
		[kg/kmol]	[kJ/kmol]
Cellulose	$C_6H_{10}O_5$	162	-936 000
Carbon	C	12	-
Oxygen	O	16	-
Nitrogen	N	14	-
Hydrogen	H	1	-
Oxygen	O_2	32	-
Nitrogen	N_2	28	-
Carbon dioxide	CO_2	44	-393 522
Water Vapour	H_2O	18	-241 826
Air	(O_2 + 3.76 N_2)	29	-

To calculate the adiabatic flame temperature for the combustion of cellulose.

An adiabatic process occurs without heat transfer (Q_{CV}) between the thermodynamic system and its surroundings,

$$Q_{CV} = 0$$

Therefore, there is no difference in enthalpy between the initial and final states of the combustion process. The enthalpy of the products (H_P) is equal to that of the reactants (H_R).

$$H_R = H_P$$

And this can also be written in a summation form,

$$\sum_R n_i \left(h_f^0 + \Delta h\right)_i = \sum_P n_e \left(h_f^0 + \Delta h\right)_e \qquad \text{(E.3.6)}$$

where Δh_e refers to each constituent in the products at the adiabatic flame temperature and Δh_i to the reactants at its reference state.

Substituting the listed values from Table 3-1 into E.3.6 gives,

$$(-936\,000)_{C_6H_{10}O_5} = 6(-393\,522 + \Delta h)_{CO_2} + 5(-241\,826 + \Delta h)_{H_2O} + 12(\Delta h)_{O_2} + 67.68(\Delta h)_{N_2}$$

Which the simplifies to,

$$6\,(\Delta h)_{CO_2} + 5\,(\Delta h)_{H_2O} + 12\,(\Delta h)_{O_2} + 67{,}68\,(\Delta h)_{N_2} = -\,2\,634\,262\ [\tfrac{kJ}{kmol}Fuel]$$

Thus, summing all the moles of the products, it quantifies to

$$N_{Total} = 6 + 5 + 12 + 67{,}68 = 90.68\ kmol\ products$$

The adiabatic flame temperature for cellulose is calculated using the following:

$$N_{Total} * M_{Air} * C_{p,Air}(T_{Adiabatic} - 298\ K) = (-2\,634\,262\,)\ [kJ/kmol\ Fuel]$$

$$T_{Adiabatic} = 1\,175.2\ K$$

$$= 902\ ℃$$

Based on the temperature yield by the combustion of cellulose with the considerations, such as metallurgical constraints, included from literature, using 600°C to 800°C as TIT's for this simulation is justified. In an EFGT study by Al-attab & Zainal (2006) stated that the turbocharger engine is much simpler than the reciprocating engine and it deals with a pure air with maximum 700°C turbine inlet temperature which leads to fewer maintenance requirements, so the unit is expected to be more suitable for the rural applications, which also supports the temperature choice used in this study.

Most EFGT cycles include a combustion air fan or flue gas fan. This study does not include this since the air mass flow through the combustor is not simulated and only uses empirical values to calculate the heat transfer in the combustion chamber. But to elaborate on the matter, the auxiliary power used by induced draft fans forms about 0.9 to 1.18 % of the total energy generation (Mandi & Yaragatti, 2014). So, in this case, the fan suited for the application would consume about 50 W. But since the flue gasses and combustion chamber itself is not simulated in detail, the ~1% reduction in total energy will be neglected.

3.3.4 Turbine

The turbine converts gaseous energy into mechanical energy by expanding the hot, high-pressure gasses to a lower temperature and pressure. The turbine converts the gaseous energy of the hot air, from the heat exchanger receiving heat from the combustor, into mechanical energy to drive

the compressor and other driven accessories such as an electric generator, typically a turbocharger-type unit.

A turbocharger consists of a compressor wheel and exhaust gas turbine wheel coupled together by a solid shaft and that is used to boost the intake air pressure of an internal combustion engine. In most automotive-type applications, both the compressor and turbine wheel are of the radial flow type. Some applications, such as medium- and low- speed diesel engines, can use an axial flow turbine wheel instead of a radial flow turbine (Schwitzer, 1991). The flow of gases through a typical turbocharger with a radial flow compressor and turbine wheels is shown in Figure 3-10.

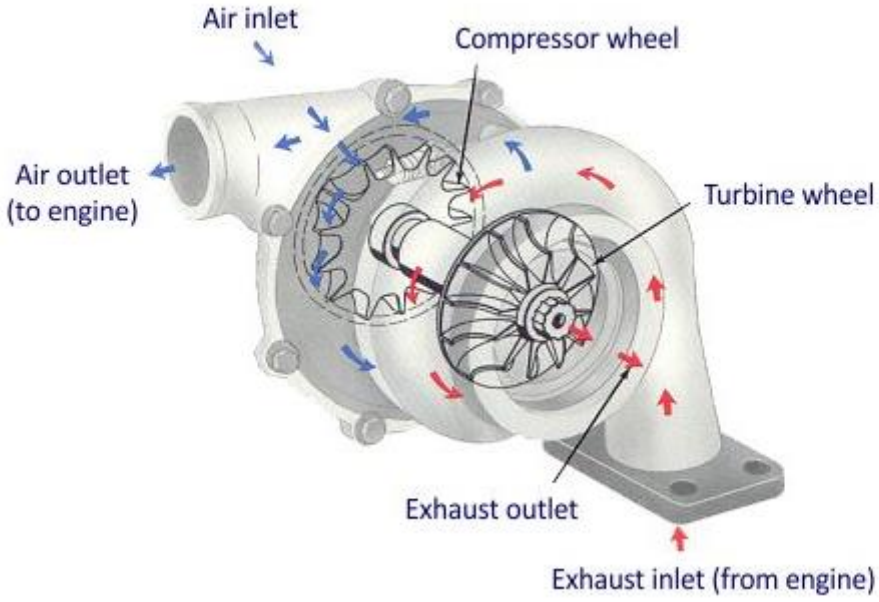

Figure 3-10: Turbocharger construction and flow of gases (Schwitzer, 1991).

The advantage of the radial flow turbine is that it maintains a relatively high expansion ratio (approaching 4:1) and is also more robust and cheaper to be manufactured (Zhu *et al.*, 2015)

Each stage of the turbine consists of a row of stationary vanes followed by a row of rotating blades. This is the reverse of the order in the compressor. In the compressor, energy is added to the gas by the rotor blades and then converted to static pressure by the stator vanes. In the turbine, the stator vanes increase gas velocity, and then the rotor blades extract energy.

The efficiency of the turbine is determined by how well it extracts mechanical energy from the hot air. Since air flows from a high-pressure zone to a low-pressure zone, this task is accomplished

fairly easily. The use of properly positioned air-foils allows a smooth flow and expansion of gases through the blades and vanes of the turbine.

A schematic of a simplified turbine is presented in Figure 3-11.

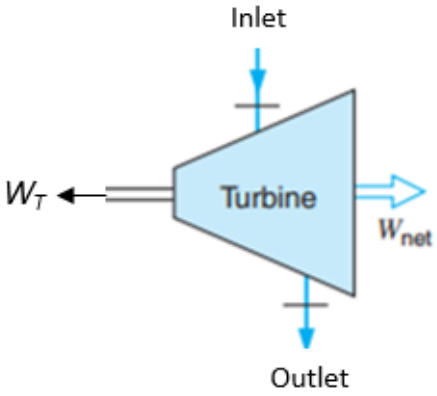

Figure 3-11: Simplified schematic of a simplified turbine (Adapted from Borgnakke & Sonntag, 2009).

The mechanical work delivered by the turbine can be calculated as follows:

$$W_T = \dot{m}\,(h_{in} - h_{out}) = \dot{m}\,Cp(T_{in} - T_{out}) \qquad \text{(E.3.7)}$$

Where,

W_T = Work supplied by the turbine per unit mass

and the other terms remain the same as for the compressor, but in this case, it is based on the inlet and outlet conditions of the turbine.

The outlet enthalpy can be calculated by using the equation for isentropic efficiency, defined as:

$$\eta_T = \frac{(h_{in} - h_{out})}{(h_{in} - h_{out,is})} \qquad \text{(E.3.8)}$$

Where,

η_T = Turbine isentropic efficiency

$h_{out,is}$ = Isentropic enthalpy of outlet fluid

h_{in} = Specific enthalpy of inlet fluid

h_{out} = Specific enthalpy of outlet fluid

(Borgnakke & Sonntag, 2009).

There are two options for the power generation set:

- High-speed generator with electronic converting.
- Low-speed generator with a speed reduction gearbox, but it needs periodic maintenance since it has a lubrication system.

According to Vaidya (2010), the best approach in interfacing the high-speed turbine to the generator is to directly couple the two by means of mechanical coupling and exclude the need for gear, belt or other mechanical transmission systems. The generator must be mounted to axially align the shaft centre line with the corresponding centre line of the turbine shaft. This allows the use of a flexible coupling or a quill shaft to drive the generator. The result is a compact generator set with no need for a gear-box that tends to adversely affect reliability as well as cost. The high-speed turbine operates most efficiently at their rated speed which varies with rated power output. Most commercial generator sets operate at a speed of 3,600 rpm (Vaidya, 2010) and based on the size and speed of the turbochargers by Garrett, direct coupling will be possible.

3.3.5 Heat Exchanger

For this simulation model the first heat exchanger will be utilized to transfer the heat from the combustion process to air in the cycle since this heat exchanger forms part of the combustion unit, it will be present in all the cycles simulated in this study. A second heat exchanger will be added for the heat recovery cycle configuration, where the turbine exhaust gasses pass through the heat exchanger to pre-heat the air moving from the compressor to the combustion chamber.

A variety of heat exchangers is available, but not all are suitable for this application. The plate type heat exchangers are very efficient, with a large surface area in a compacted size. However, the small thickness of the plates and narrow passages makes the plate type heat exchanger unsuitable for this case, because of the high temperature levels, fouling and blocking problems. The amount of small particles, ash fraction and tar that are drawn up by air towards the heat exchanger depends mostly on the type of gasifier and biomass fuel used. Even with low tar content produced by the downdraft gasifier, a small fraction of ash can easily be drawn into the heat exchanger passages. If these passages are too narrow and tight, the ash could block some of them. On the other hand, if the passages are too large, the gas flow speed will decrease, causing a reduction in the overall heat transfer.

The regenerator heat exchanger type is also not suitable for an EFTG cycle since there is a chance of mixing between the pure air and exhaust gas as a result of leakages or gases trapped in the switching process. The most suitable type of heat exchanger was found to be the shell-and-tube type as shown in Figure 3-12 (Anheden, 2000).

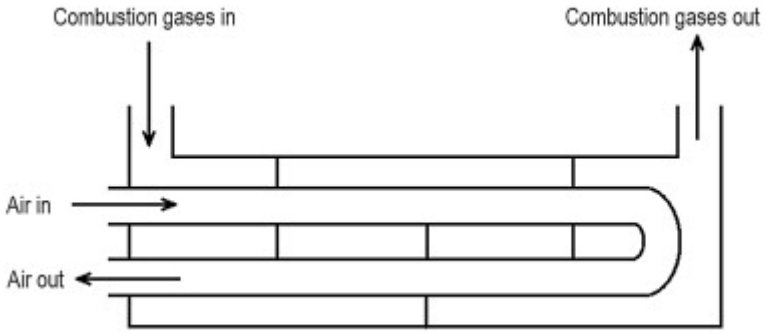

Figure 3-12: Shell-and-tube heat exchanger (Al-attab & Zainal, 2010).

The performance of the externally fired gas turbine unit depends mostly on the design of the high-temperature heat exchanger; the higher the temperature it can handle, the higher the efficiency of the unit. However, since the unit is considered to be a low-cost unit, suitable for a small power generation unit in a rural area, the development cost of the heat exchanger should be considered a major factor.

Ceramic heat exchangers can reach a high turbine inlet temperature, more than 1000°C, with a long operational life, but the development cost of these heat exchangers is very high and requires a long payback period. This option, however, may become economical in the future as developments in ceramic heat exchanger technology result in reduced costs. Metal coatings with ceramic components are a good option for high-temperature heat exchanger technology and can reduce the fabrication cost of the heat exchanger. Nickel-based super alloys allow the turbine inlet temperature to reach 800–825°C (Al-attab & Zainal, 2010). Therefore, based on the TIT range used in this study a metallic heat exchanger can be a suitable choice.

According to Kautz & Hansen (2007), the most important parameter is the temperature difference between the hot and the cold gas. At the hot end of the heat exchanger where the hot gas enters and the heated air exits the temperature difference ranges between 10 and 150 K. Based on this, a heat exchanger terminal difference of 20 K will be assumed for the shell-and-tube this simulation.

As previously stated, this study is conceptually based and therefore a detailed design of the heat exchanger will not be done. Empirical values will be used in the calculations.

A simplified schematic for a simplified heat exchanger with primary and secondary fluids between which there is heat transfer is shown in Figure 3-13.

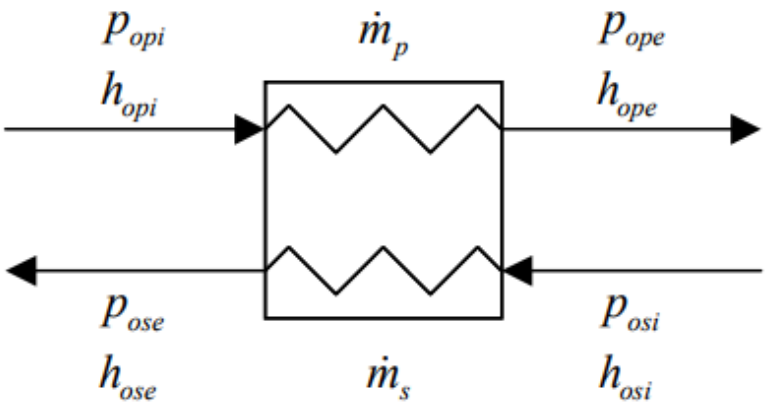

Figure 3-13: Simplified heat exchanger schematic (Rousseau, 2013).

The pressure drop for the respective primary and secondary fluids can be estimated similar to that of a pipe or duct, i.e.

$$\Delta p_{0L} = \alpha \left(\frac{p_{0i}+p_{0e}}{2}\right) \quad \text{(E.3.9)}$$

Bdour *et al*. (2016) claim that a pressure drop occurs through the heat exchanger, reducing the air stream pressure from 4 bar to 3.99995 bar (α = 0.0000125). Based on this the same alpha-value is used for the heat exchanger as for the ducting.

The simplest form used to estimate the heat transfer duty for a generic heat exchanger is to write it as a fraction of the maximum theoretically possible heat transfer (Q_{max}):

$$\dot{Q} = \varepsilon \dot{Q}_{max} \quad \text{(E.3.10)}$$

The value ε is known as the effectiveness of the heat exchanger and can range between zero and unity. The value of ε actually characterises the specific heat exchanger that is being simulated.

The maximum theoretically possible heat transfer between any two fluid streams is written as

$$\dot{Q}_{max} = C_{min}\Delta T_{max} \quad \text{(E.3.11)}$$

with $$C_{min} = \left[\dot{m}C_p\right]$$ (E3.12)

and $$\Delta T_{max} = T_{opi} - T_{osi}$$ (E3.13)

C_{min} is known as the minimum heat capacity which is equal to the minimum value of mass flow rate multiplied by the specific heat capacity of either of the two fluid streams, whereas ΔT_{max} is the maximum possible temperature change that any of the two streams can undergo (Rousseau, 2013).

3.3.6 Pre-cooling unit

The pre-cooling unit was added to see what the effect would be on the overall cycle should the compressor inlet air temperature be lower. Should it have a remarkable impact so that it would justify the additional costs, the addition of the pre-cooling unit should be considered.

The basic operating principals of the pre-cooling system can be based on a vapour-compression refrigeration cycle. Considering the vapour-compression refrigeration cycle displayed in Figure 3-14, its basic principle of operation can be summarised in 4 processes:

Process 1–2: A refrigerant gas at low pressure and temperature is compressed through the compressor to a high pressure and high temperature.

Process 2–3: Heat (Q_H) is rejected in the condenser at constant pressure. As more heat is rejected the refrigerant liquid is sub-cooled. The temperature difference between the saturated liquid point and the outlet of the condenser is referred to as the degree of sub-cool (ΔT_{sub}), usually around 8-10 ºC.

Process 3–4: From the condenser the refrigerant passes through the expansion valve where it is throttled to a low pressure and corresponding low temperature in a constant enthalpy process.

Process 4–1: The refrigerant usually enters the evaporator as a two phase mixture, where heat (Q_L) is picked up from the medium being cooled. After the refrigerant turns into a saturated vapour, it continues to pick up heat and becomes superheated. point. The temperature difference between the outlet of the evaporator and the saturated vapour point is referred to as the degree of superheat (ΔT_{sup}),), usually around 10-12 ºC.

(Rousseau, 2013).

.

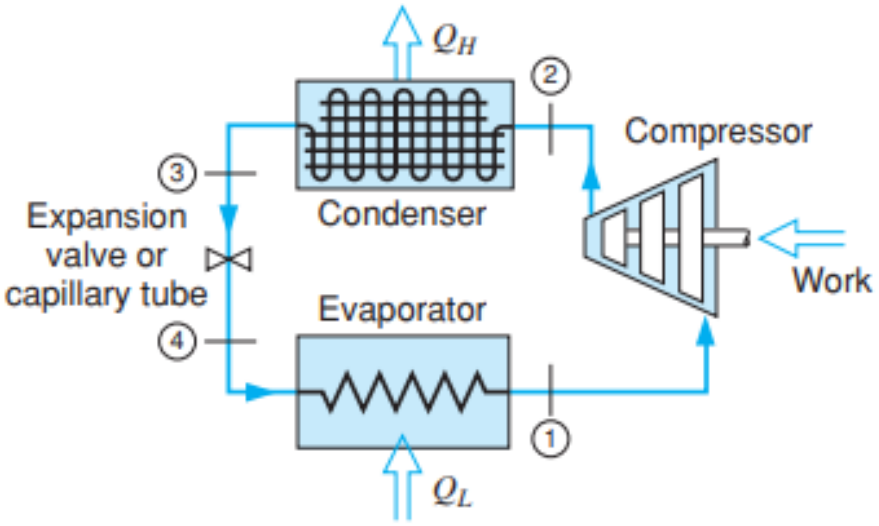

Figure 3-14: Vapor-compression refrigeration cycle (Borgnakke & Sonntag, 2009).

In the case of the actual cycle, irreversibilities and heat transfer occur during the compression process which leads to a change in entropy. Further, pressure losses occur through the condenser and the evaporator as well as heat transfer between the refrigerant and the surroundings.

In order to analyse the performance of a vapour-compression refrigeration cycle it is important to calculate the following thermodynamic properties at each of the four operating points:

P_{1-4} = Pressure

T_{1-4} = Temperature

h_{1-4} = Specific Enthalpy

s_{1-4} = Specific Entropy

The performance of a refrigerant system is expressed in terms of the coefficient of performance (COP). According to Rousseau (2013) typical COP values for refrigeration cycles are between 2 and 3. The COP of the vapour-compression refrigeration cycle involves the net work between the compressor and its cooling effect:

$$COP = \frac{Cooling\ effect}{Net\ Work\ Input} = \frac{Q_L}{W_{compressor}} \qquad \text{(E.3.14)}$$

Where,

$$Q_L = (h_1 - h_4) \qquad \text{(E.3.15)}$$

and

$$W_C = (h_2 - h_1) \quad \text{(E.3.16)}$$

The enthalpy at the compressor outlet (operation point 2) can be calculated by using the equation for isentropic efficiency, defined as:

$$\eta_C = \frac{(h_{2,is} - h_1)}{(h_2 - h_1)} \quad \text{(E.3.17)}$$

Where,

η_C = Compressor isentropic efficiency

$h_{2,is}$ = Isentropic enthalpy of fluid at compressor outlet

h_1 = Specific enthalpy of the fluid at compressor inlet

h_{out} = Specific enthalpy of the fluid at compressor outlet

(Borgnakke & Sonntag, 2009).

The pre-cooling system is also seen as an auxiliary system that needs power to operate. It can either be driven electrically or with a direct mechanical drive from the main shaft. For the purpose of the simulations, it will be driven mechanically with the available work generated by the EFGT, therefore contributing to a reduction in nett power output of the cycle.

3.3.7 The Externally Fired Gas Turbine cycle governing equations

When all the components are combined into a simulation to form a complete EFGT cycle, there are two important cycle defining parameters to be calculated:

- Net work output.
- Cycle efficiency.

The generic equation for solving the nett work output of a cycle is given by

$$W_{NET} = W_{Available} - W_{Required} \quad \text{(E.3.18)}$$

Where the available work is the power generated by the turbine and the work required is the work needed for the compressor and in the case of the pre-cooled cycle, additional compressor work is required for the compressor located in the pre-cooling system.

The cycle efficiency can then be calculated as follows:

$$\eta_{Cycle} = \frac{Net\ Work\ Output}{Heat\ Supplied} = \frac{W_{NET}}{Q_{Supplied}} \quad \text{(E.3.19)}$$

(Botha, 2010).

3.4 Conclusion

All the cycles have been derived and the simulation and evaluation of the different configurations were explained. All the components were thoroughly discussed, in terms of operating conditions, practical implementation, component choice and empirical values used in the simulations of these components were explained. The verification of the simple EFGT cycle will be covered in the next chapter by comparing the results to that of a study published in literature.

CHAPTER 4

MODEL VERIFICATION

CHAPTER 4:

MODEL VERIFICATION

4.1 Introduction

The previous chapter focused on the different cycle configurations and the relevant theoretical background needed for the development of the EFGT cycle. In this chapter, the verification of a simple EFGT model, simulated in EES, is done by comparing its results to the data of a similar study published in literature.

4.2 Verification of the simple micro EFGT cycle

The model verification was done by comparing the results of a simple EFGT cycle modelled in EES (Figure 3-1) to a simple biomass cycle published in literature, by Bdour *et al.* (2016), shown in Figure 4-1. For their model, an EFGT cycle fuelled by olive residue was modelled in Aspen Plus 8.6. Their model included a compressor, an indirect biomass combustion system, a shell-and-tube heat exchanger and a turbine.

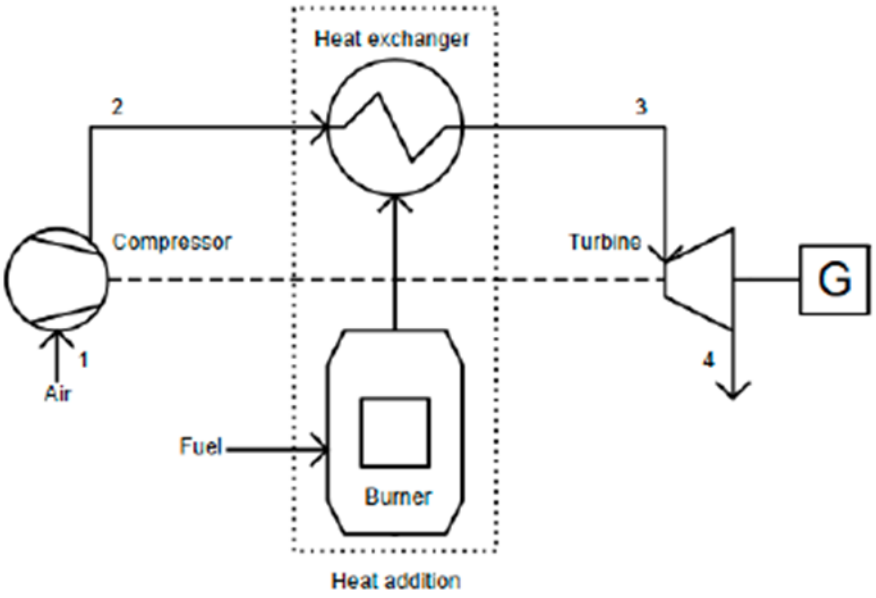

Figure 4-1: Schematic diagram for externally fired gas turbine (EFTG) cycle (Bdour *et al.*, 2016).

In order for Bdour *et al.* (2016) to study the cycle's behaviour for different operational cases, it was necessary to first develop a reference case based on specific general and operational parameters, which was stated within their study. For the verification of the simple EFGT cycle, the same general parameters used by Bdour *et al.* (2016) were used to simulate the simple EFGT in EES. Table 4-1 presents the parameters for the base case used for the model verification.

Table 4-1: Reference case general parameters.

Reference Case: General Parameters		
Parameter	**Value**	**Unit**
Ambient Temperature	300	[K]
Ambient Pressure	1	[bar]
Operating Pressure	4	[bar]
Compressor Pressure Ratio	4	[-]
Air mass flow rate	0.017	[kg/s]
Combustion heat input	10.7	[kW]
Compressor isentropic efficiency	0.78	[-]
Turbine isentropic efficiency	0.82	[-]
Electric generator efficiency	0.9	[-]
Heat Exchanger terminals difference (HED)	20	[K]
Turbine inlet temperature (TIT)	1062	[K]

The reference case presented in literature revealed that the compressor consumed 3.2 kW (mechanical power) while the gas turbine delivers 4.9 kW, resulting in 1.7 kW power generated by the system (Bdour *et al.*, 2016). The verification model is of a smaller scale than the simulation investigated in the current study, therefore the model found in literature is used for the sole purpose of verifying the EES model. The simple model simulated in EES, based on the input values tabulated in Table 4-1, delivered corresponding results, with small differences, in comparison with the Aspen Plus model. These differences can be attributed to different simulation tools using different ways to evaluate thermodynamic properties. The corresponding results are tabulated in Table 4-2, along with the deviation percentage between the values.

Table 4-2: Results obtained by the EES model in comparison with the data found in literature.

Comparative Results

Parameter	From Literature	EES Model	% Deviation
Compressor work	3.2 [kW]	3.192 [kW]	0.250
Turbine work	4.9 [kW]	4.967 [kW]	1.367
Net Power output	1.7 [kW]	1.776 [kW]	4.471

The comparison of the results was found to be within an acceptable deviation percentage of less than 5%. Figure 4-2 and Figure 4-3 are in fair correlation with one another, based on the results generated by EES and those found in literature.

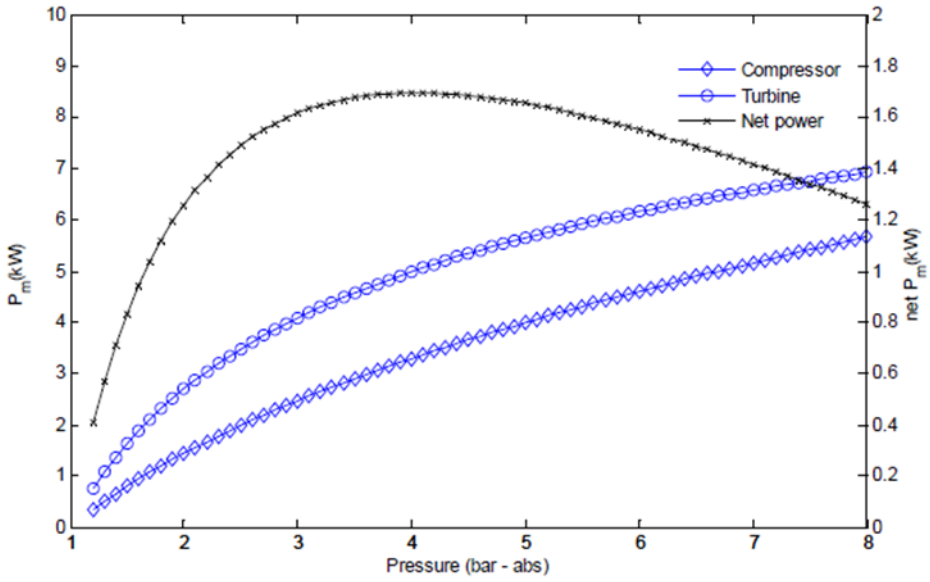

Figure 4-2: Respective power curves plotted against operating pressure (from literature - Bdour *et al.*, 2016)).

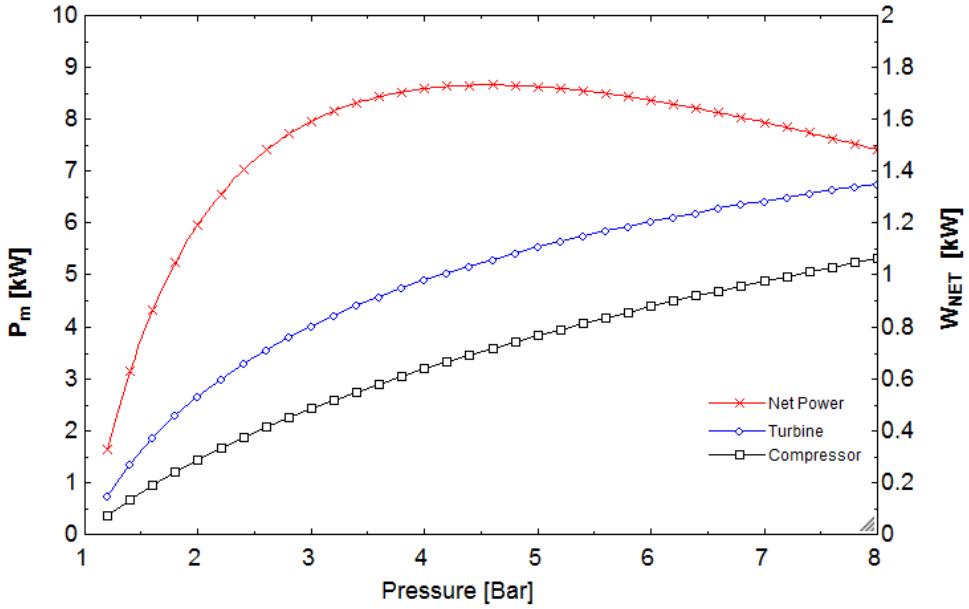

Figure 4-3: Respective power curves plotted against operating pressure (EES model).

From the figures, it is evident that for both cycles, the net power output increases until it reaches a maximum of 1.7 kW at an operating pressure of 4 bar, after which it starts to decay. With these correlating results, it can be concluded that the simple micro EFGT cycle simulated with EES is successfully verified against the results of a similar cycle simulated in Aspen Plus 8.6. Therefore, the results generated from the EES simulations can be deemed verified and trustworthy.

In the next chapter, the simulations and results obtained from the evaluation of the different cycle configurations with a net power output of 5kW are presented and discussed.

CHAPTER 5

RESULTS

CHAPTER 5:

RESULTS

5.1 Introduction

In Chapter 4 the simple EFGT cycle simulated in EES was verified by comparing its results to the data of a similar study published in literature. In this chapter, the approach for investigation and the results for the simple cycle, the heat recovery cycle, the simple pre-cooled cycle and the pre-cooled heat recovery cycle will be presented and discussed accordingly.

5.2 Results for the simple EFGT cycle

5.2.1 The Simple Reference Case

The input parameters for the simple reference case resulting in an electric generation capacity of 5 kW are tabulated in Table 5-1. The parameters were chosen based on standard ambient conditions, 25˚C and 1 bar, component efficiencies and operating parameters are in a similar region of those found in literature and the mass flow was adjusted in EES, using the stated values, in order to result in a 5 kW power output.

Table 5-1: Parameters used for the simple reference case.

Simple Reference Case: Input Parameters		
Parameter	**Value**	**Unit**
Ambient Temperature	25	[˚C]
Ambient Pressure	1	[bar]
Operating Pressure (Bdour *et al*., 2016)	4	[bar]
Air mass flow rate	0.07551	[kg/s]
Compressor isentropic efficiency (Kautz & Hansen, 2007)	0.76	[-]
Turbine isentropic efficiency (Kautz & Hansen, 2007)	0.82	[-]
Turbine inlet temperature (TIT)	700	[˚C]

The reference case was simulated for its specified input parameters listed in Table 5-1 and resulted in a 5 kW net power output, 39.73 kW heat added by the combustion chamber and a cycle efficiency of 12.58% as shown in Table 5-2.

Table 5-2: Results obtained for the simple EFGT cycle reference case.

Results for Simple EFGT Refererence Case	
Parameter	**Value**
Cycle Power Output (W_{NET})	5 kW
Heat addition (Q_{CC})	39.73 kW
Cycle Efficiency (η)	12.58%

5.2.2 Influence of turbine inlet temperature

- **The effect of turbine inlet temperature based on the reference case input parameters.**

The reference case simulation was duplicated for the same input parameters tabulated in Table 5-1, except for turbine inlet temperature. Two additional simulations were done for a TIT of 800˚C and 900˚C respectively, therefore increasing the TIT per simulation by 100˚C increments. Based on the adiabatic flame temperature of the fuel (902˚C) calculated in Chapter 3, a reduction in excess air will increase the AFR, resulting in a higher adiabatic flame temperature, making heat transfer possible for a TIT of 900˚C, therefore the TIT used in the simulations will not exceed 900˚C. The chosen TIT temperatures are very realistic compared to the actual turbine inlet temperatures found in literature.

The results obtained from simulating the simple EFGT cycle reference case for different TITs are tabulated in Table 5-3. The reference case results are included in order to be able to compare the results of the three simulations side by side.

Table 5-3: Results obtained for Simple EFGT Reference Case at different TITs.

Turbine inlet temperature	**700˚C**	**800˚C**	**900˚C**
Cycle Power Output (W_{NET})	5 kW	7.06 kW	9.11 kW
Heat addition (Q_{CC})	39.73 kW	39.73 kW	48.38 kW
Cycle Efficiency (η)	12.58%	12.58%	14.59%

The comparative results for net power output, heat addition and cycle efficiency are illustrated in Figure 5-1, which shows that an increase in TIT improves the performance of the cycle in terms of power output and efficiency. Since the mass flow was kept constant and TIT is dependent on the heat added to the cycle, the heat addition is higher to reach higher TITs, therefore more fuel will be utilised to reach higher TITs.

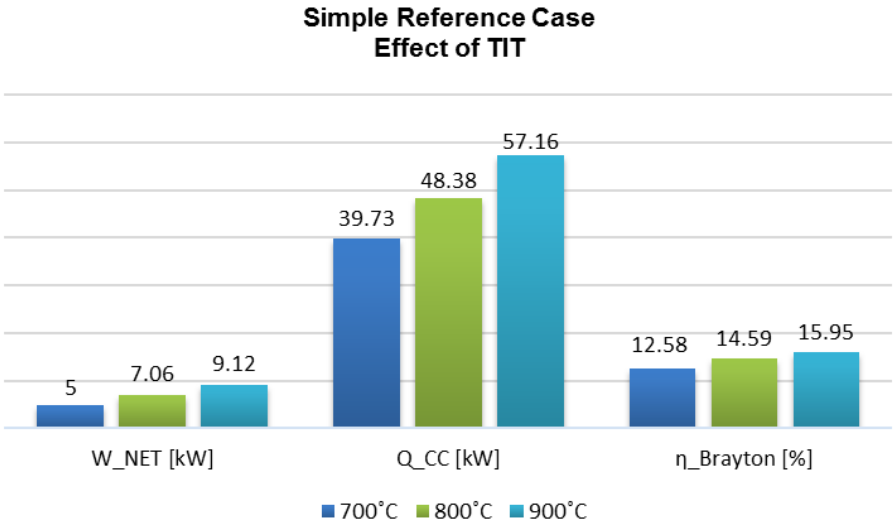

Figure 5-1: Results on the influence of TIT on reference case.

The increase in TIT increases the efficiency of the cycle with more than 3% and the power output with more than 4 kW, but the focus of the study is to maintain a 5 kW power output and improving the efficiency of the cycle.

With this said maintaining a 5 kW power output and not changing any of the component characteristics to improve the cycle, leaves only two variable parameters influencing the performance of the cycle, namely: Mass flow rate and heat input.

The air mass flow rate of the cycle can be varied by using a blower, fan or throttling valve and the heat added to the cycle can be varied by means of varying the amount of fuel (biomass or wood) added to the combustion chamber. The relationship between the two variable parameters should be correct and within an acceptable range in order to deliver the maximum cycle efficiency. Practically a compressor will stall and surge when the mass flow is too low. According to Visser *et al.* (2011), off-the-shelf turbochargers are available with rated air flows down to 30 g/s and for TIT values of 1000˚C, small turbocharger-based micro-turbines are typically rated at 35–45 g/s air flow and heat input for a simple cycle ranges between 35–40 kW.

Based on the values stated above the simple EFGT cycle should produce an electrical output of 5 kW at the maximum efficiency possible within the following constraints:

- The maximum TIT value should not exceed 900˚C.
- The mass flow should be between 35 - 45 g/s.
- The heat input should be between 30–40 kW.

(adapted from Visser *et al.*, 2011)

- **The effect of turbine inlet temperature at a fixed net power output.**

The simple EFGT was simulated for a fixed power output and specific TIT value to evaluate the performance of the cycle in terms of cycle efficiency. In this case mass flow and heat input will be determined by EES based on the fixed input parameters per simulation.

Three simulations were done for a fixed power output of 5 kW at different TITs. The fixed input parameters for each simulation are tabulated in Table 5-4.

Table 5-4: Input parameters for simple EFGT cycle with fixed power output.

Simple EFGT Cycle (Fixed power output)	**Simulation 1**	**Simulation 2**	**Simulation 3**
Turbine inlet temperature	700˚C	800˚C	900˚C
Power output (W_{NET})	5 kW	5 kW	5 kW
Mass flow	Automatically calculated in EES based on fixed inputs		
Heat input	Automatically calculated in EES based on fixed inputs		

Figure 5-2 illustrates the resulting heat input required and cycle efficiency obtained for a fixed power output of 5 kW and respective TIT values.

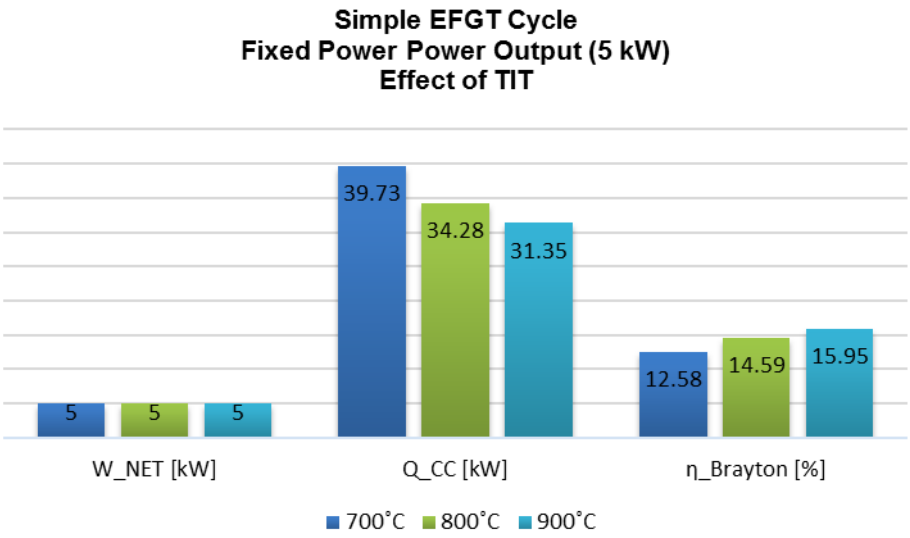

Figure 5-2: Results obtained from the simple cycle simulations with fixed power output.

From the figure, it is evident that the cycle efficiency remained unchanged due to fixed input parameters, whereas the heat input decreased as the TIT per simulation increased. This is not what one would expect for a TIT being increased, but the heat input was one of two parameters being calculated per simulation, governed by the fixed input values. The mass flows calculated per simulation are shown in Table 5-5 which also decreased for simulations at higher TITs.

Table 5-5: Results obtained from the simple cycle simulations with fixed power output.

Power Output	TIT	Heat Supplied	Cycle Efficiency	Air mass flow
5 kW	700˚C	39.73 kW	12.58%	0.07551 kg/s
5 kW	800˚C	34.77 kW	14.59%	0.0535 kg/s
5 kW	900˚C	31.27 kW	15.95%	0.04141 kg/s

The results obtained from the third simulation (TIT of 900˚C and power output 5 kW) falls within the criteria of the constraints, with a cycle efficiency of 15.95%. But to ensure that this is the best possible efficiency obtainable for the given input parameters and constraints a parametric study was conducted by varying the mass flow from 0.035 kg/s to 0.045 kg/s to determine the heat input, while all other input parameters stay fixed. The results are displayed in Table 5-6.

Table 5-6: Simple EFGT cycle results for varying mass flow.

Run #	m_dot [kg/s]	W_NET [kW]	Q_CC [kW]	ETA_ BRAYTON	TIT [C]
1	0.035	5	26.49	0.1887	900
2	0.036	5	27.25	0.1835	900
3	0.037	5	28.01	0.1785	900
4	0.038	5	28.77	0.1738	900
5	0.039	5	29.52	0.1694	900
6	0.04	5	30.28	0.1651	900
7	0.041	5	31.04	0.1611	900
8	0.042	5	31.79	0.1573	900
9	0.043	5	32.55	0.1536	900
10	0.044	5	33.31	0.1501	900
11	0.045	5	34.06	0.1468	900

For a mass flow of 0.04 kg/s, a heat input of 30.28 kW is required to reach a TIT of 900˚C and still deliver a power output of 5 kW. The heat input falls within the constraints for the simple cycle. With this adjustment, the best possible cycle efficiency is 16.15%.

The detailed results for the simulation at the above-mentioned conditions are tabulated in Table 5-7 and Table 5-8.

Table 5-7: Simple cycle results for each operating point at the maximum possible efficiency.

Operating Point	Pressure	Temperature	Isentropic Enthalpy	Enthalpy	Entropy
	P[i]	T[i]	h_s[i]	h[i]	s[i]
[#]	[kPa]	[C]	[kJ/kg]	[kJ/kg]	[kJ/kg·K]
1	100	25	-	298.4	6.862
2	99.01	25	-	298.4	6.865
3	99	25	-	298.4	6.865
4	396	213.9	443.9	489.9	6.964
5	395.98	213.9	-	489.9	6.964
6	395.98	900	-	1247	7.925
7	395.96	900	-	1247	7.925
8	105	628	866.1	934.6	8.004
9	104.99	628	-	934.6	8.004

Table 5-8: Simple cycle operating conditions at the maximum possible efficiency.

Parameter Description	Parameter	Value	Unit
Mass Flow Rate	m_dot	0.04	[kg/s]
Combustion Chamber Heat	Q_CC	30.28	[kW]
Cycle Efficiency	Eta_Brayton	0.1651	[-]
Power Output	W_Net	5	[kW]
Turbine Inlet Temperature	TIT	900	[°C]
Compressor Work	W_C	7.66	[kW]
Compressot Pressure Ratio	PR_C	4	[-]
Turbine Work	W_T	12.49	[kW]
Turbine Pressure Ratio	PR_T	3.771	[-]

In the following section, the heat recovery cycle will be discussed, and its results will be compared to that of the simple cycle.

5.2.3 Results for the heat recovery EFGT cycle

The heat recovery EFGT cycle was simulated in order to recover exhaust heat from the turbine to preheat the compressed air before it enters the combustion chamber and by doing so reducing the amount of heat input required by the system. The heat recovery cycle was simulated for the reference case input parameters listed in Table 5-1.

The results for the heat recovery cycle based on the reference case input parameters are tabulated in Table 5-9 and Table 5-10.

Table 5-9: Heat recovery cycle results for each operating point based on reference case parameters.

Operating Point	Pressure	Temperature	Isentropic Enthalpy	Enthalpy	Entropy
	P[i]	T[i]	h_s[i]	h[i]	s[i]
[#]	[kPa]	[C]	[kJ/kg]	[kJ/kg]	[kJ/kg·K]
1	100.00	25		298.4	6.862
2	99.01	25		298.4	6.865
3	99.00	25		298.4	6.865
4	396.00	213.9	443.9	489.9	6.964
5	395.98	213.9		489.9	6.964
6	395.98	399.8		684.6	7.303
7	395.96	399.8		684.6	7.303

8	395.96	700		996.9	7.709
9	395.94	683.1		996.9	7.689
10	102.00	450.5	682.6	739.2	7.771
11	101.99	450.5		739.2	7.771
12	101.99	266.6		544.4	7.460
13	103.00	266.6		544.4	7.457

Table 5-10: Heat recovery cycle operating conditions based on reference case parameters.

Parameter Description	Parameter	Value	Unit
Mass Flow Rate	m_dot	0.07551	[kg/s]
Combustion Chamber Heat	Q_CC	23.58	[kW]
Cycle Efficiency	Eta_Brayton	0.2121	[-]
Power Output	W_Net	5	[kW]
Turbine Inlet Temperature	TIT	700	[°C]
Compressor Work	W_C	14.46	[kW]
Compressot Pressure Ratio	PR_C	4	[-]
Turbine Work	W_T	19.46	[kW]
Turbine Pressure Ratio	PR_T	3.88	[-]

When comparing the heat recovery cycle to the simple cycle based on the input parameters specified for the reference case, it was found that for the same power output of 5 kW, the cycle efficiency increases with 68% from 12.58% to 21.21% and the heat added by the combustion chamber, as required by the cycle, decreases by 40.6% due to heat rejected from the turbine, which is recovered in the heat exchanger. The comparative results of the two different cycles are graphically presented in Figure 5-3.

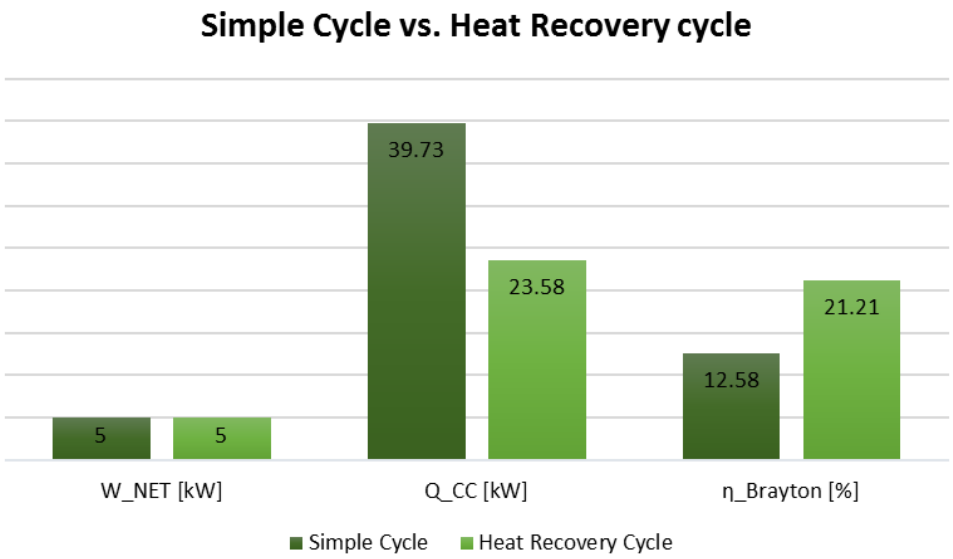

Figure 5-3: Simple cycle vs. heat recovery cycle

This shows that for the same input parameters the heat recovery cycle would need less fuel to supply the lower amount of heat required from the combustor.

- **Improving the heat recovery cycle for a fixed power output**

As stated in the cycle development the potential improvement of the heat recovery cycle is investigated. An increase in component efficiency will automatically improve the performance of the cycle in terms of power output and cycle efficiency, but this will also increase the cost of the components. Within this study, the component efficiencies will stay constant throughout the evaluation of the different cycle configurations.

From previous evaluations, it is evident that the TIT, mass flow and heat input are influential parameters to the EFGT cycle. In an effort to improve the performance of the heat recovery EFGT cycle an additional simulation was carried out. To compare the improved heat recovery cycle to the simple EFGT cycle, corresponding input parameters should be used, therefore the heat recovery cycle was simulated for the following input conditions and constraints:

Table 5-11: Heat recovery cycle input parameters and constraints

Parameter	Value	Unit
Power output	5	[kW]
TIT	900	[˚C]
Mass flow rate	0.035 - 0.045	[kg/s]

Once again verification should be done to determine whether the results meet all constraints. According to Visser et al. (2011), the heat input for the heat recovery cycle of this scale ranges between 10–18 kW. This will be used to govern the heat input for the heat recovery cycle.

Incorporating the mass flow of 0.4 kg/s, obtained from the simple cycle parametric study, in the heat recovery cycle for a fixed power output of 5 kW, a TIT of 900˚C and PR of 4, improved the heat recovery cycle efficiency to 29.93%, and reduced the heat input required to with 16.71 kW which is well within the 10 – 18 kW range.

The detailed results for the improved heat recovery cycle simulation are tabulated in Table 5-12 and Table 5-13.

Table 5-12: Heat recovery cycle results for each operating point for the improved cycle.

Operating Point	Pressure	Temperature	Isentropic Enthalpy	Enthalpy	Entropy
	P[i]	T[i]	h_s[i]	h[i]	s[i]
[#]	[kPa]	[C]	[kJ/kg]	[kJ/kg]	[kJ/kg·K]
1	100.00	25		298.4	6.862
2	99.01	25		298.4	6.865
3	99.00	25		298.4	6.865
4	396.00	213.9	443.9	489.9	6.964
5	395.98	213.9		489.9	6.964
6	395.98	565.7		823.2	7.491
7	395.96	565.7		823.2	7.491
8	395.96	900		1241	7.925
9	395.94	894.9		1241	7.92
10	102.00	618.8	854.9	924.4	8
11	101.99	618.8		924.4	8
12	101.99	311.3		591.1	7.453
13	103.00	311.3		591.1	7.451

Table 5-13: Heat recovery cycle operating conditions for the improved cycle.

Parameter Description	Parameter	Value	Unit
Mass Flow Rate	m_dot	0.04	[kg/s]
Combustion Chamber Heat	Q_CC	16.71	[kW]
Cycle Efficiency	Eta_Brayton	29.93	[-]
Power Output	W_Net	5	[kW]

Turbine Inlet Temperature	TIT	900	[°C]
Compressor Work	W_C	7.66	[kW]
Compressot Pressure Ratio	PR_C	4	[-]
Turbine Work	W_T	12.49	[kW]
Turbine Pressure Ratio	PR_T	3.771	[-]

In comparison with the simple cycle, the improved heat recovery cycle requires 13.57 kW less heat than the simple cycle with an increased efficiency of 29.93% (16.51% for the same setup for the simple cycle). This shows for this combination of operating parameters the heat recovery cycle is 81.2% more efficient as the simple cycle based on the same input parameters.

5.2.4 Results for the pre-cooled EFGT cycles

5.2.4.1 The pre-cooling unit

The pre-cooling unit was included in the study to evaluate the effect it would have on the simple and heat recovery EFGT cycle should the temperature of the air entering the EFGT cycle compressor be lower, especially in areas known for high ambient temperatures. An independent simulation of the pre-cooling unit, also known as the vapour-compression refrigeration cycle, was included to investigate the performance of such a cycle based on realistic values with regard to the environment it will be utilised before incorporating it into the EFGT cycles.

The following assumptions were made and applied to simulate the vapour-compression refrigeration cycle:

- Ambient air is cooled from 30°C to 12°C.
- Superheating of 12°C.
- Subcooling of 8°C.
- The temperature of heat rejected to the surroundings (Q_H) is 20°C above the ambient temperature.
- Pressure drops in pipes and components are neglected.

Other input parameters incorporated in the simulation, such as ambient conditions, refrigerant mass flow and the compressor's isentropic efficiency, are displayed in Table 5-14.

Table 5-14: Input parameters for the vapour-compression refrigeration cycle simulation.

Vapor-Compression Refrigeration Cycle: Input Parameters		
Parameter	**Value**	**Unit**
Ambient Temperature	30	[˚C]
Ambient Pressure	100	[kPa]
Refrigerant mass flow rate	0.03	[kg/s]
Compressor isentropic efficiency	0.60	[-]

The simulation was used to investigate properties such as the COP, the work input for the compressor and the cooling effect (Q_L) of the cycle. Figure 5-4 displays a temperature-entropy (T-s) diagram of the simulated cycle.

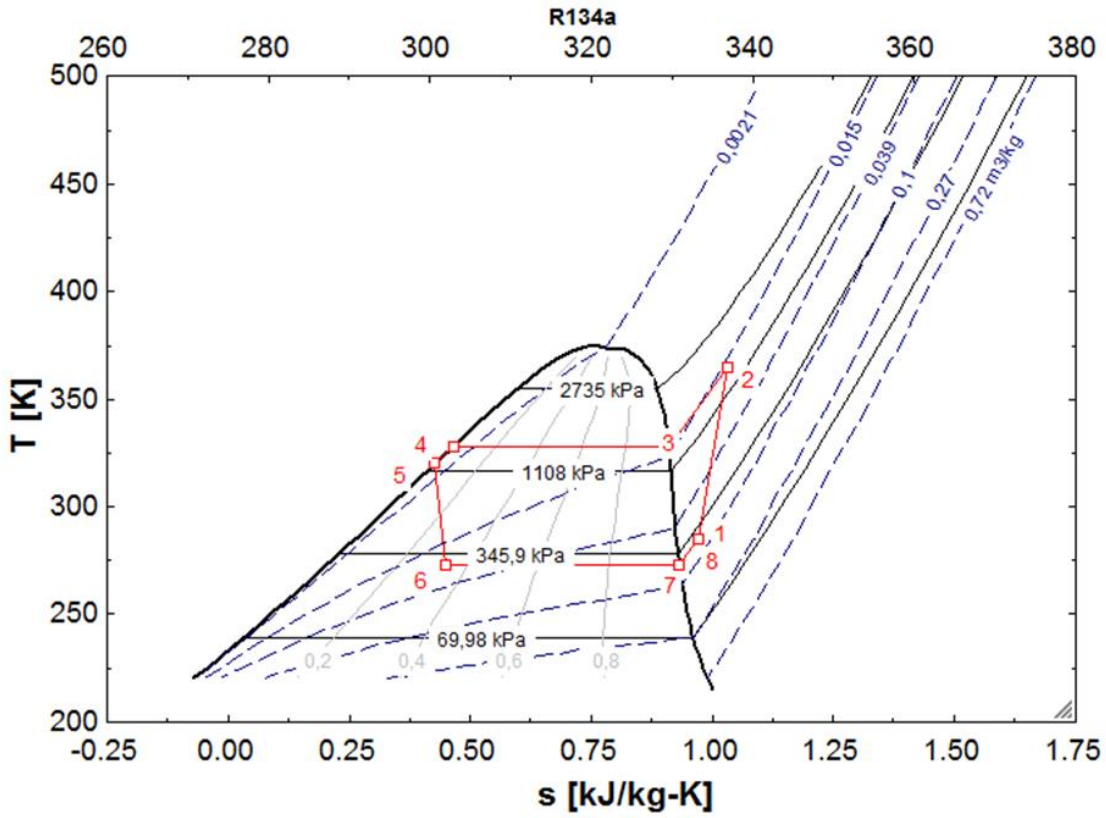

Figure 5-4: T-s diagram of the simulated vapour-compression refrigeration cycle.

Based on the given input parameters and assumptions governing the simulation, the cycle resulted in a COP of approximately 2.694, a cooling effect of 4.498 kW and a compressor power input of 1.67 kW. The results obtained from the simulation are displayed in Table 5-15.

Table 5-15: Results obtained from the simulated vapour-compression refrigeration cycle.

Vapor-Compression Refrigeration Cycle: Results		
Parameter	**Value**	**Unit**
COP	2.694	[-]
Compressor Work (W_C)	1.669	[kW]
Cooling effect (Q_L)	4.498	[kW]
Air mass flow rate	0.194	[kg/s]

After simulating the vapour-compression refrigeration cycle for the stated conditions and obtaining results regarding its performance, it can realistically be incorporated into the EFGT cycles to evaluate whether it could have an improving effect on the overall EFGT cycle performance.

The pre-cooling unit was incorporated in the EFGT cycle simulations by including parameters such as the COP (2.694) and temperature difference (ΔT of 18°C) adapted from the independent vapour-compression refrigeration cycle simulation. For these simulations, the ambient temperature will be increased to 30°C since this application would be more suitable in regions with higher ambient temperatures. From the independent vapour-compression refrigeration cycle simulation it is evident that the mass flow rate of the refrigerant is approximately 15% of the mass flow rate of air. Therefore, for the following simulations, it was assumed that the mass flow rate of the refrigerant is 15% of the mass flow rate of air flowing through the cycle. The EES models for the pre-cooled EFGT cycles are available in Appendix A.

5.2.4.2 The simple pre-cooled cycle

- **The effect of the pre-cooler on the simple EFGT cycle based on reference case parameters.**

The first simple pre-cooled EFGT cycle simulation was based on the reference case simulation input parameters listed in Table 5-1 as well as incorporating the above-mentioned parameters for the pre-cooling unit. Table 5-16 shows the results obtained from the simple pre-cooled EFGT simulation compared to the results of the simple EFGT reference case simulation.

Table 5-16: Results for the simple pre-cooling cycle based on reference case parameters.

Description	Simple Reference Case	Simple Pre-cooled Reference Case
Net Work Output	5 kW	5 kW
Cycle Efficiency	12.58%	13.43%
Heat Input	30.28 kW	37.23 kW

Based on the reference case parameters and pre-cooling unit parameters and assumptions, the simple pre-cooled cycle simulation results in an improvement in cycle efficiency, but at the cost of an additional 6.9 kW heat input required.

- **The effect of the pre-cooler temperature difference.**

In order to investigate the simple pre-cooled cycle in terms of the temperature difference (ΔT) between the ambient air and the compressor inlet initiated by the pre-cooler, three simulations were done. The simulations were based on the same ambient conditions and operating conditions as for the reference case simple cycle each of the three respective TITs. For each simulation, the pre-cooling unit has a COP of 2.5 and its ΔT was varied in a parametric table from 5 to 25˚C. Furthermore, it is important to note that the pressure ratios referred to in this section are the pressure ratio of the EFGT cycle and not that of the compressor in the pre-cooling cycle. The effect of the ΔT with respect to combustion heat input and cycle efficiency at the three different TITs are illustrated in Figure 5-5 and Figure 5-6 respectively.

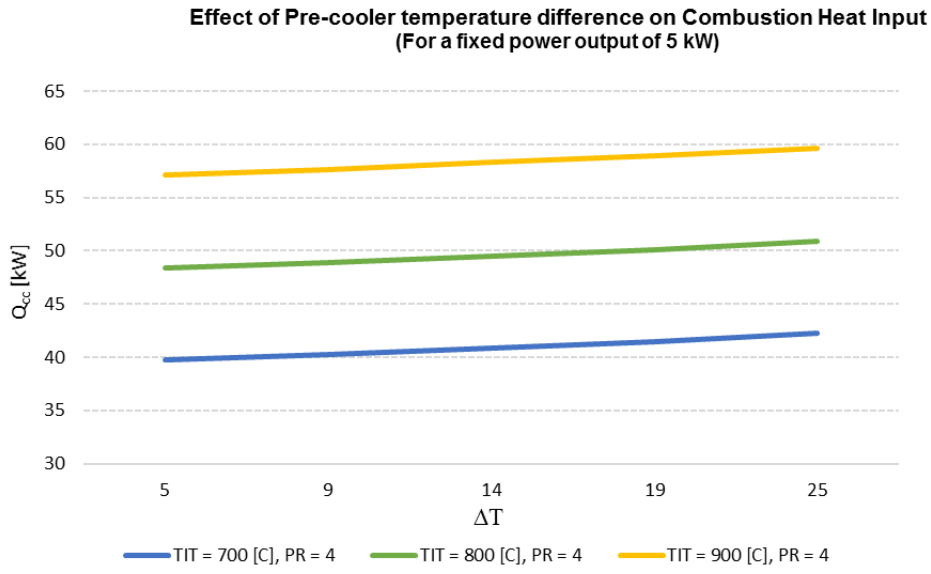

Figure 5-5: Effect of Pre-cooler temperature difference on combustion heat input.

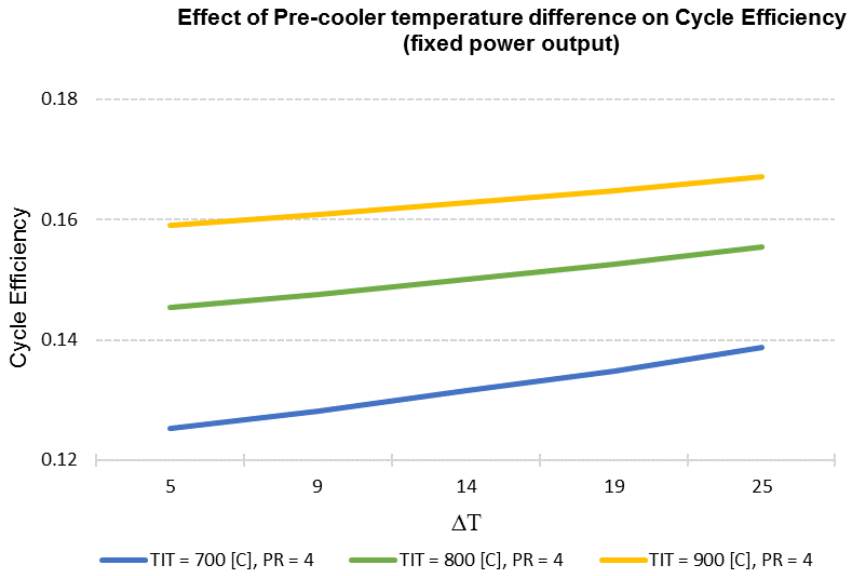

Figure 5-6: Effect of Pre-cooler temperature difference on cycle efficiency.

The general effect was that an increase in ΔT (an increase in cooling effect) at the compressor causes a linear increase in heat supplied to the EFGT cycle and a linear increase in the EFGT cycle efficiency per operation point. Therefore an increase in ΔT leads to an improvement in cycle efficiency, but at the same time would require a higher heat input.

- **The effect of the COP**

In order to illustrate the influence of the COP of the pre-cooler on the simple EFGT cycle, a cycle with a TIT of 700 ˚C, PR of 4 and a ΔT of 18 ˚C was simulated. The effect of the COP on the cycle efficiency and power output is illustrated in Figure 5-7.

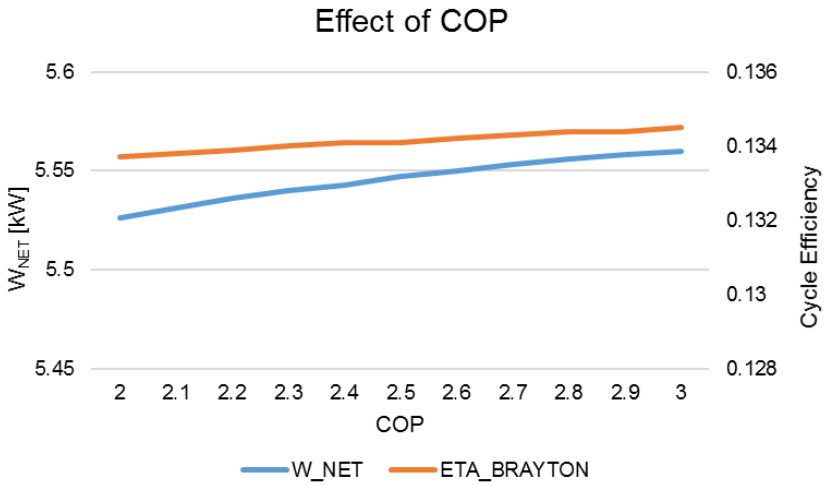

Figure 5-7: Effect of COP on power output and cycle efficiency.

It is clear that an increase in the COP of the pre-cooling unit initiates an increase in cycle efficiency and power output. Only the one graph is presented, for the cycles at 800˚C and 900˚C shows the same tendency only for respective higher and lower power output and cycle efficiency values.

- **The effect of the pre-cooler on the simple EFGT cycle based on best performance parameters.**

In order to compare the best performing simple EFGT cycle to the simple pre-cooled cycle, it is necessary to use the same input parameters for both simulations. The best results obtained for the simple EFGT cycle with a fixed power output of 5 kW was at the following input parameters:

  - TIT of 900 ˚C
  - PR of 4
  - 5 kW power output
  - Mass flow of 0.4 kg/s

Using these input parameters for the simple pre-cooled cycle along with the previously stated input parameters for the pre-cooling unit, COP and ΔT, the simulation delivered the following results.

Table 5-17: Results for the simple pre-cooling cycle based on the simple cycle best performance parameters.

Description	Simple Cycle	Simple Pre-cooled Cycle
Net Work	5 kW	5 kW
Cycle Efficiency	16.51%	15.72%
Heat Input	30.28 kW	31.81 kW

From the results, it is evident that the pre-cooling unit did not have an improving effect on the simple EFGT cycle delivering 5 kW power for the given input parameters. Further investigation should be done to evaluate additional parameters and its effect on an EFGT cycle i.e. compressor pressure ratio.

5.2.4.3 The pre-cooled heat recovery cycle

The pre-cooled heat recovery cycle was investigated in order to compare its performance to that of the heat recovery cycle. The best results obtained for the heat recovery cycle with a fixed power output of 5 kW was at the following input parameters:

- TIT of 900 ˚C
- PR of 4
- 5 kW power output
- Mass flow of 0.4 kg/s

Using these input parameters for the pre-cooled precooled heat recovery cycle along with the previously stated input parameters for the pre-cooling unit, COP and ΔT, the simulation delivered the results tabulated in Table 5-18.

Table 5-18: Results obtained for the pre-cooled heat recovery cycle.

Description	Simple Cycle	Simple Pre-cooled Cycle
Net Work	5 kW	5 kW
Cycle Efficiency	29.93%	30.07 %
Heat Input	29.93 kW	30.07 kW

The pre-cooled heat recovery cycle with a power output of 5 kW showed an improvement in cycle efficiency 30.07% along with a heat input required of 16.86 kW. The detailed results for the improved heat recovery cycle simulation are tabulated in Table 5-19 and Table 5-20.

Table 5-19: Pre-cooled Heat recovery cycle results for each operating point for the improved cycle.

Operating Point	Pressure	Temperature	Isentropic Enthalpy	Enthalpy	Entropy
	P[i]	T[i]	h_s[i]	h[i]	s[i]
[#]	[kPa]	[C]	[kJ/kg]	[kJ/kg]	[kJ/kg·K]
1	100.00	12		285.3	6.818
2	99.00	12		285.3	6.82
3	99.00	12		285.3	6.82
4	396.00	193.1	424.5	468.5	6.919
5	395.98	193.1		468.5	6.919
6	395.98	525.6		821.1	7.489
7	395.96	525.6		821.1	7.489
8	395.96	900		1247	7.925
9	395.94	900		1247	7.925
10	102.00	622.9	859.2	928.9	8.006
11	101.99	622.9		928.9	8.006
12	101.99	297.2		576.3	7.518
13	104.00	297.2		576.3	7.512

Table 5-20: Pre-cooled Heat recovery cycle operating conditions for the improved cycle.

Parameter Description	Parameter	Value	Unit
Mass Flow Rate	m_dot	0.04	[kg/s]
Combustion Chamber Heat	Q_CC	16.86	[kW]
Cycle Efficiency	Eta_Brayton	30.07	[-]
Power Output	W_Net	5	[kW]
Turbine Inlet Temperature	TIT	900	[°C]
Compressor Work	W_C	7.254	[kW]
Compressot Pressure Ratio	PR_C	4	[-]
Turbine Work	W_T	12.59	[kW]
Turbine Pressure Ratio	PR_T	3.882	[-]
Cooling effect	Q_L	0.717	[kW]
Pre-cooling unit work	W_PC_Net	0.266	[kW]

5.2.5 Summary of results

The simple cycle simulation based on the reference case input parameters resulted in a 5 kW power output, 39.73 kW heat supplied by the combustion chamber and a cycle efficiency of

12.58%. Increasing the TIT to 900˚C increased the cycle efficiency to 16.51% and reducing the heat required to 30.28 kW, due to fixed power output and adjusting the mass flow of the air.

The heat recovery cycle showed to be 81% more efficient than the simple cycle for simulations based on the same input parameters. Resulting in a cycle efficiency of 29.93%. This configuration delivers the best results based on the specified parameters.

The simple pre-cooled cycle showed that the pre-cooling unit did not have an improving effect on the simple EFGT cycle based on the given input parameters and for a ΔT of 18℃ and a COP of 2.5. The cycle efficiency decresed from 16.51% to 15.72%.

The investigation of the COP revealed that it has a greater influence on cycles with lower TIT values, but has an overall improving effect on all simulations when the COP, as well as the ΔT, is increased.

The pre-cooled heat recovery cycle showed the best results in terms of cycle performance. The simulation for a 5 kW EFGT-cycle deemed the highest cycle efficiency of 30.07%.

CHAPTER 6

CONCLUSION

CHAPTER 6:

CONCLUSION

6.1 Introduction

In this concluding chapter, a summary will be provided with the most important results that were discussed in the previous chapters. From these results, certain conclusions will be made and suggested financial considerations will be given, leading to recommendations for further research.

6.2 Summary

In the first chapter of this study, the background and problem statement were given, emphasizing the need for a micro-scale EFGT biomass application suitable to provide rural communities with the minimum electricity. In Chapter 2 a literature survey was conducted on the history, components, working principals and previous studies conducted on EFGT cycles. It was found that very little research has been done on micro-scaled EFGT biomass applications in contrast to what is available in the 100 – 150 kW range.

In Chapter 3 the cycle development was discussed in terms of different configurations and simulation methodology. Chapter 3 also provided the theoretical background on the governing equations needed to simulate the components configured within an EFGT cycle as well as the equations to evaluate the performance of such a cycle.

The cycle verification was covered in Chapter 4, verification of the simple EES model was done using information from a published study into the use of a simple biomass-fuelled, micro-scale EFGT modelled in Aspen Plus 8.6. The correlating results obtained for compressor work needed was accurate within 99.75%, where the generated work by the turbine and net work of the cycle was found to be accurate within 98.5% and 95%, respectively.

In chapter 5 the results obtained from the different simulations were presented graphically and discussed in terms of performance and the influences of selected parameters, such as turbine inlet temperature, pressure ratio, COP of the pre-cooling unit and heat added by the combustion chamber.

6.3 Conclusion

The purpose of this study was to evaluate different EFGT configurations using developed simulation models for a micro-scale EFGT biomass application with an electricity generation capacity in the region of 5 kW and to use the simulation models to investigate different cycle configurations, operating conditions, and their comparative system efficiencies.

The study results demonstrate a micro-scaled biomass simulation models which was successfully derived and the four different cycle configurations were evaluated for different operating conditions.

Based on the results obtained, the EFGT cycle incorporating heat recovery will be the best-suited cycle for rural applications. Since biomass is abundantly available, additional fuel can be used if needed. The results show the EFGT cycle incorporating heat recovery can be up to 81% more efficient as the simple cycle based on the parameters specified.

For pre-cooling the air of the EFGT cycle and incorporating heat recovery the cycle efficiency is increased by ~1%. Although the pre-cooling unit improves the performance of the cycle, further investigation should be conducted regarding the implementation of the pre-cooling unit to determine whether it will be feasible and practically viable for rural applications.

6.4 Financial considerations

This section does not form part of the current scope of this study but it is relevant when considering which configuration of the cycle would be most viable. In chapter 5 the results for different configurations were given and the effect of adding a heat exchanger and pre-cooling unit were discussed. For most applications, the decision of which configuration to implement is not purely technical, but rather financial.

The improvement of the cycle, by adding these additional components, do seem rather attractive but on micro-scale, the feasibility is questionable when considering all the costing factors. Therefore, it is important to do a financial feasibility study before making the final decision. Factors and costs to consider are:

- Cost of components
- Implementation costs
- Operation and maintenance costs
- Fuel costs

- Fuel transportation costs
- The cost of the generated electricity
- The current cost of electricity
- Return on investment
- Life cycle costing

Even for the simple model, this will be a rather important exercise and by adding the cost of additional components and their effects, the viability can be investigated.

6.5 Recommendations for further research

Recommendations for further research are as follows:

- Detailed investigation of biomass fuels to determine their chemical compilation and combustion capability especially for use in EFGTs.
- Based on an industrial approach, a feasibility study/financial model can be investigated for micro-scale biomass applications taking all costing variables into account.
- The detail design of the heat exchangers utilized in EFGTs and heat recovery cycles.

BIBLIOGRAPHY

Al-Attab, K.A. & Zainal, Z.A. 2010. Turbine startup methods for externally fired micro gas turbine (EFMGT) system using biomass fuels. *Applied energy*, 87(4):1336-1341.

Al-Attab, K.A. & Zainal, Z.A. 2010. Performance of high-temperature heat exchangers in biomass fuel powered externally fired gas turbine systems. Applied energy, 35(5):913-920.

Al-Attab, K.A. & Zainal, Z.A. 2015. Externally fired gas turbine technology: a review. *Applied energy*, 138:474–487.

Anheden, M. 2000. Analysis of gas turbine systems for sustainable energy conversion. Sweden: Royal Institute of Technology. (Thesis – PhD)

Ansaldo Energia. 2019. AE-T100 Externally Fired Micro Turbine. [Web:] https://www.ansaldoenergia.com/business-lines/new-units/microturbines/ae-t100e Date of access: 12 Feb 2019.

Bdour, M., Al-Addous, M., Nelles, M. & Ortwein, A. 2016. Determination of optimized parameters for the flexible operation of a biomass-fuelled, microscale externally fired gas turbine (EFGT). *Energies*, 9(10):856. DOI: 10.3390/en9100856.

Borgnakke, C. & Sonntag, R.E. 2009. Fundamentals of thermodynamics. 7th ed. Wiley.

Botha, B.W. 2010. Gas turbine theory and performance: course notes for MGII 887. NWU, Potchefstroom: Faculty of Engineering. (Unpublished).

Brayton Energy. 2019. 1.2 MW Gas Turbine For Biomass Burning. [Web:] https://www.braytonenergy.net/our-projects/1-2-mw-gas-turbine/ Date of access: 14 Feb 2019.

Capstone Turbine Corporation. 2019. C30 Microturbine. [Web:] https://www.capstoneturbine.com/products/c30 Date of access: 20 Feb 2019.

Chen, H. 2014. Biotechnology of Lignocellulose. Theory and Practice. Springer Netherlands. 510 p.

Cocco, D., Deiana, P. & Cau, G. 2006. Performance evaluation of small size externally fired gas turbine (EFGT) power plants integrated with direct biomass dryers. *Energy*, 31:1459–1471.

Datta, A., Ganguly, R. & Sarkar, L. 2010. Energy and exergy analyses of an externally fired gas turbine (EFGT) cycle integrated with biomass gasifier for distributed power generation. *Energy,* 35:341–350.

De Mello, P.E.B. & Monteiro, D.B. 2012. Thermodynamic study of an EFGT (externally fired gas turbine) cycle with one detailed model for the ceramic heat exchanger. *Energy,* 45:497–502.

Durante, A., Pena-Vergara, G., Curto-Risso, P.L., Medina, A. & Calvo Hernández, A. 2017. Thermodynamic simulation of a multi-step externally fired gas turbine powered by biomass. *Energy conversion and management,* 140:182-191.

Environmental Protection Agency. 2018. [Web:] https://www.epa.gov/greenpower/what-green-power Date of access: 23 Jul 2017

Eskom. 2016a. Company information. [Web:] http://www.eskom.co.za/OurCompany/Company Information/Pages/Company_Information.aspx Date of access: 14 May 2016.

Eskom. 2016b. Renewable energy. [Web:] http://www.eskom.co.za/AboutElectricity/ RenewableEnergy/Pages/Renewable_Energy.aspx Date of access: 14 May 2016.

Garrett. 2018. [Web:] https://www.garrettmotion.com/turbo-replacement/aftermarket-turbochargers-turbo-identification/ Date of access: 22 Aug. 2018.

Habboush, M. 2016. Renewable energy focus could boost global economic growth. Bloomberg News: 18 Jan. [Web:] http://www.renewableenergyworld.com/articles/2016/01/ renewable-energy-focus-could-boost-global-economic-growth.html Date of access: 22 May 2016.

Hamilton, S.L. 2001. Microturbines. (*In* Chambers, A. *ed.* Distributed generation: a nontechnical guide. USA: Pennwell Corporation. p. 33-72).

Henne, R.H., Friedrich, K.A. 2009. APPLICATIONS – TRANSPORTATION | Auxiliary Power Units: Fuel Cells. Encyclopedia of Electrochemical Power Sources, 157-173.

Howstuffworks. 2006. [Web:] https://auto.howstuffworks.com/supercharger4.htm Date of access: 6 June 2018.

Hydraulics and Pneumatics. 2016. Power and refrigeration cycles: Brayton cycle: The ideal cycle for gas-turbine engines. [Web:] http://machineryequipmentonline.com/hydraulics-and-

pneumatics/power-and-refriger-a-tion-cyclesbrayton-cycle-the-ideal-cycle-for-gas-turbine-engines/ Date of access: 26 May 2017.

Horlock, J. 2003. Advanced gas turbine cycles. Oxford: Pergamon.

Kautz, M. & Hansen, U. 2007. The externally-fired gas-turbine (EFGT-cycle) for decentralized use of biomass. *Applied energy*, 84:795–805.

Liss, W.E. 1999. Natural Gas Power Systems for the Distributed Generation Market. Power-Gen International '99 Conference. CD-Rom. New Orleans, Louisiana, USA.

Mandi, R.P. & Yaragatti, U.R. 2014. Reducing Auxiliary Power of Induced Draft Fans in Coal Fired Thermal Power Plants by Energy Audit. The Journal of CPRI. 10(1):65-74.

McAllister, S., Chen, J.Y. & Fernendez-Pello, A.C. 2011. Fundamentals of Combustion Processes. New York: Springer. 304 p.

McKendry, P. 2002. Energy production from biomass (part 2): conversion technologies. *Bioresource Technology,* 83:47-54.

MTT (Micro Turbine Technology BV). 2018. [Web:] https://www.mtt-eu.com/applications/micro-chp/ Date of access: 26 Feb 2019.

Nascimento, M.A., Rodrigues, L.O., Santos, E.C., Gomes, E.B., Dias, F.L.G., Velásques, E.I.G. & Carrillo, R.A.M. 2014. Micro gas turbine engine: a review. (*In* Bernini, E. *ed.* Progress in gas turbine performance. InTech, DOI: 10.5772/54444).

Nascimento, M.A.R. & Santos, E.C. 2011. Biofuel and gas turbine engines. (*In* Bernini, E. *ed.* Advances in gas turbine technology. InTech, DOI: 10.5772/22305).

Nelson, V.C. 2011. Introduction to renewable energy. CRC Press.

Pantaleo, A.M., Camporeale, S.M. & Shah, N. 2013. Thermo-economic assessment of externally fired micro-gas turbine fired by natural gas and biomass: applications in Italy. *Energy conversion and management*, 75:202–213.

Pilavachi, P.A. 2000. Power generation with gas turbine systems and combined heat and power. *Applied thermal engineering*, 20:1421-1429.

Rodgers, C., Watts, J., Thoren, D., Nichols, K. & Brent, R. 2001. Microturbines. (*In* Borbely, A. & Kreider, J.F. *eds*. Distributed generation – the power paradigm for the new millennium. USA: CRC Press LLC. p. 120-148).

Rousseau, P.G. 2013. Thermal-fluid systems modelling I - course notes for MGII 885. NWU Potchefstroom: Faculty of Engineering. (Unpublished).

Saravanamuttoo, H.I.H., Rogers, G.F.C., Cohen, H. & Straznicky, P.V. 2009. Gas turbine theory. 6th ed. England: Pearson Education Limited.

Sayers, A.T. 1990. Hydraulic And Compressible Flow Turbomachines. McGraw-Hill. 301 p.

Schmid, M. 2007. Dezentrale Stromerzeugung Mit Feststoffbiomasse. Ökozentrum Langenbruck: Langenbruck, Switzerland.

Schwitzer Turbochargers, 1991. Introduction to Turbochargers. Indianapolis, Indiana.

Smil, V. 1983. Biomass energies: resources, links, constraints. Springer US.

Statistics South Africa. 2016. The state of basic service delivery in South Africa: In-depth analysis of the Community Survey 2016 data, Report 03-01-22.

Vaidya, J.G. 2007. Electric generators for direct coupled high speed turbo Generators in distributed power systems. Cogeneration and Distributed Generation Journal 22(3):50-62.

Vera, D., Juradoa, F., De Menab, B. & Schories, B.G. 2011. Comparison between externally fired gas turbine and gasifier-gas turbine system for the olive oil industry. *Energy*, 36:6720–6730.

Visser, W.P.J., Shakariyants, S.A., Oostveen, M. 2011. Development of a 3 kW Microturbine for CHP Applications. Journal of Engineering for Gas Turbines and Power. Vol. 133 / 042301-1.

Wilcox, M., Kruz, R. & Burn, K. 2012. Technology Review of Modern Gas Turbine Inlet Filtration Systems. International Journal of Rotating Machinery. Vol. 2012. 15 p.

Zhu, S., Deng, K. & Liu, S. 2015. Modeling and extrapolating mass flow characteristics of a radial turbocharger turbine. *Energy*, 87:628-637.

CLAIMS FOR HAVING ATTAINED THE REQUIREMENTS FOR A MASTERS DEGREE

The following list serves as a summary of the content covered within this study. Each point speaks to a different relative outcome required to obtain a master's degree.

- The problem statement, research objective and methodology of this study was clearly stated and identified in chapter 1.
- A literature survey was conducted on the working principals, the different components and configurations of an EFGT cycle. Different operating parameters were investigated as well as a few previous studies conducted on these type of biomass cycles, outlining relevant results obtained from the studies.
- The relevant theoretical background was investigated for each of the components as well as the theory associated with the output and performance of the cycle.
- The cycles were developed based on the relevant background theory, identifying working points used within the cycle simulations and diagrams were used to illustrate the configuration of each cycle presented.
- The investigation of each cycle was stipulated in chapter 3, each configuration was investigated in terms of power output and cycle efficiency based on the effect of different parameters.
- Model verification was done by comparing the results of a simple model simulated in EES to that of a similar model found in literature, modelled in Aspen Plus 8.6. The verification was conclusive due to the fact that the comparison between the results was in fair correlation.
- The results based on the investigation of the effect of different parameters were thorough and influences on the different configurations were revealed.
- In conclusion of this document, its content was summarized, the results were discussed, and financial considerations were listed.

APPENDIX A

EES Simulations

I. EES simulation model for the simple EFGT cycle

```
//CYCLE VERIFICATION
//SIMPLE OPEN BRAYTON CYCLE vs. BDOUR ET AL.

"INPUT VALUES"
"_____"

T_MAX =1062

T_AMB = 300

m_dot =0.017

"PRESSURE DROP %"
"_____"

alpha_AF =0
alpha_P = 0.00025

"COMPONENT CHARACTERISTICS"
"_____"

"COMPRESSOR PRESSURE RATIO"
PR_C=4

 "COMPRESSOR EFFICIENCY"
ETA_C=0.78

"TURBINE EFFICIENCY"
ETA_T=0.82

"POINT 1 - AMBIENT"
"_____"

P[1]=100 [kPa]
T[1]= T_AMB
h[1] =Enthalpy(Air_ha,T=T[1],P=P[1])
s[1] =Entropy(Air_ha,T=T[1],P=P[1])

"POINT 2 - AIR FILTER OUTLET"
"_____"

DELTA_AF =alpha_AF *((P[1] +P[2])/2)
P[2] =P[1]-DELTA_AF
h[2] =h[1]
T[2] =Temperature(Air_ha,P=P[2],h=h[2])
s[2] =Entropy(Air_ha,T=T[2],P=P[2])
```

```
"POINT 3 - COMPRESSOR INLET"
"_____"

DELTA_P23 =alpha_P *((P[2]+P[3])/2)

P[3]=P[2] -DELTA_P23
h[3] =h[2]
T[3] =Temperature(Air_ha,P=P[3],h=h[3])
s[3] =Entropy(Air_ha,T=T[3],P=P[3])

"POINT 4 - COMPRESSOR OUTLET"
"_____"

P[4]=P[3]*PR_C
h_s[4] =Enthalpy(Air_ha,P=P[4],s=s[3])                    "ISENTROPIC ENTHALPY"

W_C = (1/ETA_C) * m_dot*(h_s[4] -h[3])
W_C=m_dot * (h[4]-h[3])                                   "WORK NEEDED BY COMPRESSOR"

T[4]=Temperature(Air_ha,P=P[4],h=h[4])
s[4]=Entropy(Air_ha,T=T[4],P=P[4])

"POINT 5 - COMBUSTION CHAMBER INLET"
"_____"

DELTA_P45 =alpha_P *((P[4] +P[5])/2)

P[5]=P[4] -DELTA_P45
h[5] =h[4]
T[5] =Temperature(Air_ha,P=P[5],h=h[5])
s[5] =Entropy(Air_ha,T=T[5],P=P[5])

"POINT 6 - COMBUSTION CHAMBER OUTLET"
"_____"

T[6]=T_MAX
P[6]=P[5]

h[6]=Enthalpy(Air_ha,T=T[6],P=P[6])
s[6]=Entropy(Air_ha,T=T[6],P=P[6])

Q_CC=m_dot *(h[6]-h[5])

"POINT 7 - TURBINE INLET"
"_____"

DELTA_P67 =alpha_P *((P[6] +P[7])/2)
P[7] =P[6] -DELTA_P67
h[7] = h[6]
T[7] = Temperature(Air_ha,P=P[7],h=h[7])
s[7] = Entropy(Air_ha,T=T[7],P=P[7])


"POINT 8 - TURBINE OUTLET"
"_____"

P[8]=100
h_s[8]=Enthalpy(Air_ha,s=s[7],P=P[8])
```

```
W_T = ETA_T * m_dot*(h[7]-h_s[8])
W_T=m_dot * (h[7]-h[8])

T[8] = temperature(Air_ha,h = h[8], P = P[8])
s[8] = Entropy(Air_ha,T=T[8],P=P[8])

"POINT 9 - EXHAUST"
"_____"

DELTA_P89 =alpha_P *((P[8] +P[9])/2)

P[9 ]= P[1]+2
h[9] = h[8]
T[9] = Temperature(Air_ha,P=P[9],h=h[9])
s[9] = Entropy(Air_ha,T=T[9],P=P[9])

"POWER OUTPUT CALCULATIONS"
"_____"

W_NET= W_T - W_C

"CYCLE EFFICIENCY"
"_____"

ETA_BRAYTON = (W_NET/Q_CC)
```

II. EES simulation model for the simple EFGT cycle

```
//SIMPLE OPEN BRAYTON CYCLE

"INPUT VALUES"
"_____"

T_MAX =273.15+700

T_AMB = 273.15+25

P_AMB = 100

m_dot =0.07551

{Q_CC = 39.73}

{W_NET= 5.00}

"PRESSURE DROP %"
"_____"

alpha_AF =0.01
alpha_P = 0.00005

"COMPONENT CHARACTERISTICS"
"_____"

 "COMPRESSOR PRESSURE RATIO"
PR_C=4

 "COMPRESSOR EFFICIENCY"
ETA_C=0.76

"TURBINE EFFICIENCY"
ETA_T=0.82

"POINT 1 - AMBIENT"
"_____"

P[1]=P_AMB
T[1]= T_AMB
h[1] =Enthalpy(Air_ha,T=T[1],P=P[1])
s[1] =Entropy(Air_ha,T=T[1],P=P[1])


"POINT 2 - AIR FILTER OUTLET"
"_____"

DELTA_AF =alpha_AF *((P[1] +P[2])/2)

P[2] =P[1]-DELTA_AF
h[2] =h[1]
T[2] =Temperature(Air_ha,P=P[2],h=h[2])
s[2] =Entropy(Air_ha,T=T[2],P=P[2])
```

```
"POINT 3 - COMPRESSOR INLET"
"_____"

DELTA_P23 =alpha_P *((P[2]+P[3])/2)

P[3]=P[2] -DELTA_P23
h[3] =h[2]
T[3] =Temperature(Air_ha,P=P[3],h=h[3])
s[3] =Entropy(Air_ha,T=T[3],P=P[3])


"POINT 4 - COMPRESSOR OUTLET"
"_____"

P[4]=P[3]*PR_C

h_s[4] =Enthalpy(Air_ha,P=P[4],s=s[3])          "Isentropic Enthalpy"

W_C = (1/ETA_C) * m_dot*(h_s[4] -h[3] )
W_C=m_dot * (h[4]-h[3])                         "Work needed by compressor"

T[4]=Temperature(Air_ha,P=P[4],h=h[4])
s[4]=Entropy(Air_ha,T=T[4],P=P[4])


"POINT 5 - COMBUSTION CHAMBER INLET"
"_____"

DELTA_P45 =alpha_P *((P[4]+P[5])/2)

P[5]=P[4] -DELTA_P45
h[5] =h[4]
T[5] =Temperature(Air_ha,P=P[5],h=h[5])
s[5] =Entropy(Air_ha,T=T[5],P=P[5])


"POINT 6 - COMBUSTION CHAMBER OUTLET"
"_____"

T[6]=T_MAX
P[6]=P[5]
h[6]=Enthalpy(Air_ha,T=T[6],P=P[6])
s[6]=Entropy(Air_ha,T=T[6],P=P[6])

Q_CC=m_dot *(h[6]-h[5])


"POINT 7 - TURBINE INLET"
"_____"

DELTA_P67 =alpha_P *((P[6]+P[7])/2)

P[7] = P[6] - DELTA_P67
h[7] = h[6]
T[7] = Temperature(Air_ha,P=P[7],h=h[7])
s[7] = Entropy(Air_ha,T=T[7],P=P[7])
```

```
 "POINT 8 - TURBINE OUTLET"
"_____"

 P[8] = P[1]+5
 P[8]=  P[7]*(1 / PR_T)

h_s[8]=Enthalpy(Air_ha,s=s[7],P=P[8])

W_T = ETA_T * m_dot*(h[7]-h_s[8])
W_T=m_dot * (h[7]-h[8])

T[8] = temperature(Air_ha,h = h[8], P = P[8])
s[8] = Entropy(Air_ha,T=T[8],P=P[8])

"POINT 9 - EXHAUST"
"_____"

DELTA_P89 =alpha_P *((P[8]+P[9])/2)

P[9] =P[8] - DELTA_P89
h[9] = h[8]
T[9] = Temperature(Air_ha,P=P[9],h=h[9])
s[9] = Entropy(Air_ha,T=T[9],P=P[9])

"_____CALCULATIONS_____"

W_NET= W_T - W_C

"_____EFFICIENCY_____”

ETA_BRAYTON = (W_NET/Q_CC)
```

III. EES simulation model for the heat recovery EFGT cycle

```
//HEAT RECOVERY CYCLE

"INPUT VALUES"
"_____"

T_MAX =700+273.15

T_AMB = 25+273.15

P_AMB = 100 [kPa]

{m_dot =0.07551}

{Q_CC=39.73}

 W_NET =5

"PRESSURE DROP %"
"_____"

alpha_AF =0.01
alpha_P = 0.00005

"COMPONENT CHARACTERISTICS"
"_____"


 "COMPRESSOR PRESSURE RATIO"
PR_C=4

 "COMPRESSOR EFFICIENCY"
ETA_C=0.76

"TURBINE EFFICIENCY"
ETA_T=0.82

"HEAT EXCHANGER EFFECTIVENESS"

Epsilon = 0.8

//#########################################################################

"POINT 1 - AMBIENT"
"_____"

P[1]=P_AMB
T[1]= T_AMB
h[1] =Enthalpy(Air_ha,T=T[1],P=P[1])
s[1] =Entropy(Air_ha,T=T[1],P=P[1])

Cp=Cp(Air_ha,T=T[1],P=P[1])

"POINT 2 - AIR FILTER OUTLET"
"_____"
```

```
DELTA_AF =alpha_AF *((P[1] +P[2])/2)

P[2] =P[1]-DELTA_AF
h[2] =h[1]
T[2] =Temperature(Air_ha,P=P[2],h=h[2])
s[2] =Entropy(Air_ha,T=T[2],P=P[2])


"POINT 3 - COMPRESSOR INLET"
"_____"
//PIPE SECTION 2-3

DELTA_P23 =alpha_P *((P[2]+P[3])/2)

P[3]=P[2] -DELTA_P23
h[3] =h[2]
T[3] =Temperature(Air_ha,P=P[3],h=h[3])
s[3] =Entropy(Air_ha,T=T[3],P=P[3])


"POINT 4 - COMPRESSOR OUTLET"
"_____"

P[4]=P[3]*PR_C

h_s[4] =Enthalpy(Air_ha,P=P[4],s=s[3])          "Isentropic enthalpy"

W_C = (1/ETA_C) * m_dot*(h_s[4] -h[3] )
W_C=m_dot * (h[4]-h[3])                         "Work needed by compressor"

T[4]=Temperature(Air_ha,P=P[4],h=h[4])
s[4]=Entropy(Air_ha,T=T[4],P=P[4])


"POINT 5 - HEAT EXCHANGER PRIMARY SIDE INLET"
"_____"
 //PIPE SECTION 4-5

DELTA_P45 =alpha_P *((P[4]+P[5])/2)

P[5]=P[4] -DELTA_P45
h[5] =h[4]
T[5] = Temperature(Air_ha,P=P[5],h=h[5])
s[5] =Entropy(Air_ha,T=T[5],P=P[5])
Cp_[5]=Cp(Air_ha,T=T[5],P=P[5])

 "POINT 6 - HEAT EXCHANGER PRIMARY SIDE OUTLET"
"_____"

DELTA_P_HX_PS = 0 [kPa]                         "Pressure Drop HX Primary Side
P[6] = P[5] - DELTA_P_HX_PS                     "Primary Side Outlet Pressure"

Q_dot_max =C_min * (T[11] - T[5])
Q_dot = Epsilon * Q_dot_max
Q_DOT = m_dot * (h[6] - h[5])

C_min = MIN(Cp_[5] * m_dot, Cp_[11] * m_dot)    "Minimum Heat Capacity"
```

```
T[6] = Temperature(Air_ha,P = P[6],h = h[6])                "Primary Side Outlet Temperature"
s[6] = Entropy(Air_ha,T = T[6],P = P[6])

"POINT 7 - COMBUSTION CHAMBER INLET"
"_____"

 //PIPE SECTION 6-7

DELTA_P67 =alpha_P *((P[6] +P[7])/2)

P[7]=P[6] -DELTA_P67
h[7] =h[6]
T[7] =Temperature(Air_ha,P=P[7],h=h[7])
s[7] =Entropy(Air_ha,T=T[7],P=P[7])

"POINT 8 - COMBUSTION CHAMBER OUTLET"
"_____"

T[8]=T_MAX
P[8]=P[7]

h[8]=Enthalpy(Air_ha,T=T[8],P=P[8])
s[8]=Entropy(Air_ha,T=T[8],P=P[8])

Q_CC=m_dot *(h[8]- h[7])

"POINT 9 - TURBINE INLET"
"_____"

DELTA_P89 =alpha_P *((P[8] +P[9])/2)

P[9] =P[8] - DELTA_P89
h[9] = h[8]
T[9] = Temperature(Air_ha,P=P[9],h=h[9])
s[9] = Entropy(Air_ha,T=T[9],P=P[9])

 "POINT 10 - TURBINE OUTLET"
"_____"

//P[10] = P[9]*(1 / PR_T)
P[10]=P[1]+5

h_s[10]=Enthalpy(Air_ha,s=s[9],P=P[10])

W_T = ETA_T * m_dot*(h[9]-h_s[10])

W_T=m_dot * (h[9]- h[10])

T[10] = temperature(Air_ha,h = h[10], P = P[10])
s[10] = Entropy(Air_ha,T=T[10],P=P[10])

"POINT 11 - HEAT EXCHANGER PRIMARY SIDE INLET"
 "_____"

 //PIPE SECTION 10-11
```

```
DELTA_P1011 =alpha_P *((P[10 ]+P[11])/2)

P[11]=P[10] -DELTA_P1011
h[11] =h[10]
T[11] =Temperature(Air_ha,P=P[11],h=h[11])
s[11] =Entropy(Air_ha,T=T[11],P=P[11])
 Cp_[11]=Cp(Air_ha,T=T[11],P=P[11])

" POINT 12 - HEAT EXCHANGER SECONDARY SIDE OUTLET"
"_____"

{DELTA_P_HX_SS = Alpha_HX * ((P[12] + P[11]) / 2)}   "Pressure Drop HX Secondary Side"
DELTA_P_HX_SS = 0 [kPa]
P[12] = P[11] - DELTA_P_HX_SS                        "Secondary Side Outlet Pressure"

Q_Dot = -m_dot * (h[12] - h[11])

T[12] = Temperature(Air_ha, h = h[12], P = P[12])    "Secondary Side Outlet Temperature"
s[12] = Entropy(Air_ha, T = T[12], P = P[12])        "Secondary Side Outlet Entropy"

 "POINT 13 - EXHAUST"
"_____"

  //PIPE SECTION 12-13

//DELTA_P1213 =alpha_P *((P[12]+P[13])/2)
  //P[13] = P[12] - DELTA_P1213
P[13] =P[1] +5
h[13] = h[12]
T[13] = Temperature(Air_ha,P=P[13],h=h[13])
s[13] = Entropy(Air_ha,T=T[13],P=P[13])

//#########################################################################

"_____CALCULATIONS_____"

W_NET= W_T - W_C

"_____CYCLE EFFICIENCY_____"

ETA_BRAYTON = (W_NET/Q_CC)
```

IV. EES simulation model for the simple pre-cooled EFGT cycle

```
//PRE-COOLED SIMPLE OPEN BRAYTON CYCLE

"INPUT VALUES"
"_____________________________________________________________"

T_MAX =700+273.15

T_AMB = 15+273.15

P_AMB = 100

{m_dot =0,07551}

Cp=Cp(Air_ha,T=T_AMB,P=P_AMB)

{Q_CC=39,73}

W_NET = 5.00

"PRESSURE DROP %"
"_____________________________________________________________"

alpha_AF =0.05
alpha_P = 0.00005

"COMPONENT CHARACTERISTICS"
"_____________________________________________________________"

"PRE-COOLER COP"

COP = 1.9

 "COMPRESSOR PRESSURE RATIO"
PR_C=4

 "COMPRESSOR EFFICIENCY"
ETA_C=0.76

"TURBINE EFFICIENCY"
ETA_T=0.82

"POINT 01 - AMBIENT / PRE-COOLER INLET"
"_____________________________________________________________"

P[01]=P_AMB
T[01]= T_AMB
h[01] =Enthalpy(Air_ha,T=T[01],P=P[01])
s[01] =Entropy(Air_ha,T=T[01],P=P[01])

 "POINT 1 - PRE-COOLER OULET"
"_____________________________________________________________"

P[1]=P_AMB

DELTA_T = 12
```

```
T[1]= T_AMB - DELTA_T
h[1] =Enthalpy(Air_ha,T=T[1],P=P[1])
s[1] =Entropy(Air_ha,T=T[1],P=P[1])

Q_L= m_dot*(h[01]-h[1])

COP = Q_L / W_PC_Net

"POINT 2 - AIR FILTER OUTLET"
"_____"

DELTA_AF =alpha_AF *((P[1] +P[2])/2)

P[2] =P[1]-DELTA_AF
h[2] =h[1]
T[2] =Temperature(Air_ha,P=P[2],h=h[2])
s[2] =Entropy(Air_ha,T=T[2],P=P[2])

"POINT 3 - COMPRESSOR INLET"
"_____"

DELTA_P23 =alpha_P *((P[2]+P[3])/2)

P[3]=P[2] -DELTA_P23
h[3] =h[2]
T[3] =Temperature(Air_ha,P=P[3],h=h[3])
s[3] =Entropy(Air_ha,T=T[3],P=P[3])

"POINT 4 - COMPRESSOR OUTLET"
"_____"

 P[4]=P[3]*PR_C
 h_s[4] =Enthalpy(Air_ha,P=P[4],s=s[3])                    "ISENTROPIC"

W_C = (1/ETA_C) * m_dot*(h_s[4] -h[3] )
W_C=m_dot * (h[4]-h[3])                                    "WORK NEEDED BY COMPRESSOR"

T[4]=Temperature(Air_ha,P=P[4],h=h[4])
s[4]=Entropy(Air_ha,T=T[4],P=P[4])

"POINT 5 - COMBUSTION CHAMBER INLET"
"_____"

DELTA_P45 =alpha_P *((P[4]+P[5])/2)

P[5]=P[4] -DELTA_P45
h[5] =h[4]
T[5] =Temperature(Air_ha,P=P[5],h=h[5])
s[5] =Entropy(Air_ha,T=T[5],P=P[5])

"POINT 6 - COMBUSTION CHAMBER OUTLET"
"_____"

T[6]=T_MAX
P[6]=P[5]
 h[6]=Enthalpy(Air_ha,T=T[6],P=P[6])
s[6]=Entropy(Air_ha,T=T[6],P=P[6])
```

```
Q_CC=m_dot *(h[6]-h[5])

"POINT 7 - TURBINE INLET"
"_____"

DELTA_P67 =alpha_P *((P[6]+P[7])/2)

 P[7] = P[6] - DELTA_P67
h[7] = h[6]
T[7] = Temperature(Air_ha,P=P[7],h=h[7])
s[7] = Entropy(Air_ha,T=T[7],P=P[7])

"POINT 8 - TURBINE OUTLET"
"_____"

 //P[8] = P[7]*(1 / PR_T)
P[8]=P[1] +2
 h_s[8]=Enthalpy(Air_ha,s=s[7],P=P[8])

W_T = ETA_T * m_dot*(h[7]-h_s[8])
 W_T=m_dot * (h[7]-h[8])

T[8] = temperature(Air_ha,h = h[8], P = P[8])
s[8] = Entropy(Air_ha,T=T[8],P=P[8])

"POINT 9 - EXHAUST"
"_____"


DELTA_P89 =alpha_P *((P[8]+P[9])/2)
P[9] = P[8] - DELTA_P89
h[9] = h[8]
T[9] = Temperature(Air_ha,P=P[9],h=h[9])
s[9] = Entropy(Air_ha,T=T[9],P=P[9])

"_____CALCULATIONS_____"

W_NET= W_T - W_C- W_PC_NET

"EFFICIENCY"
"_____"

ETA_BRAYTON = (W_NET/Q_CC)
```

V. EES simulation model for the heat recovery pre-cooled EFGT cycle

```
//PRE-COOLED HEAT RECOVERY CYCLE

"INPUT VALUES"
"_____"

T_MAX =700+273.15

T_AMB = 25+273.15

P_AMB = 100 [kPa]

{m_dot =0.07551}

Cp=Cp(Air_ha,T=T_AMB,P=P_AMB)

W_NET = 5.00

{Q_CC=39.73}

"PRESSURE DROP %"
"_____"

alpha_AF =0.01
alpha_P = 0.00005

"COMPONENT CHARACTERISTICS"
"_____"

 "PRE-COOLER COP"

COP = 1.9

 "COMPRESSOR PRESSURE RATIO"
PR_C=4

"TURBINE PRESSURE RATIO"
{PR_T=4,2}

 "COMPRESSOR EFFICIENCY"
ETA_C=0.76

"TURBINE EFFICIENCY"
ETA_T=0.82

"HEAT EXCHANGER EFFECTIVENESS"

Epsilon = 0.8

//#########################################################################

"POINT 01 - AMBIENT / PRE-COOLER INLET"
"_____"

P[01]=P_AMB
T[01]= T_AMB
```

```
h[01] =Enthalpy(Air_ha,T=T[01],P=P[01])
s[01] =Entropy(Air_ha,T=T[01],P=P[01])

 "POINT 1 - PRE-COOLER OULET"
"_____"

P[1]=100 [kPa]

DELTA_T = 12
T[1]= T_AMB - DELTA_T
h[1] =Enthalpy(Air_ha,T=T[1],P=P[1])
s[1] =Entropy(Air_ha,T=T[1],P=P[1])

m_dot_ref = m_dot*0.1
Q_L= m_dot_ref*(h[01]-h[1])

COP = Q_L / W_PC_Net

"POINT 2 - AIR FILTER OUTLET"
"_____"

DELTA_AF =alpha_AF *((P[1] +P[2])/2)

P[2] =P[1]-DELTA_AF
h[2] =h[1]
T[2] =Temperature(Air_ha,P=P[2],h=h[2])
s[2] =Entropy(Air_ha,T=T[2],P=P[2])

"POINT 3 - COMPRESSOR INLET"
"_____"
//PIPE SECTION 2-3

DELTA_P23 =alpha_P *((P[2]+P[3])/2)
P[3]=P[2] -DELTA_P23
h[3] =h[2]
T[3] =Temperature(Air_ha,P=P[3],h=h[3])
s[3] =Entropy(Air_ha,T=T[3],P=P[3])

"POINT 4 - COMPRESSOR OUTLET"
"_____"

 P[4]=P[3]*PR_C
h_s[4] =Enthalpy(Air_ha,P=P[4],s=s[3])    "ISENTROPIC ENTHALPY"

W_C = (1/ETA_C) * m_dot*(h_s[4] -h[3] )
W_C=m_dot * (h[4]-h[3])                    "WORK NEEDED BY COMPRESSOR"

T[4]=Temperature(Air_ha,P=P[4],h=h[4])
s[4]=Entropy(Air_ha,T=T[4],P=P[4])

 "POINT 5 - HEAT EXCHANGER PRIMARY SIDE INLET"
"_____"

 //PIPE SECTION 4-5

DELTA_P45 =alpha_P *((P[4]+P[5])/2)

P[5]=P[4] -DELTA_P45
```

```
h[5] =h[4]
T[5] = Temperature(Air_ha,P=P[5],h=h[5])
s[5] =Entropy(Air_ha,T=T[5],P=P[5])
Cp_[5]=Cp(Air_ha,T=T[5],P=P[5])

 "POINT 6 - HEAT EXCHANGER PRIMARY SIDE OUTLET"
"_____"

DELTA_P_HX_PS = 0 [kPa]                          "Pressure Drop HX Primary Side:
P[6] = P[5] - DELTA_P_HX_PS                      "Primary Side Outlet Pressure"

Q_dot_max =C_min * (T[11] - T[5])
Q_dot = Epsilon * Q_dot_max
Q_DOT = m_dot * (h[6] - h[5])

C_min = MIN(Cp_[5] * m_dot, Cp_[11] * m_dot)     "Minimum Heat Capacity"

T[6] = Temperature(Air_ha,P = P[6],h = h[6])     "Primary Side Outlet Temperature"
s[6] = Entropy(Air_ha,T = T[6],P = P[6])

"POINT 7 - COMBUSTION CHAMBER INLET"
"_____"
 //PIPE SECTION 6-7

DELTA_P67 =alpha_P *((P[6]+P[7])/2)

P[7]=P[6] -DELTA_P67
h[7] =h[6]
T[7] =Temperature(Air_ha,P=P[7],h=h[7])
s[7] =Entropy(Air_ha,T=T[7],P=P[7])

"POINT 8 - COMBUSTION CHAMBER OUTLET"
"_____"

T[8]=T_MAX
P[8]=P[7]
 h[8]=Enthalpy(Air_ha,T=T[8],P=P[8])
s[8]=Entropy(Air_ha,T=T[8],P=P[8])

Q_CC=m_dot *(h[8]-h[7])

 "POINT 9 - TURBINE INLET"
"_____"

DELTA_P89 =alpha_P *((P[8]+P[9])/2)


P[9] =P[8] - DELTA_P89
h[9] = h[8]
T[9] = Temperature(Air_ha,P=P[9],h=h[9])
s[9] = Entropy(Air_ha,T=T[9],P=P[9])

"POINT 10 - TURBINE OUTLET"
 "_____"

P[10] = P[9]*(1 / PR_T)
P[10]= P[1] +2
h_s[10]=Enthalpy(Air_ha,s=s[9],P=P[10])
```

```
W_T = ETA_T * m_dot*(h[9]-h_s[10])
W_T=m_dot * (h[9]-h[10])

T[10] = temperature(Air_ha,h = h[10], P = P[10])
s[10] = Entropy(Air_ha,T=T[10],P=P[10])

" POINT 11 - HEAT EXCHANGER PRIMARY SIDE INLET"
"_____"

 //PIPE SECTION 10-11

DELTA_P1011 =alpha_P *((P[10]+P[11])/2)

P[11]=P[10] -DELTA_P1011
h[11] =h[10]
T[11] =Temperature(Air_ha,P=P[11],h=h[11])
s[11] =Entropy(Air_ha,T=T[11],P=P[11])
 Cp_[11]=Cp(Air_ha,T=T[11],P=P[11])

" POINT 12 - HEAT EXCHANGER SECONDARY SIDE OUTLET"
"_____"

{DELTA_P_HX_SS = Alpha_HX * ((P[12] + P[11]) / 2)}   "Pressure Drop HX Secondary Side"
DELTA_P_HX_SS = 0 [kPa]
P[12] = P[11] - DELTA_P_HX_SS                        "Secondary Side Outlet Pressure"

Q_Dot = -m_dot * (h[12] - h[11])

T[12] = Temperature(Air_ha, h = h[12], P = P[12])    "Secondary Side Outlet Temperature"
s[12] = Entropy(Air_ha, T = T[12], P = P[12])        "Secondary Side Outlet Entropy"

"POINT 13 - EXHAUST"
"_____"
//PIPE SECTION 12-13

//DELTA_P1213 =alpha_P *((P[12]+P[13])/2)
//P[13] = P[12] - DELTA_P1213
P[13]=P[1]+4
h[13] = h[12]
T[13] = Temperature(Air_ha,P=P[13],h=h[13])
s[13] = Entropy(Air_ha,T=T[13],P=P[13])

//#########################################################################

"_____CALCULATIONS_____"

W_NET= W_T - W_C –(ABS(W_PC_Net))

 "_____CYCLE EFFICIENCY_____"

ETA_BRAYTON = (W_NET/Q_CC)
```

APPENDIX B

Garrett
ADVANCING MOTION

Installer Connect

Turbo Catalog

Corresponding Part Numbers for: TATA Ace

OE Number	Garrett Number	Reman	Engine Model	Engine Code	Power	Displacement	Years
571014510101	789997-5001S	-	Ace	0.8L DICOR	40HP@4000RPM	0.8L	2010

Corresponding Part Numbers for: CHEVROLET (GM) Aveo

OE Number	Garrett Number	Reman	Engine Model	Engine Code	Power	Displacement	Years
* 9S516K682BA	799171-5001S	-	Aveo	LDV	75HP@4000RPM	1.3L	2011-2015
* 9S516K682BA	799171-5001S	-	Aveo	LDV	75HP@4000RPM	1.3L	2011-2015
* DS516K682AA	799171-5002S	-	Aveo	LDV	75HP@4000RPM	1.3L	2011-2015
* 9S516K682BA	799171-5001S	-	Aveo	Z13DTE	95HP@4000RPM	1.3L	2011-2015
* DS516K682AA	799171-5002S	-	Aveo	Z13DTE	95HP@4000RPM	1.3L	2011-2015

Corresponding Part Numbers for: CHEVROLET (GM) Cruze

OE Number	Garrett Number	Reman	Engine Model	Engine Code	Power	Displacement	Years
* 96832200	771903-5003S	-	Cruze	Z20S1	150HP@2000RPM	2.0L	2009
* 96832200	771903-5003S	-	Cruze	Z20S1	125HP@2000RPM	2.0L	2009-2011
* E55565353	781504-5001S	-	Cruze	A14NET	140HP@6000RPM	1.4L	2012
* E55565353	781504-5002S	-	Cruze	A14NET	140HP@6000RPM	1.4L	2012
* E55565353	781504-5004S	-	Cruze	A14NET	140HP@6000RPM	1.4L	2012

Corresponding Part Numbers for: CHEVROLET (GM) Captiva

OE Number	Garrett Number	Reman	Engine Model	Engine Code	Power	Displacement	Years
96440365	762463-5002S	-	Captiva	Z20S	147HP@4000RPM	2.0L	2008
96440365	762463-5003S	-	Captiva	Z20S	147HP@4000RPM	2.0L	2008
96440365	762463-5004S	-	Captiva	Z20S	147HP@4000RPM	2.0L	2008
96440365	762463-5006S	762463-9006S	Captiva	Z20S	147HP@4000RPM	2.0L	2008
* 96440365	762463-5002S	-	Captiva	Z20S	150HP@4000RPM	2.0L	2006-2011
* 96440365	762463-5003S	-	Captiva	Z20S	150HP@4000RPM	2.0L	2006-2011
* 96440365	762463-5004S	-	Captiva	Z20S	150HP@4000RPM	2.0L	2006-2011
* 96440365	762463-5006S	762463-9006S	Captiva	Z20S	150HP@4000RPM	2.0L	2006-2011
* 96440365	762463-9006S	-	Captiva	Z20S	150HP@4000RPM	2.0L	2006-2011
* 96440365	762463-5002S	-	Captiva	Z20S	126HP@4000RPM	2.0L	2006-2009

APPENDIX C

Simulation of the vapour-compression refrigeration cycle

Assumptions:

- Superheating of 12°C.
- Subcooling of 8°C.
- Pressure drops in pipes and components are neglected.
- Ambient air is cooled from 30°C to 12°C.

Vapor-Compression Refrigeration Cycle: Input Parameters

Parameter	Value	Unit
Ambient Temperature	30	[˚C]
Ambient Pressure	100	[kPa]
Condensing Temperature	50	[˚C]
Evaporating Temperature	0	[˚C]
Refrigerant mass flow rate	0.03	[kg/s]
Compressor isentropic efficiency	0.60	[-]

Results for Vapor-Compression Simulation:

Vapour-Compression Refrigeration Cycle: Results

Parameter	Value	Unit
COP	2.694	[-]
Compressor Work (W_C)	1.669	[kW]
Cooling effect (Q_L)	4.498	[kW]
Air mass flow rate	0.194	[kg/s]

T-s Diagram for Vapour-Compression Simulation:

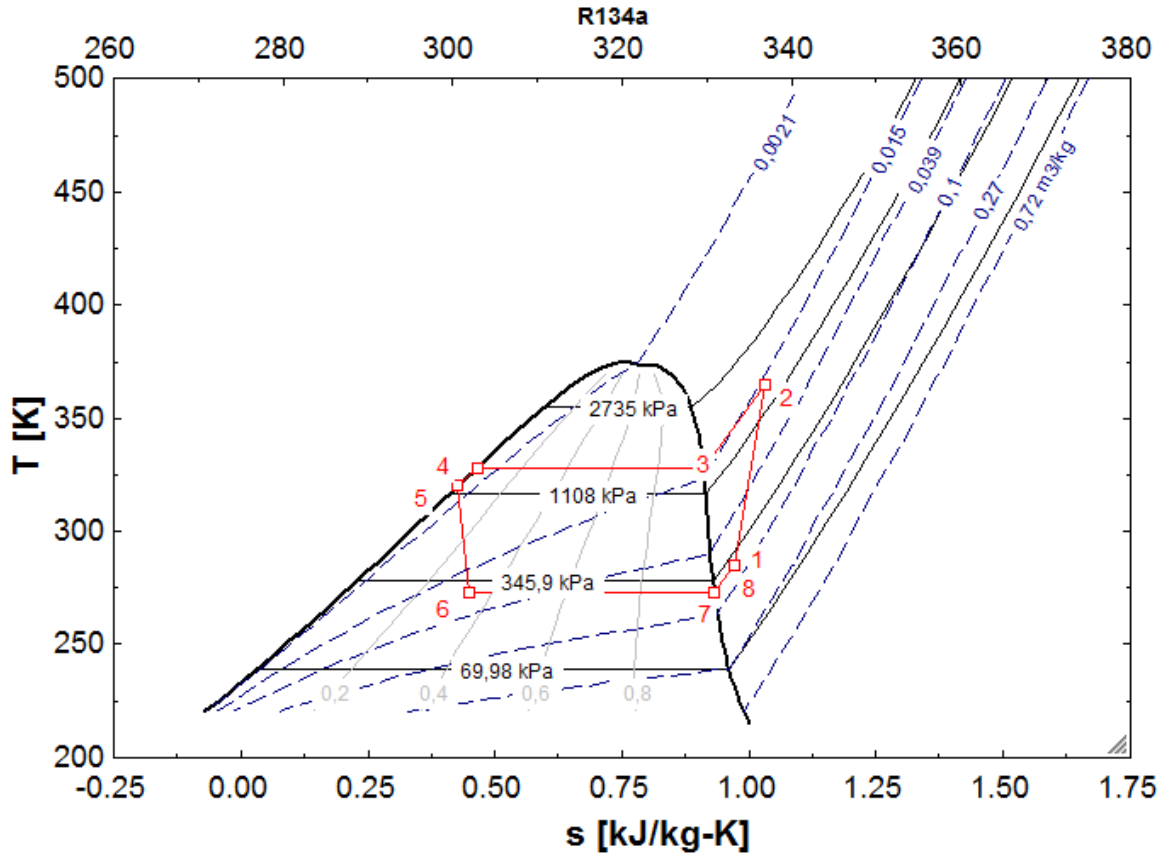

Results obtained per operating point:

Operating point	Temperature T[i]	Pressure P[i]	Enthalpy h[i]	Entropy s[i]	Quality x[i]
#	[K]	[kPa]	[kJ/kg]	[kJ/kg·K]	[-]
1	285.2	293	261.1	0.9697	1
2	359.7	1319	316.8	1.033	1
3	323.1	1319	275.3	0.9115	1
4	323.1	1319	123.5	0.4418	0
5	315.1	1319	111.2	0.4034	0
6	273.1	293	111.2	0.4217	0.29
7	273.2	293	250.5	0.9314	1
8	285.2	293	261.1	0.9697	1

EES Program for Vapour-Compression Simulation:

```
//Actual Vapour-Compression Cycle

"                    Ambient Conditions                    "
"__________________________________________________________"

T_AMB=30+273.15                                    "Ambient Temperature"
P_AMB=100                                          "Ambient Pressure"

"                    Input Properties                    "
"__________________________________________________________"

T_c = 50+273.15                                    "Condensing Temperature"
T_e=0+273.15                                       "Evaporating Temperature"
 DELTA_T_sup=12                                    "Super heating"
 DELTA_T_sub=8                                     "Sub Cooling"

T_ai = 30+273.15
T_ae = 12+273.15

m_dot_gas= 0.03

"                Point 1 - Compressor Inlet                "
"__________________________________________________________"
P[1]=pressure(R134a,T=T_e,x=1)
T[1]=T_e+ DELTA_T_sup
 h[1]=enthalpy(R134a,T=T[1],P=P[1])
s[1]=entropy(R134a,T=T[1],P=P[1])


"              Point 2 - Compressor outlet                 "
"__________________________________________________________"

P[2]=pressure(R134a,T=T_c,x=1)
s_2_isen=s[1]
h_2_isen=enthalpy(R134a,P=P[2],s=s_2_isen)
T[2]=temperature(R134a,P=P[2],h=h[2])
s[2]=entropy(R134a,T=T[2],h=h[2])

ETA_C=0.60
ETA_C=((h_2_isen-h[1])/(h[2]-h[1]))
W_C=m_dot_gas*(h[2]-h[1])


h_g[2] = enthalpy(R134a,x=1, P=P[2])
h_f[2] = enthalpy(R134a,x=0, P=P[2])

"                  Point 3 - Condenser                   "
"__________________________________________________________"

h[3] = h_g[2]
P[3] = P[2]
T[3]=temperature(R134a,P=P[3],x=1)
s[3]=entropy(R134a,T=T[3],x=1)
```

```
"        Point 4 - Condenser two-phase region          "
"______________________________________________________"

P[4]=P[3]
h[4] = enthalpy(R134a,x=0, P=P[2])
T[4]=temperature(R134a,P=P[4],h=h[4])
s[4]=entropy(R134a,h=h[4],T=T[4])

"              Point 5 - sub-cooled region             "
"______________________________________________________"

P[5]=P[4]
T[5]=T[4]-DELTA_T_sub
h[5]=enthalpy(R134a,P=P[5],T=T[5])
s[5]=entropy(R134a,h=h[5],T=T[5])

//Heating
Q_Con=m_dot_gas*(h[5]-h[2])

"              Point 6 - Expansion Valve               "
"______________________________________________________"

h[6]=h[5]
P[6]=P[1]
T[6]=temperature(R134a,P=P[6],h=h[6])
s[6]=entropy(R134a,h=h[6],T=T[6])
x[6]=quality(R134a,P=P[6],h=h[6])

"              Point 7 - Evaporator                    "
"______________________________________________________"

h_g[1] = enthalpy(R134a,x=1, P=P[1])
h[7]=h_g[1]
P[7]=P[6]
T[7]=T_e
s[7]=entropy(R134a,P=P[7],x=1)

"              Point 8 - Evapotator Outlet             "
"______________________________________________________"

P[8]=P[7]
T[8]=T[7]+DELTA_T_sup
h[8] = enthalpy(R134a,T=T[8], P=P[8])
s[8]=entropy(R134a,P=P[8],h=h[8])

//Cooling
Q_e=m_dot_gas*(h[8]-h[6])

COP=Q_e/W_C
"                      Air Side                        "
"______________________________________________________"

h_ai=enthalpy(Air_ha,T=T_ai,P=P_AMB)
h_ae=enthalpy(Air_ha,T=T_ae,P=P_AMB)
-Q_e=m_dot_air*(h_ae-h_ai)
```